DEVELOPMENT OF A MONTE CARLO CODE SYSTEM WITH CONTINUOUS ENERGY ADJOINT TRANSPORT CAPABILITIES FOR NEUTRONS AND PHOTONS

by

Alex P. Robinson

A preliminary report submitted in partial fulfillment of
the requirements for the degree of

Doctor of Philosophy

(Nuclear Engineering and Engineering Physics)

at the

UNIVERSITY OF WISCONSIN–MADISON

14 February 2014

Table of Contents

List of Tables

List of Figures

Chapter 1

Introduction

The Monte Carlo method has a rich history going back as far back as Babylonian times. However, its use in the field of radiation transport began in the 1940s and can be attributed to the work of von Neumann, Ulam, Metropolis, Kahn, Fermi and their collaborators [1]. The first successful application of the method in the field of radiation transport coincided with the construction of the first digital computers [2]. Because computational resources were relatively scarce and expensive, the computer codes implementing the Monte Carlo method to solve radiation transport problems were full of approximations to both the physical models and the cross section data. As the availability of computer resources increased, it became feasible to do high fidelity Monte Carlo simulations with regard to both the physical models and the cross section data [3]. Today, the Monte Carlo method is regarded as the gold standard of computational methods for solving radiation transport problems because all variables of interest (i.e. energy, direction and position) can be treated on a continuous scale and because the problem geometry can be modeled nearly completely. As computers continue to grow in size and speed, the Monte Carlo method will continue to be used for more and more challenging problems*.

1.1 The Monte Carlo Method

The Monte Carlo method is a stochastic method in which samples are drawn from a parent population through sampling procedures governed by a set of probability laws. From the samples, statistical data is acquired and analyzed to make inferences about the parent population.

In radiation transport problems, the system of interest is a collection of bounded regions which can contain one or more of the following: a material, a vacuum, a source, a detector. The parent population is the set of all possible radiation histories and the samples are histories drawn from this set. The particle history can be regarded as a random walk from a source region to a problem domain boundary or some other terminating location (i.e. absorption point). Each phase

*Already, the Monte Carlo method is appearing in full reactor core simulation codes where it was once deemed too costly and inefficient to use [4].

of the random walk is governed by a set of probability laws that are related to the material interaction cross sections of the particular form of radiation. The portion of a random walk that passes through a finite detector region is recorded or scored.

While radiation transport problems are typically solved by sampling radiation histories that start in what can be regarded as a model of the physical source and recorded in what can be regarded as a model of the physical detector, the opposite can also be true. The process of sampling the starting point of a radiation history in the model of the physical source and recording information in the model of the physical detector is often called a forward process. The probability laws used in a forward process can be derived from the Boltzmann equation, which will be referred to as the transport equation. The forward process is most effective when the detector region is large relative to the source region. As the detector region decreases in size, the probability of any given history passing through the detector region decreases until, for a point detector, the probability goes to zero [5]. The process of sampling the starting point of a history in the model of a physical detector and recording information in the model of the physical source is referred to in the literature as an adjoint or reverse process [5, 6]. The reverse process is most effective when the source region is large compared to the detector region. When the detector region is a point, only the reverse process can be used without resorting to special procedures. The probability laws that govern this process can be derived from the adjoint Boltzmann equation, which will be referred to as the adjoint transport equation. The derivation of these probability laws will be a major focus of this report.

1.2 Motivations for using the Adjoint Process

As mentioned in the previous section, one of the primary motivations for using the adjoint process is that problems with detectors that are small relative to the source can be solved more efficiently. This motivation for the adjoint process is encountered often in the literature [5, 7, 8].

While a wide range of shielding problems could benefit from the adjoint process based on the above motivation, there is a particular class of problems, which are of particular interest in the fusion community, that could benefit. In these problems the photon dose in a particular region of an experiment, fusion device or fission device, which results from neutron activation of the surrounding material, is desired. This information is particularly important for planning maintenance on the experiment

or device. These problems are often solved using a method called the rigorous 2-step (R2S) method [9–11]. In this method the neutron flux throughout the experiment or device is calculated. This neutron flux data is then given to an activation code which calculates the source of photons due to the decay of material that is activated by the neutrons. Finally, the dose due to photons is calculated in the areas of interest using a forward process. Usually, the amount of activated material is much larger than the region where the dose distribution is desired, which indicates that these problems could potentially benefit from the adjoint process for photons. The use of the adjoint photon process in the rigorous 2-step method has been coined the rigorous 2-step adjoint (R2SA) method [11].

Another motivation for using the adjoint process exists. However, discussion of this motivation requires a physical interpretation of the adjoint flux that is estimated by using the adjoint process. As explained in the previous section, during an adjoint process an adjoint random walk starts in the detector and when it enters the source, information about the problem is gathered. It is therefore common to interpret the adjoint flux as the importance or sensitivity of a particular point of the source (in phase space) to the detector response [8]. This source importance data can be invaluable when the exact source distribution is not known, which can occur in source distribution optimization calculations.

In the medical physics community there has been a good deal of work done over the last decade in which adjoint data is used for this very reason. In both brachytherapy and external beam treatment planning optimization, the use adjoint flux data interpreted as a source importance distribution has been shown to allow for faster and simpler treatment planning optimization algorithms [12–14].

The adjoint flux or importance can also be useful when designing detectors. Essentially, the adjoint flux can allow for the spectral performance of a detector to be predicted for an arbitrary source distribution, which allows the detector design to be optimized before it is constructed. This can be especially important for detectors that utilize rare materials, such as He^3 detectors [15].

1.3 Monte Carlo Codes Available Today

Most Monte Carlo codes available today focus on the forward process described before. The forward process has been developed to a level where very few approximations are used. For instance, it is very common to treat radiation histories on a continuous energy scale. This is also made possible by the very accurate cross

section data that is available. The adjoint process has not been developed to the same level yet. Only a few Monte Carlo codes have implemented the adjoint process in a way that is relatively free of approximation. The GEANT4 toolkit has implemented the adjoint process on a continuous energy scale for electromagnetic radiation and charged particles. In this implementation there are still some approximations that lead to discrepancies in results compared to results from the forward process [6]. FOCUS, a research code written by Hoogenboom, was the first code to implement the adjoint process for neutrons on a continuous energy scale. This code was not able to model the coupled adjoint process for neutrons and photons [16]. Today only the commercial United Kingdom code MCBEND has implemented the adjoint process for neutrons [17]. The implementation in MCBEND has some approximations that can be eliminated as well. Like FOCUS, MCBEND can not model the coupled adjoint process for neutrons and photons. Table 1.3 summarizes the continuous energy modeling capabilities of most Monte Carlo codes available today. Please note that two of the most powerful and popular codes, MCNP5 and MCBEND are not open source codes. GEANT4, though a software development kit and not a true code, is the only open source software that has some continuous energy adjoint capabilities. Several codes, such as MCNP5 and MORSE have implemented the adjoint process with a discrete or multigroup energy format.

Table 1.1: **Continuous Energy Capabilities of Monte Carlo Codes Available Today.** *The final column shows the proposed capabilities of the Forward-Adjoint Continuous Energy Monte Carlo (FACEMC) code.*

Code	n	γ	$n^\dagger$	$\gamma^\dagger$
EGS4	-	$\surd$	-	-
EGSnrc	-	$\surd$	-	-
ITS6	-	$\surd$	-	-
PENELOPE	-	$\surd$	-	-
MORSE	-	-	-	-
TART2005	$\surd$	$\surd$	-	-
MCNP5/6	$\surd$	$\surd$	-	-
MCNPX	$\surd$	$\surd$	-	-
GEANT4	$\surd$	$\surd$	-	$\surd$
MCBEND	$\surd$	$\surd$	$\surd$	-
FACEMC	$\surd$	$\surd$	$\surd$	$\surd$

The main reason for the apparent lack of codes that have implemented the adjoint process on a continuous energy scale is the lack of available adjoint cross section

data necessary for the adjoint process. The popular ENDF libraries only supply cross section data for the forward process. In addition, most of the literature only discusses sampling procedures for the forward process based on differential cross sections. Fortunately, Hoogenboom has shown that both the total and differential adjoint cross sections can be derived from the forward cross sections. The calculation of these cross sections is costly, but only needs to be done once and can be done in the popular ENDF format [16].

1.4 The FACEMC Code

To address the limitations of current Monte Carlo codes and to bring the adjoint process up to the level of the forward process, the Forward-Adjoint Continuous Energy Monte Carlo (FACEMC) code will be developed along with any adjoint cross sections and sampling techniques that are currently lacking. This code will be open source to foster adoption and development by other researchers. As mentioned previously, the scope of this code will only encompass fixed source problems. The energy range over which the forward and adjoint neutron processes will be explored is 10^{-5} eV to 20.0 MeV. For the forward and adjoint photon processes, the energy range that will be explored is 1.0 keV to 20.0 MeV. These energy ranges will be sufficient to model a large number of problems important to both the nuclear engineering community and the medical physics community.

1.5 Report Outline

Most of this report will focus on the theory behind the Monte Carlo random walk process used to simulate the transport of the types of radiation that are of interest. Many texts tend to skip over the detailed derivations that are shown in the following chapters because the forward process is very easy to conceptualize. The probability laws that govern the forward process are also very easy to derive based solely on one's intuition of how radiation travels through a material. The adjoint process is much more difficult to conceptualize. To derive the probability laws that govern the adjoint process, one must rely solely on the adjoint transport equation since one is not likely to have any intuition for how adjoint radiation travels through a material. The goal of the following three chapters is therefore to derive the probability laws that govern the adjoint process from the adjoint transport equation.

Once the probability laws that govern the adjoint process have been derived, a chapter will be devoted to sampling techniques specific to photons and adjoint photons. A single chapter will also be devoted to describing the FACEMC code. This description will include the proposed code requirements, the high-level code design, and the code validation plan.

Chapter 2

Monte Carlo Methods for Fredholm Integral Equations

While Monte Carlo processes can be used to estimate the solutions to a variety of quadrature problems, the focus in this report will fall solely on the specific Monte Carlo process that is used to estimate the solutions of Fredholm integral equations of the second kind (FIESKs). This class of equations is of interest because, through a series of manipulations that will be shown in the following chapters, both the transport equation and the adjoint transport equation become a FIESK. Before discussing the particular Monte Carlo process that is used to solve a FIESK, some background into this class of integral equations will be given.

2.1 The Fredholm Integral Equations of the Second Kind

A FIESK has the following form:

$$F(x) = S(x) + \lambda \int_a^b K(x, y)F(y)dy. \tag{2.1}$$

In this equation, the functions $K(x, y)$ and $S(x)$ are known. The function $S(x)$ is a forcing function and the function $K(x, y)$ is called the kernel of the integral equation, which can be interpreted as a function characterizing the transition from some initial state y to the state x. Due to this interpretation, the kernel is sometimes written as $K(y \to x)$. This notation will be adopted throughout the rest of this report.

Another equation exists that is very similar to the FIESK. It is called the Volterra Integral equation of the second kind:

$$F(x) = S(x) + \lambda \int_a^x K(x, y)F(y)dy. \tag{2.2}$$

The only difference between the two equations is that the Volterra Integral equation of the second kind has a limits of integration that is variable. The Volterra integral

equation is particularly important for radiation transport because it comes about whenever there is a preferred direction for the independent variable*. However, the Volterra integral equation is just a special case of the FIESK and in fact, all Volterra integral equations can be written as a FIESK through the use of a modified kernel [18]:

$$K'(y \to x) = \begin{cases} K(y \to x) & \text{if } y < x \\ 0 & \text{if } y > x. \end{cases} \tag{2.3}$$

It is for this reason that only FIESKs will be of interest in the rest of this report.

There are many ways to analytically solve a FIESK [18, 19]. The method of successive approximations will be shown because of its relevance to the Monte Carlo process that will be described in the next sections. To start, set the zeroth order approximation equal to the forcing function $S(x)$. The first through n-th order approximations will then be defined as follows:

$$\begin{aligned} f_0(x) &= S(x) \\ f_1(x) &= S(x) + \lambda \int_a^b K(y \to x) f_0(y) dy \\ f_2(x) &= S(x) + \lambda \int_a^b K(y \to x) f_1(y) dy \\ &\vdots \\ f_n(x) &= S(x) + \lambda \int_a^b K(y \to x) f_{n-1}(y) dy. \end{aligned} \tag{2.4}$$

As the order of the approximation goes to ∞, the exact solution of the FIESK is recovered:

$$F(x) = \lim_{n \to \infty} f_n(x). \tag{2.5}$$

The solution can also be represented as a Neumann series. First, define a new function $g_n(x)$:

$$g_n(x) = \begin{cases} \int_a^b K(y \to x) S(y) dy & n = 1 \\ \int_a^b K(y \to x) g_{n-1}(y) dy & n > 1. \end{cases} \tag{2.6}$$

*Due to conservation of energy and momentum, the energy of a particle after scattering off of a massive scattering center cannot be greater than the energy prior to the scattering event, assuming that the massive scattering center is stationary

Then equation 2.4 can be written in terms of the function $g_n(x)$:

$$f_n(x) = S(x) + \sum_{j=1}^{n} \lambda^j g_j(x). \tag{2.7}$$

Finally, the exact solution of the FIESK becomes

$$F(x) = S(x) + \sum_{j=1}^{\infty} \lambda^j g_j(x). \tag{2.8}$$

When the function $g_n(x)$ is expanded, the solution in terms of a Neumann series has the following form:

$$\begin{aligned} F(x) = S(x) &+ \lambda \int_a^b K(y \to x) S(y) dy \\ &+ \lambda^2 \int_a^b \int_a^b K(y \to x) K(y_1 \to y) S(y_1) dy_1 dy \\ &+ \lambda^3 \int_a^b \int_a^b \int_a^b K(y \to x) K(y_1 \to y) K(y_2 \to y_1) S(y_2) dy_2 dy_1 dy \\ &+ \cdots \end{aligned} \tag{2.9}$$

If an integral operator $\hat{K} = \int_\Gamma K(y \to x) dy^*$ is defined, then the Neumann series will converge if and only if the spectrum of $\hat{K}$ is contained on the open unit disk [5, 18, 19]. In other words, successive application of the operator $\hat{K}$ do not cause the function being operated on to grow in magnitude.

2.2 The Monte Carlo Random Walk Process

The Monte Carlo process that is used to estimate the solution of a FIESK simulates the movement of entities from state to state in some phase space. The process of moving some entity from state to state is commonly referred to as a random walk processes. The derivation of this Monte Carlo process is outside the scope of this report. It will only be proven that this process does indeed recover the solution to a FIESK given an appropriate random variable. The work by Spanier and Gelbard should be consulted for a detailed discussion of the process [5].

The random walk process for the solution of a Fredholm integral equation of the second kind is completely specified by the following probability distribution

*$\hat{K} \cdot f = \int_\Gamma K(y \to x) f(y) dy$

functions (PDFs) [5]:

$$\text{Random Walk:} \begin{cases} p^1(x) & = P(x_1 = x) \\ p(y \to x) & = P(x_{n+1} = x \mid x_n = y, k > n) \\ p(x) & = P(k = n \mid x_n = x). \end{cases} \tag{2.10}$$

The variable x represents one point, or state, in continuous phase space Γ. The PDF $p^1(x)$ characterizes the probability that the first event of a random walk will occur in state x ($x_1 = x$). The PDF $p(y \to x)$ characterizes the probability of a transition from an initial state y to a new state x ($x_{n+1} = x$ given that $x_n = y$). Finally, the probability $p(x)$ characterizes the probability of termination in state x. The probability of survival in state x will be represented by $q(x)$. The random walk is assumed to undergo k events where x_1 is the first event and x_k is the final event. The PDFs that define the random walk process have the following properties:

1. $p^1(x) \geqslant 0$
   $\int_\Gamma p^1(x)dx = 1$

   and

2. $p(y \to x) \geqslant 0$
   $\int_\Gamma p(y \to x)dx = q(y) = 1 - p(y)$.

The PDF $p^1(x)$ can be generalized to a PDF that characterizes the probability of an entity having its n^{th} event in state x:

$$P^n(x) = \begin{cases} P(x_n = x \mid k > n-1) & \text{if } n >= 2 \\ P(x_1 = x) = p^1(x) & \text{if } n = 1. \end{cases} \tag{2.11}$$

To calculate the PDF in equation 2.11, the following recursion relation may be used:

$$P^n(x) = \int_\Gamma p(y \to x) P^{n-1}(y) dy \tag{2.12}$$

A discrete random variable $X(x)$ can now be defined on the space of random walks, which represents the number density of events that happen in state x. The

expected value of this discrete random variable is

$$\begin{aligned} E[X(x)] &= 1 \cdot P^1(x) + 1 \cdot P^2(x) + \dots \\ &= \sum_{n=1}^{\infty} P^n(x). \end{aligned} \tag{2.13}$$

Finally, a continuous random variable $P(x)$ can be defined, which is equal to $E[X(x)]$. This new random variable is called the continuous event density at x, or simply the event density*. Using this random variable for the event density, and equation 2.12, a proof will be shown that the Monte Carlo random walk process outlined in equation 2.10 will indeed recover the solution of a Fredholm integral equation, which has the form shown in equation 2.1. This proof assumes that $S(x)$ and $K(y \to x)$ from equation 2.1 have the same properties as $p^1(x)$ and $p(y \to x)$ respectively:

$$\begin{aligned} P(x) &= \sum_{n=1}^{\infty} P^n(x) \\ &= p^1(x) + \sum_{n=2}^{\infty} \int_\Gamma p(y \to x) P^{n-1}(y) dy \\ &= p^1(x) + \int_\Gamma p(y \to x) \sum_{n=2}^{\infty} P^{n-1}(y) dy \\ &= p^1(x) + \int_\Gamma p(y \to x) \sum_{n=1}^{\infty} P^n(y) dy \\ &= p^1(x) + \int_\Gamma p(y \to x) P(y) dy. \end{aligned}$$

The random variables $X(x)$ and $P(x)$ are purely mathematical contrivances used to motivate the use of the random walk process and will never be used to estimate values of interest in a problem. While one could count the number of events that occur at a particular point in phase space, given the continuous nature of the phase space, the probability of any one event occurring at exactly the point of interest is zero. In the next section, more practical random variables will be discussed that allow one to estimate the solution of a FIESK in some finite portion of the phase space.

To conduct the random walk process that has been outlined, one must first

*The collision density is the name given in most texts but for the sake of generality, event density has been chosen.

sample a starting state x_1 from the PDF $p^1(x)$. With probability $p(x_1)$ this random walk will end in state x_1. If the random walk continues, a new state x_2 is sampled from

$$\begin{aligned} p(x \mid x_1) &= \frac{p(x_1 \to x)}{\int p(x_1 \to x)dx} \\ &= \frac{p(x_1 \to x)}{q(x_1)}. \end{aligned} \tag{2.14}$$

This process will then continue until the random walk eventually ends in some state x_k. The variable $\alpha = (x_1, \ldots, x_{k-1}, x_k)$ will be used to represent the random walk.

Depending on how the random walk process is derived from the model equation (in the form of a FIESK), the random walk process can fall into one of two categories: analogue or non-analogue. In an analogue random walk process, the random walks simulate the physical behavior of the entity that would be expected based on the model equation. A common misconception is that an analogue process is one where the weight of a particle is always unity. For multiplying systems where particle multiplication is treated implicitly, an analogue process will use particle weights. However, this is rarely done and the latter description will usually suffice. Non-analogue random walk processes typically employ one or more variance reducing techniques to aid in the estimation of rare events. A few common forms of variance reduction are importance sampling, Russian roulette and splitting, all of which are described in detail by Spanier and Gelbard [5].

To determine if a random walk process is analogue, one must look at the source PDF $p^1(x)$ and the state transition PDF $p(y \to x)$. If the source PDF is equal to the source function $S(x)$ divided by a normalization constant and the state transition PDF is equal to the state transition kernel $K(y \to x)$ the random walk process is analogue (usually).

In terms of radiation transport, analogue random walk processes are rarely used due to the difficulty in estimating low probability events. For example, if an estimate of some quantity on the back side of a thick shield is desired and an analogue random walk process is employed, the probability of any random walk passing through the shield model will be very small. Acquiring good estimates of the quantity of interest will therefore require a very large amount of random walks to compensate for the very small probability of any one random walk passing through the shield.

2.3 Monte Carlo Inner Product Estimators

As mentioned in the previous section, the continuous nature of the phase space where the Monte Carlo random walk process is conducted makes the estimation of quantities at a point very challenging. In most problems where Monte Carlo is used, one is instead interested in the estimation of a quantity in some finite portion of the phase space. This quantity of interest can be represented by an inner product of two functions. One function will be a known function and the other will be the solution to a FIESK, which is unknown.

As an example, consider a photon shielding problem where the dose in a particular region behind the shield is desired. In this problem, the known function is the flux-to-dose conversion function and the unknown function is the photon flux distribution in the region of interest behind the shield. The inner product of the flux-to-dose conversion function and the photon flux distribution in the region of interest gives the dose in the region of interest. In equation 2.15, $g(x)$ is the known function and $F(x)$ is the solution to the FIESK of interest:

$$I = \int_{\Gamma} g(x)F(x)dx. \tag{2.15}$$

In this section, two random variables, often referred to as estimators, will be introduced that can be used to gather information from the random walks to estimate the value I. These estimators are defined over the entire phase space instead of one particular point, which makes them quite useful.

The first estimator that will be discussed gathers information about every event of the random walk, but only contributes to the estimation of I when the random walk terminates. Because of this property, it is called the termination estimator. To conduct the random walks using the procedure described in the previous section, the PDFs $p^1(x)$ and $p(y \to x)$ must be constructed by normalizing $S(x)$ and $K(y \to x)$ respectively. This random variable will then reincorporate the magnitude of these functions into the estimate of I. In equation 2.16, the variable α is a random walk beginning at x_1 and ending at x_k:

$$\varepsilon(\alpha) = \frac{S(x_1)}{p^1(x_1)} w(x_1 \to x_2) \cdots w(x_{k-1} \to w_k) \frac{g(x_k)}{p(x_k)}. \tag{2.16}$$

The weight function $w(y \to x)$ is defined in the following equation:

$$w(y \to x) = \begin{cases} \frac{K(y \to x)}{p(y \to x)} & \text{if } p(y \to x) \neq 0 \\ 0 & \text{otherwise.} \end{cases} \tag{2.17}$$

Note that for an analogue random walk process, the weight function after each event will be unity*, since $p(y \to x)$ is equal to $K(y \to x)$. In addition, $\frac{S(x_1)}{p^1(x_1)}$ will be equal to the constant $C = \int_\Gamma S(x)dx$. Therefore, for an analogue random walk process, the termination estimator reduces to

$$\varepsilon(\alpha) = C\frac{g(x_k)}{p(x_k)}.$$

It will now be shown that the expected value of this estimator is equal to the value of the inner product, which will prove that this estimator is unbiased [5]. Equation 2.9, which shows $F(x)$ as a Neumann series will be useful in verifying this proof:

$$\begin{aligned} E[\varepsilon(\alpha)] &= \sum_\alpha P(\alpha)\varepsilon(\alpha) \\ &= \sum_{k=1}^{\infty} \int \cdots \int dx_1 \cdots dx_k p^1(x_1)p(x_1 \to x_2) \cdots p(x_{k-1} \to x_k)p(x_k) \cdot \\ &\quad \frac{S(x_1)}{p^1(x_1)} w(x_1 \to x_2) \cdots w(x_{k-1} \to w_k) \frac{g(x_k)}{p(x_k)} \\ &= \sum_{k=1}^{\infty} \int \cdots \int dx_1 \cdots dx_k S(x_1)K(x_1 \to x_2) \cdots K(x_{k-1} \to x_k)g(x_k) \\ &= \int_\Gamma g(x)F(x)dx. \end{aligned}$$

If the function g(x) is only non-zero in some finite portion of the phase space Γ_d, which will be the case for most problems, only the random walks that terminate in the phase space Γ_d will contribute to the estimation of I.

Another more efficient estimator exists, which estimates I every time a random walk has an event in the phase space Γ_d. This estimator, defined in equation 2.18, is called the event estimator since every event can potentially contribute to the

*As mentioned in the previous section, the weight function for an analogue random walk process where multiplication is treated implicitly will not generally be unity.

estimation of the value of interest*:

$$\eta(\alpha) = \sum_{m=1}^{k} \frac{S(x_1)}{p^1(x_1)} w(x_1 \to x_2) \cdots w(x_{m-1} \to x_m) g(x_m)$$
$$= \sum_{m=1}^{k} W_m(\alpha) g(x_m). \tag{2.18}$$

The value $W_m(\alpha)$ can be interpreted as the weight of the entity after the m^{th} event of the random walk.

Again, for an analogue random walk process, the weight function after each event will be unity and the value $\frac{S(x_1)}{p^1(x_1)}$ will be equal to the constant $C = \int_\Gamma S(x)dx$. Therefore, for an analogue random walk process, the event estimator reduces to

$$\eta(\alpha) = C \sum_{m=1}^{k} g(x_k).$$

The proof that this estimator is an unbiased random variable is quite lengthy and requires a more in-depth discussion of probability theory. Details of this proof can be found in the work by Spanier and Gelbard [5].

As the size of the phase space Γ_d decreases, the event estimator will perform slightly better than the termination estimator because each random walk will have more opportunities to contribute to the estimate of the inner product I. Note that as the size of the phase space Γ_d decreases to a point, the function $g(x)$ becomes a delta function and both of the estimators become ineffective at estimating the value I. In the next section, this problem will be addressed specifically without resorting to special estimators†.

When the Monte Carlo random walk process is used to calculate the inner product I, only a finite number of random walks can be simulated and therefore, only an estimate of the value I can be obtained. The estimate will correspond to the following equation, where N is the number of random walks conducted and $f(\alpha_i)$ is the value of the estimator for random walk α_i:

$$\bar{I} = \frac{1}{N} \sum_{i=1}^{N} f(\alpha_i). \tag{2.19}$$

*The collision estimator is the name given in most texts but for the sake of generality, event estimator has been chosen.

†Kalos has shown how to estimate the flux at a point using a modified collision estimator [20]

To quantify the uncertainty of the estimate of I, the sample standard deviation must also be calculated. The unbiased sample standard deviation is

$$s = \sqrt{\frac{1}{N-1}\sum_{i=1}^{N} f(\alpha_i)^2 - \frac{N}{N-1}\bar{I}}. \tag{2.20}$$

Before moving on, an assumption that was made, which has not been mentioned until now, must be discussed. In order for any of the above estimators to converge to the value I, they must be bounded [5]. This means that the random walks must terminate after $k < \infty$ events with probability unity. Because the random walk process is in effect estimating the terms of a Neumann series, the convergence criteria for a Neumann series will also apply to the random walks. As mentioned in section 2.1, the Neumann series will converge if the spectrum of the operator $\hat{K} = \int_\Gamma K(y \to x)dy$ is contained on the open unit disk, and consequently random walks will terminate with probability unity. In the context of neutron transport problems, this means that only subcritical problems can be handled. This is an acceptable limitation since this report will not address criticality problems.

2.4 The Dual Fredholm Integral Equation of the Second Kind

It has been noted in the previous two sections that estimating a value of interest at a point using a Monte Carlo random walk process is challenging. In this section, a new problem will be introduced that will allow for the estimation of a value of interest at a point using the same general Monte Carlo random walk process from section 2.2.

First consider an operator H with the following property when operating on the function $F(x)$, where x again is a state in the continuous phase space Γ:

$$H \cdot F(x) = F(x) - \int_\Gamma K(y \to x)F(y)dy. \tag{2.21}$$

Based on the equation 2.1, which describes a FIESK, $H \cdot F(x)$ is equal to $S(x)$, the forcing function. If $F(x)$ is assumed to be a real-valued function, the adjoint operator

$H^\dagger$ is defined by the following identity [19]:

$$\int_\Gamma F^\dagger(x)H \cdot F(x)dx = \int_\Gamma F(x)H^\dagger \cdot F^\dagger(x)dx. \tag{2.22}$$

The function $F^\dagger(x)$ is the solution of a different FIESK, which will be called the dual FIESK. From this identity the adjoint operator $H^\dagger$ can be determined:

$$\begin{aligned}
\int_\Gamma F^\dagger(x)H \cdot F(x)dx &= \int_\Gamma \left[F^\dagger(x)F(x) - F^\dagger(x)\int_\Gamma K(y \to x)F(y)dy\right]dx \\
&= \int_\Gamma \left[F^\dagger(x)F(x) - \int_\Gamma K(y \to x)F^\dagger(x)F(y)dy\right]dx \\
&= \int_\Gamma F(y)F^\dagger(y)dy - \int_\Gamma F(y)\int_\Gamma K(y \to x)F^\dagger(x)dxdy \\
&= \int_\Gamma F(x)H^\dagger \cdot F^\dagger(x)dx
\end{aligned}$$

$$H^\dagger \cdot F^\dagger(x) = F^\dagger(x) - \int_\Gamma K(x \to y)F^\dagger(y)dy. \tag{2.23}$$

If the function $H^\dagger \cdot F^\dagger(x)$ is set equal to the function $g(x)$ from the inner product that was defined in equation 2.15, the dual FIESK can be defined as

$$F^\dagger(x) = g(x) + \int_\Gamma K(x \to y)F^\dagger(y)dy. \tag{2.24}$$

The forcing function for the dual FIESK is the function $g(x)$, which means that random walks for the dual FIESK will start in the region Γ_d where the function $g(x)$ is defined. The kernel of the dual FIESK is the same as the kernel for the original FIESK. However, in the dual FIESK the integration is over final states, which will cause the behavior of the kernel, and thus the random walks, to be different.

With the dual FIESK defined in this way, the inner product from equation 2.15 can now be defined as

$$\begin{aligned}
I &= \int_\Gamma F(x)g(x)dx \\
&= \int_\Gamma F(x)H^\dagger \cdot F^\dagger(x)dx \\
&= \int_\Gamma F^\dagger(x)H \cdot F(x)dx \\
I &= \int_\Gamma F^\dagger(x)S(x)dx.
\end{aligned} \tag{2.25}$$

As equation 2.15 and 2.25 indicate, either the solution to the original FIESK or to the dual FIESK can be used to determine the value I, which is why the two equation are duals. The question of which one to use can be answered by analyzing the functions $g(x)$ and $S(x)$.

In the limiting case where $g(x)$ is a delta function, which will occur when the value of I is desired at a point, only a Monte Carlo random walk process for the dual FIESK, combined with any of the estimators described in the previous section, will be able to estimate I. Conversely, in the limiting case where $S(x)$ is a delta function, only a Monte Carlo random walk process for the original FIESK, combined with any of the estimators described in the previous section, will be able to estimate I. This is because delta functions can be handled easily as source terms by the Monte Carlo random walk process but are very challenging to handle with estimators.

In general, if the portion of the phase space Γ_s, in which the source is non-zero is larger than the portion of the phase space Γ_d, in which the function $g(x)$ is non-zero, the dual problem will be be able to take advantage of estimators with smaller variance, assuming that the dual FIESK has similar properties to the original FIESK*. This is one of the primary motivations for studying the dual problem in this report.

2.5 Chapter Summary

Several points from this chapter must be emphasized before moving on to the next chapter. They are summarized in the following list:

- The FIESK is an important equation with applications in radiation transport problems.
- While the FIESK can be solved analytically using the method of successive approximations, it is more common to solve it numerically using the Monte Carlo random walk process. This is especially true when the system the FIESK describes is complex.
- The Monte Carlo random walk process is governed by a set of PDFs that are derived from the FIESK.

*The properties of the dual FIESK are often much different, as will be shown in chapter 4. In general though, this point is still valid since the probability of random walks entering a larger region will be greater than the probability of random walks entering a smaller region.

- The solution to any FIESK can be estimated using the Monte Carlo random walk process assuming that the PDFs derived from the FIESK have certain necessary properties.
- To estimate the solution of a FIESK in some finite portion of phase space, the termination estimator and the event estimator can be used.
- If an estimation of the solution of a FIESK at a point of the phase space is desired, the Dual FIESK and its associated Monte Carlo random process must be used (unless special estimators are used which will not be discussed in this report).
- More generally, if the size of the source region is larger than the size of the detector region (the region of interest), the Dual FIESK and its associated Monte Carlo random walk process should be used.

Chapter 3

The Monte Carlo Random Walk Process for Radiation Transport

In the previous chapter, the Monte Carlo random walk process was discussed in a very general mathematical sense. In this chapter, it will be shown how to apply the general Monte Carlo random walk process to radiation transport problems. This will require the derivation of the PDFs that govern the random walk process from the transport equation. This derivation will be done in some detail so that each step of the derivation is very clear. The same steps that are shown in this chapter will then be followed in the next chapter to derive the PDFs that govern the random walk process for adjoint radiation transport.

3.1 The Integro-Differential Transport Equation

The equation that describes the average behavior of both photons and neutrons in a medium is the transport equation:

$$\begin{aligned}\frac{1}{\nu}\frac{\partial\varphi(\vec{r},E,\hat{\Omega},t)}{\partial t}+\hat{\Omega}\cdot\vec{\bigtriangledown}\varphi(\vec{r},E,\hat{\Omega},t)+\Sigma_T(\vec{r},E)\varphi(\vec{r},E,\hat{\Omega},t)=\\ S(\vec{r},E,\hat{\Omega},t)+\int\int\Sigma_T(\vec{r},E'\rightarrow E,\hat{\Omega}'\rightarrow\hat{\Omega})\varphi(\vec{r},E',\hat{\Omega}',t)dE'd\hat{\Omega}'\end{aligned} \tag{3.1}$$

where

$$\begin{aligned}\vec{r}&=\text{spacial coordinate}\\ E&=\text{energy}\\ \hat{\Omega}&=\text{flight direction}\\ t&=\text{time}\\ \nu&=\text{speed.}\end{aligned} \tag{3.2}$$

The transport equation only characterizes the average or expected behavior of the radiation in a system. Therefore, the continuous function $\varphi(\vec{r},E,\hat{\Omega},t)$ in equation

3.1 can be interpreted as the expected particle flux at $\vec{r}$ and time t for particles with energy E and direction $\hat{\Omega}$ per unit energy per unit solid angle. The external particle source density is described by the function $S(\vec{r}, E, \hat{\Omega}, t)$. It can be interpreted as the probability per unit time that a particle of energy E will appear at $\vec{r}$ per unit volume per unit energy per unit solid angle. The function $\Sigma_T(\vec{r}, E)$ is the total macroscopic cross section at $\vec{r}$ for particles with energy E. It can be interpreted as the probability of a particle interaction per unit distance of particle travel. The double differential collision cross section is represented by the function $\Sigma_T(\vec{r}, E' \to E, \hat{\Omega}' \to \hat{\Omega})$, which can be interpreted as the total probability per unit distance per unit energy per unit solid angle at $\vec{r}$ for the transfer of a particle with energy E' and direction $\hat{\Omega}'$ to the energy E and direction $\hat{\Omega}$ as a result of a collision. This double differential collision cross section can be expanded into the total macroscopic cross section and a total double differential transfer function. Also note that the total macroscopic cross section is just the sum of all partial macroscopic cross sections [7]:

$$\Sigma_T(\vec{r}, E' \to E, \hat{\Omega}' \to \hat{\Omega}) = \Sigma_T(\vec{r}, E')f(\vec{r}, E' \to E, \hat{\Omega}' \to \hat{\Omega}) \tag{3.3}$$

$$= \sum_i \Sigma_i(\vec{r}, E')c_i(\vec{r}, E')f_i(\vec{r}, E' \to E, \hat{\Omega}' \to \hat{\Omega}). \tag{3.4}$$

Because the transport equation only takes into account average behavior, reactions that result in the emission of additional particles are handled implicitly. The double differential transfer function for each reaction can therefore only describe the average outgoing energy and direction distribution for all particles emitted from the reaction. Some texts on neutron transport normalize the double differential transfer function for each reaction to the number of particles emitted from the reaction [7]. However, to facilitate eventual sampling from these distributions, they will instead be normalized to unity:

$$\int\int f_i(\vec{r}, E' \to E, \hat{\Omega}' \to \hat{\Omega}) dE d\hat{\Omega} = 1 \tag{3.5}$$

The number of particles emitted from reaction i will then be accounted for by the function $c_i(\vec{r}, E')$. For absorption reactions like the (n,γ) and (n,α) neutron reactions and the photoelectric effect for photons, the function $c_i(\vec{r}, E')$ must be set equal to zero. For the elastic and inelastic scattering reactions of neutrons and gamma rays, the function $c_i(\vec{r}, E')$ will be set equal to unity. For the (n,2n) neutron reaction and the pair production photon reaction (neglecting charged particle creation), the function $c_i(\vec{r}, E')$ will be set equal to two. For fission reactions, the function $c_i(\vec{r}, E')$

will be set equal to the average number of neutrons produced by a fission caused by a neutron of energy E', $\nu(\vec{r}, E')$. Based on these definitions for the function $c_i(\vec{r}, E')$ the normalization for the total double differential transfer function can be determined:

$$\int\int \Sigma_T(\vec{r}, E') f(\vec{r}, E' \to E, \hat{\Omega}' \to \hat{\Omega}) dE d\hat{\Omega} = \int\int \sum_i \Sigma_i(\vec{r}, E') c_i(\vec{r}, E') \cdot f_i(\vec{r}, E' \to E, \hat{\Omega}' \to \hat{\Omega}) dE d\hat{\Omega}$$

$$\int\int f(\vec{r}, E' \to E, \hat{\Omega}' \to \hat{\Omega}) dE d\hat{\Omega} = \frac{\sum_i \Sigma_i(\vec{r}, E') c_i(\vec{r}, E')}{\Sigma_T(\vec{r}, E')} = c(\vec{r}, E'). \tag{3.6}$$

The function $c(\vec{r}, E')$ is simply a cross section weighted average of the $c_i(\vec{r}, E')$ functions for each reaction. It can be interpreted as the mean number of particles (of the same type as the primary) emerging per collision at $\vec{r}$ given a particle of energy E'.

While this consolidation of the double differential transfer function for each reaction into a total double differential transfer function is necessary in the context of the transport equation, it is not necessary in a Monte Carlo random walk process. In fact, the creation of a total double differential transfer function that adequately described the behavior of the particle is quite challenging. Instead, one must model each reaction type separately by using the double differential transfer function for an associated reaction.

3.2 The Transport equation in Integral Form

The transport equation is often given in an integro-differential form, as seen in equation 3.1. In order to use the Monte Carlo random walk process that was discussed in the previous chapter, the integro-differential form of the transport equation must be converted to a FIESK. Once it is in the appropriate form the PDFs that govern the random walk process for the radiation type of interest can be determined. Similar derivations to the one that will be shown can also be found in several references [7, 8, 16, 21].

In this report all problems discussed will be assumed to be steady state. Therefore, the time dependence of the transport equation, shown in equation 3.1, will be ignored from here. To further simplify equation 3.1 the right hand side of the

equation will be referred to simply as the emission density $\chi(\vec{r}, E, \hat{\Omega})$:

$$\chi(\vec{r}, E, \hat{\Omega}) = S(\vec{r}, E, \hat{\Omega}) + \int\int \Sigma_T(\vec{r}, E' \to E, \hat{\Omega}' \to \hat{\Omega})\varphi(\vec{r}, E', \hat{\Omega}')dE'd\hat{\Omega}'. \tag{3.7}$$

The simplified transport equation then becomes

$$\hat{\Omega} \cdot \vec{\nabla}\varphi(\vec{r}, E, \hat{\Omega}) + \Sigma_T(\vec{r}, E)\varphi(\vec{r}, E, \hat{\Omega}) = \chi(\vec{r}, E, \hat{\Omega}). \tag{3.8}$$

From the reduced transport equation, the method of characteristics will be used to transform it to its integral form. The characteristic for the transport equation is the line defined by the fixed point $\vec{r}$ and the direction $\hat{\Omega}$. This line can be parameterized by the variable R resulting in the following equation:

$$\vec{r}' = \vec{r} - R\hat{\Omega}. \tag{3.9}$$

Using equation 3.9 a directional derivative along the characteristic can be determined:

$$\begin{aligned} \frac{d}{dR} &= \frac{dx'}{dR}\frac{\partial}{\partial x} + \frac{dy'}{dR}\frac{\partial}{\partial y} + \frac{dz'}{dR}\frac{\partial}{\partial z} \\ &= -\Omega_x\frac{\partial}{\partial x} - \Omega_y\frac{\partial}{\partial y} - \Omega_z\frac{\partial}{\partial z} \\ &= -\hat{\Omega} \cdot \vec{\nabla}. \end{aligned} \tag{3.10}$$

By using this directional derivative along the characteristic the transport equation can be reduced to a first order ordinary differential equation (ODE):

$$-\frac{d}{dR}\varphi(\vec{r}', E, \hat{\Omega}) + \Sigma_T(\vec{r}', E)\varphi(\vec{r}', E, \hat{\Omega}) = \chi(\vec{r}', E, \hat{\Omega}). \tag{3.11}$$

This ODE can be easily solved with the integrating factor

$$\exp\left[-\int_0^R \Sigma_T(\vec{r} - R'\hat{\Omega}, E)dR'\right],$$

as will be shown.

First, the left two terms of equation 3.11 can be combined into a single term using

the integrating factor:

$$-\frac{d}{dR}\left[\varphi(\vec{r}',E,\hat{\Omega})\exp\left[-\int_0^R \Sigma_T(\vec{r}-R'\hat{\Omega},E)dR'\right]\right] = \chi(\vec{r}',E,\hat{\Omega})\exp\left[-\int_0^R \Sigma_T(\vec{r}-R'\hat{\Omega},E)dR'\right]$$

Next, the derivative along the characteristic can be eliminated by integrating from zero to infinity:

$$-\varphi(\vec{r}-R\hat{\Omega},E,\hat{\Omega})\exp\left[-\int_0^R \Sigma_T(\vec{r}-R'\hat{\Omega},E)dR'\right]\Big|_0^\infty = \int_0^\infty \chi(\vec{r}-R\hat{\Omega},E,\hat{\Omega})\exp\left[-\int_0^R \Sigma_T(\vec{r}-R'\hat{\Omega},E)dR'\right]dR.$$

If the flux is assumed to go to zero as R goes to infinity, the integral transport equation is obtained:

$$\varphi(\vec{r},E,\hat{\Omega}) = \int_0^\infty \chi(\vec{r}-R\hat{\Omega},E,\hat{\Omega})\exp\left[-\int_0^R \Sigma_T(\vec{r}-R'\hat{\Omega},E)dR'\right]dR. \tag{3.12}$$

It is often more convenient to represent the integral transport equation as an integral over all space instead of a line integral. To convert equation 3.12 to a volume integral, note that

$$\begin{aligned} R &= |\vec{r}-\vec{r}'|, \\ \hat{\Omega} &= \frac{\vec{r}-\vec{r}'}{|\vec{r}-\vec{r}'|} \text{ and} \\ dV' &= R^2 dR d\hat{\Omega}. \end{aligned} \tag{3.13}$$

With the above definitions, the integral transport equation becomes

$$\varphi(\vec{r},E,\hat{\Omega}) = \int \chi(\vec{r}',E,\hat{\Omega})\exp\left[-\int_0^{|\vec{r}-\vec{r}'|} \Sigma_T(\vec{r}-R'\hat{\Omega},E)dR'\right]\frac{\delta\left(\hat{\Omega}-\left[\frac{\vec{r}-\vec{r}'}{|\vec{r}-\vec{r}'|}\right]\right)}{|\vec{r}-\vec{r}'|^2}dV'.$$

To further simplify the integral transport equation, one more function will be introduced:

$$\tau(\vec{r}',\vec{r},E,\hat{\Omega}) = \exp\left[-\int_0^{|\vec{r}-\vec{r}'|} \Sigma_T(\vec{r}-R'\hat{\Omega},E)dR'\right]\frac{\delta\left(\Omega-\left[\frac{\vec{r}-\vec{r}'}{|\vec{r}-\vec{r}'|}\right]\right)}{|\vec{r}-\vec{r}'|^2}. \tag{3.14}$$

The simplified integral transport equation is now simply

$$\varphi(\vec{r}, E, \hat{\Omega}) = \int \chi(\vec{r}', E, \hat{\Omega}) \tau(\vec{r}', \vec{r}, E, \hat{\Omega}) dV'. \tag{3.15}$$

With the transport equation now in an integral form, only minor manipulations are needed in order to turn it into a FIESK.

3.3 The Flux FIESK

To derive the flux FIESK, the emission density defined in equation 3.7 will be substituted back into the integral transport equation shown in equation 3.15:

$$\begin{aligned}
\varphi(\vec{r}, E, \hat{\Omega}) = & \int \left[S(\vec{r}', E, \hat{\Omega}) + \int\int \Sigma_T(\vec{r}', E' \to E, \hat{\Omega}' \to \hat{\Omega}) \varphi(\vec{r}', E', \hat{\Omega}') dE' d\hat{\Omega}' \right] \\
& \cdot \tau(\vec{r}', \vec{r}, E, \hat{\Omega}) dV' \\
\varphi(\vec{r}, E, \hat{\Omega}) = & \int S(\vec{r}', E, \hat{\Omega}) \tau(\vec{r}', \vec{r}, E, \hat{\Omega}) dV' + \\
& \int\int\int \tau(\vec{r}', \vec{r}, E, \hat{\Omega}) \Sigma_T(\vec{r}', E' \to E, \hat{\Omega}' \to \hat{\Omega}) \varphi(\vec{r}', E', \hat{\Omega}') dE' d\hat{\Omega}' dV'.
\end{aligned} \tag{3.16}$$

Since equation 3.16 is a FIESK that describes the flux, a random walk process can be created to simulate the flux. The source PDF will be created first (using the same notation from the previous chapter):

$$p^1(\vec{r}, E, \hat{\Omega}) = \frac{\int S(\vec{r}', E, \hat{\Omega}) \tau(\vec{r}', \vec{r}, E, \hat{\Omega}) dV'}{\int\int S(\vec{r}', E, \hat{\Omega}) \tau(\vec{r}', \vec{r}, E, \hat{\Omega}) dV' dV dE d\hat{\Omega}}. \tag{3.17}$$

The state transition PDF can be broken into two parts; one part will govern the movement of the particle through space and the other part will govern the movement of the particle through energy and direction:

$$\begin{aligned}
p(y \to x) &= p(\vec{r}' \to \vec{r}, E' \to E, \hat{\Omega}' \to \hat{\Omega}) \\
&= p(\vec{r}' \to \vec{r} \quad | E, \hat{\Omega}) p(E' \to E, \hat{\Omega}' \to \hat{\Omega} \quad | \vec{r}').
\end{aligned} \tag{3.18}$$

The PDF that governs the movement through space is simply the function

$\tau(\vec{r}', \vec{r}, E, \hat{\Omega})$ defined in equation 3.14 normalized to unity:

$$p(\vec{r}' \rightarrow \vec{r} \quad | E, \hat{\Omega}) = \frac{\tau(\vec{r}', \vec{r}, E, \hat{\Omega})}{w_1(\vec{r}', E, \hat{\Omega})}, \tag{3.19}$$

where

$$w_1(\vec{r}', E, \hat{\Omega}) = \int \tau(\vec{r}', \vec{r}, E, \hat{\Omega}) dV. \tag{3.20}$$

The random walk process that would correspond to the flux FIESK has many disadvantages. First, during the random walk process the weight of the particle after every collision will be multiplied by the factor w_1. Unfortunately, this factor is not bounded to the interval $(0, 1)$ and will likely increase the variance of the estimator used [5]. Another disadvantage of this random walk process comes about from the conditional state transition PDF $p(\vec{r}' \rightarrow \vec{r} \quad | E, \hat{\Omega})$. Because this PDF does not contain the factor $\Sigma_T(\vec{r}, E)$, it is possible to sample an event position in a vacuum. This peculiar property is due to the fact that the flux does not go to zero in a vacuum. The final disadvantage is that sampling from the source would be very challenging given that the source is defined as an integral which is difficult to evaluate in general.

The Monte Carlo random walk process for estimating the flux directly is not ideal and in practice is rarely done. An event density should have a preferable random walk process because at the very least, the event density goes to zero in a vacuum.

3.4 The Emission Density FIESK

A FIESK will now be constructed for the emission density. To construct the flux FIESK, the emission density given in equation 3.7 was substituted into the integral transport equation shown in equation 3.15. To construct the emission density FIESK, the opposite will be done.

$$\begin{aligned}\chi(\vec{r}, E, \hat{\Omega}) &= S(\vec{r}, E, \hat{\Omega}) + \int\int \Sigma_T(\vec{r}, E' \rightarrow E, \hat{\Omega}' \rightarrow \hat{\Omega}) \int \chi(\vec{r}', E', \hat{\Omega}') \tau(\vec{r}', \vec{r}, E', \hat{\Omega}') dV' dE' d\hat{\Omega}' \\ &= S(\vec{r}, E, \hat{\Omega}) + \int\int\int \frac{\Sigma_T(\vec{r}, E' \rightarrow E, \hat{\Omega}' \rightarrow \hat{\Omega})}{\Sigma_T(\vec{r}, E')} \Sigma_T(\vec{r}, E') \tau(\vec{r}', \vec{r}, E', \hat{\Omega}') \\ &\qquad \cdot \chi(\vec{r}', E', \hat{\Omega}') dV' dE' d\hat{\Omega}'\end{aligned}$$

Two kernels must now be introduced to simplify the emission density FIESK.

The first will be called the collision kernel and is defined as

$$\begin{aligned} C(\vec{r}, E' \to E, \hat{\Omega}' \to \hat{\Omega}) &= \frac{\Sigma_T(\vec{r}, E' \to E, \hat{\Omega}' \to \hat{\Omega})}{\Sigma_T(\vec{r}, E')} \\ &= f(\vec{r}, E' \to E, \hat{\Omega}' \to \hat{\Omega}) \end{aligned} \tag{3.21}$$

Note that the collision kernel is simply the total double differential transfer function that was discussed in section 3.1. The second kernel will be called the transport kernel and is defined as

$$\begin{aligned} T(\vec{r}' \to \vec{r}, E, \hat{\Omega}) &= \Sigma_T(\vec{r}, E)\tau(\vec{r}', \vec{r}, E, \hat{\Omega}) \\ &= \Sigma_T(\vec{r}, E) \exp\left[-\int_0^{|\vec{r}-\vec{r}'|} \Sigma_T(\vec{r} - R'\hat{\Omega}, E) dR'\right] \frac{\delta\left(\hat{\Omega} - \left[\frac{\vec{r}-\vec{r}'}{|\vec{r}-\vec{r}'|}\right]\right)}{|\vec{r} - \vec{r}'|^2}. \end{aligned} \tag{3.22}$$

Note that the quantity $T(\vec{r}' \to \vec{r}, E, \hat{\Omega})dV$ can be interpreted as the probability that a particle at $\vec{r}'$ with energy E and direction $\hat{\Omega}$ will have its next collision in volume element dV at $\vec{r}$.

Using the above kernels, the simplified emission density FIESK becomes

$$\begin{aligned} \chi(\vec{r}, E, \hat{\Omega}) = S(\vec{r}, E, \hat{\Omega}) + \int\int\int C(\vec{r}, E' \to E, \hat{\Omega}' \to \hat{\Omega}) T(\vec{r}' \to \vec{r}, E', \hat{\Omega}') \\ \cdot \chi(\vec{r}', E', \hat{\Omega}') dV' dE' d\hat{\Omega}'. \end{aligned} \tag{3.23}$$

The state transition kernel for the emission density FIESK is simply

$$\begin{aligned} K(y \to x) &= K(\vec{r}' \to \vec{r}, E' \to E, \hat{\Omega}' \to \hat{\Omega}) \\ &= C(\vec{r}, E' \to E, \hat{\Omega}' \to \hat{\Omega}) T(\vec{r}' \to \vec{r}, E', \hat{\Omega}'). \end{aligned} \tag{3.24}$$

3.5 The Collision Density FIESK

Up to this point, only the flux and the emission density have been discussed. However, there is another quantity that can be very useful: the collision density. It is

related to the flux and the emission density by the following equations:

$$\psi(\vec{r}, E, \hat{\Omega}) = \Sigma_T(\vec{r}, E)\varphi(\vec{r}, E, \hat{\Omega}) \tag{3.25}$$

$$= \int T(\vec{r}' \rightarrow \vec{r}, E, \hat{\Omega})\chi(\vec{r}', E, \hat{\Omega})dV'. \tag{3.26}$$

The kernel $T(\vec{r}' \rightarrow \vec{r}, E, \hat{\Omega})$ is the transport kernel that was defined in equation 3.22. Whereas the emission density is the expected density of particles exiting a collision or the source, the collision density is the expected density of particles entering a collision.

To construct the collision density FIESK, equation 3.26 and the emission density FIESK given in equation 3.23 will be used:

$$\psi(\vec{r}, E, \hat{\Omega}) = \int S(\vec{r}', E, \hat{\Omega})T(\vec{r}' \rightarrow \vec{r}, E, \hat{\Omega})dV' + \iiint T(\vec{r}' \rightarrow \vec{r}, E, \hat{\Omega})C(\vec{r}', E' \rightarrow E, \hat{\Omega}' \rightarrow \hat{\Omega})\psi(\vec{r}', E', \hat{\Omega}')dE'd\hat{\Omega}'dV'. \tag{3.27}$$

Notice that the source term for the collision density FIESK is the first collided source.

The state transition kernel for the collision density FIESK is simply

$$L(y \rightarrow x) = L(\vec{r}' \rightarrow \vec{r}, E' \rightarrow E, \hat{\Omega}' \rightarrow \hat{\Omega})$$

$$= T(\vec{r}' \rightarrow \vec{r}, E, \hat{\Omega})C(\vec{r}', E' \rightarrow E, \hat{\Omega}' \rightarrow \hat{\Omega}). \tag{3.28}$$

3.6 Emission and Collision Density State Transition Kernel Properties

Before the PDFs that govern the random walk process for the emission and collision densities are derived, the transport and collision kernels must be investigated a bit

further. First, note that for an infinite medium the transport kernel is normalized:

$$\begin{aligned}\int T(\vec{r}^{\,'} \to \vec{r}, E, \hat{\Omega})dV &= \int \Sigma_T(\vec{r}, E) \cdot exp\Big[-\int_0^{|\vec{r}-\vec{r}^{\,'}|} \Sigma_T(\vec{r} - R^{'}\hat{\Omega}, E)dR^{'}\Big] \frac{\delta\left(\Omega - \left[\frac{\vec{r}-\vec{r}^{\,'}}{|\vec{r}-\vec{r}^{\,'}|}\right]\right)}{|\vec{r}-\vec{r}^{\,'}|^2} dV \\ &= \int_0^{\infty} \Sigma_T(\vec{r}^{\,'} + R\hat{\Omega}, E) \cdot exp\left[-\int_0^{R} \Sigma_T(\vec{r}^{\,'} + R^{''}\hat{\Omega}, E)dR^{''}\right] dR \\ &= -\int_0^{\infty} \frac{d}{dR} exp\left[-\int_0^{R} \Sigma_T(\vec{r}^{\,'} + R^{''}\hat{\Omega}, E)dR^{''}\right] dR \\ &= 1.\end{aligned}$$

However, if the domain of interest in a problem is finite, the transport kernel will no longer be normalized. Fortunately, this is taken care of by terminating random walks that exit the domain of interest, which is equivalent to surrounding the domain of interest with a purely absorbing medium of infinite extent [21].

The collision kernel, being equal to the total double differential transfer probability, has the following property:

$$\int\int C(\vec{r}, E^{'} \to E, \hat{\Omega}^{'} \to \hat{\Omega})dEd\hat{\Omega} = c(\vec{r}, E^{'}), \tag{3.29}$$

where $c(\vec{r}, E^{'})$ is the mean number of particles emitted per collision at $\vec{r}$ given a particle of energy $E^{'}$. In regions where no multiplying reactions occur, the collision kernel has the following, more familiar property:

$$\begin{aligned}\int\int C(\vec{r}, E^{'} \to E, \hat{\Omega}^{'} \to \hat{\Omega})dEd\hat{\Omega} &= \frac{\Sigma_s(\vec{r}, E^{'})}{\Sigma_T(\vec{r}, E^{'})} \\ &= P_{NA}(\vec{r}, E^{'}).\end{aligned} \tag{3.30}$$

The macroscopic cross section $\Sigma_s(\vec{r}, E^{'})$ is the total macroscopic scattering cross section. The ratio of the total macroscopic scattering cross section and the total macroscopic cross section is often referred to as the non-absorption or survival probability, $P_{NA}(\vec{r}, E)$.

Based on these properties of the transport and collision kernels, the emission density state transition kernel normalization can be determined. If multiplying

reactions are possible in a region, the normalization is the following:

$$\begin{aligned}\int K(y \to x)dx &= \int\int\int C(\vec{r}, E' \to E, \hat{\Omega}' \to \hat{\Omega})T(\vec{r}' \to \vec{r}, E', \hat{\Omega}')dEd\hat{\Omega}dV \\ &= \int c(\vec{r}, E')T(\vec{r}' \to \vec{r}, E', \hat{\Omega}')dV \\ &= \bar{c}(\vec{r}', E'). \end{aligned} \tag{3.31}$$

The normalization function $\bar{c}(\vec{r}', E')$ can be interpreted as an average of the mean number of particles emerging per collision along the line from $\vec{r}'$ to $\vec{r}$ given a particle of energy E'. If multiplying reactions are not possible in a region, the normalization is instead

$$\begin{aligned}\int K(y \to x)dx &= \int\int\int C(\vec{r}, E' \to E, \hat{\Omega}' \to \hat{\Omega})T(\vec{r}' \to \vec{r}, E', \hat{\Omega}')dEd\hat{\Omega}dV \\ &= \int P_{NA}(\vec{r}, E')T(\vec{r}' \to \vec{r}, E', \hat{\Omega}')dV \\ &= \overline{P}_{NA}(\vec{r}', E'). \end{aligned} \tag{3.32}$$

The normalization function $\overline{P}_{NA}(\vec{r}', E')$ can be interpreted as the average survival probability along the line from $\vec{r}'$ to $\vec{r}$ given a particle of energy E'.

The collision density state transition kernel normalization can also be determined with the properties of the transport and collision kernels that were discussed. If multiplying reactions are possible in a region, the normalization is

$$\begin{aligned}\int L(y \to x)dx &= \int\int\int T(\vec{r}' \to \vec{r}, E, \hat{\Omega})C(\vec{r}', E' \to E, \hat{\Omega}' \to \hat{\Omega})dVdEd\hat{\Omega} \\ &= \int\int C(\vec{r}', E' \to E, \hat{\Omega}' \to \hat{\Omega})dEd\hat{\Omega} \\ &= c(\vec{r}', E'). \end{aligned} \tag{3.33}$$

In regions where multiplying reactions are not possible, the normalization is instead

$$\begin{aligned}\int L(y \to x)dx &= \int\int\int T(\vec{r}' \to \vec{r}, E, \hat{\Omega})C(\vec{r}', E' \to E, \hat{\Omega}' \to \hat{\Omega})dVdEd\hat{\Omega} \\ &= \int\int C(\vec{r}', E' \to E, \hat{\Omega}' \to \hat{\Omega})dEd\hat{\Omega} \\ &= P_{NA}(\vec{r}', E'). \end{aligned} \tag{3.34}$$

The properties of the two state transition kernels are summarized below:

1. $K(y \to x) > 0$
   $L(y \to x) > 0$

   and

2. $\int K(y \to x)dx = \bar{c}(y) >= \overline{P}_{NA}(y)$
   $\int L(y \to x)dx = c(y) >= P_{NA}(y).$

In section 2.2, where the necessary properties of the random walk PDFs where enumerated, it was stated that the state transition PDF integrated over final states must be equal to the survival probability in the initial state:

$$\int_{\Gamma} p(y \to x)dx = q(y) = 1 - p(y)$$

The state transition kernel for the emission density and the collision density will only have this property when multiplying reactions aren't possible. When multiplying reactions are possible, the emission density state transition kernel will have to be multiplied by the factor

$$\frac{\overline{P}_{NA}(y)}{\bar{c}(y)},$$

and the collision density state transition kernel will have to be multiplied by the factor

$$\frac{P_{NA}(y)}{c(y)}.$$

Due to these factors, it would appear that conducting an analogue random walk process for radiation transport without using weights is impossible in a system where multiplying reactions are possible. This is indeed true if particle multiplication is handled implicitly. However, if particle multiplication is handled explicitly, with separate random walks conducted for each additional particle emitted, an analogue random walk process can be conducted without using weights. To handle particle multiplication explicitly, the collision kernel must be expanded into its constituent parts, which will be shown in the next section.

3.7 Expansion of the Collision Kernel

As mentioned in the previous sections, to treat particle multiplication explicitly, the collision kernel must be expanded:

$$\begin{aligned} C(\vec{r}, E' \to E, \hat{\Omega}' \to \hat{\Omega}) &= \frac{\Sigma_T(\vec{r}, E' \to E, \hat{\Omega}' \to \hat{\Omega})}{\Sigma_T(\vec{r}, E')} \\ &= f(\vec{r}, E' \to E, \hat{\Omega}' \to \hat{\Omega}) \\ &= \sum_j \frac{\Sigma_j(\vec{r}, E') c_i(\vec{r}, E') f_i(\vec{r}, E' \to E, \hat{\Omega}' \to \hat{\Omega})}{\Sigma_T(\vec{r}, E')} \\ &= \sum_A \frac{\Sigma_A(\vec{r}, E')}{\Sigma_T(\vec{r}, E')} \sum_j \frac{\sigma_{A,j}(E')}{\sigma_A(E')} c_{A,j}(E') p_{A,j}(E' \to E, \hat{\Omega}' \to \hat{\Omega}) \\ &= \sum_A p_A(\vec{r}, E') \sum_j p_{A,j}(E') \sum_{k=1}^{2} p_{A,j,k}(E') \\ &\qquad \cdot \sum_{l=1}^{x_k} p_{A,j,l}(E' \to E, \hat{\Omega}' \to \hat{\Omega}). \end{aligned} \tag{3.35}$$

In this expansion, the subscript A denotes a particular nuclide or element, the subscript j denotes a particular type of reaction and the subscript l denotes a particular emitted particle. The function $p_{A,j,l}(E' \to E, \hat{\Omega}' \to \hat{\Omega})$ is the double differential transfer probability for the initial particle and emitted particle l given a collision of type j on nuclide or element A. This transfer probability is normalized to unity. Since it is desired to conduct separate random walks for each emitted particle, only an integer number of particles can be emitted from a collision*. The probabilities $p_{A,j,k}(E')$ restrict the number of particles emitted to integer values. They are defined as follows along with the corresponding value of x_k:

$$p_{A,j,1} = \begin{cases} \lceil c_{A,j}(E') \rceil - c_{A,j}(E') & \text{if } c_{A,j}(E') \text{ not an integer} \\ 1 & \text{otherwise} \end{cases} \tag{3.36}$$

$$p_{A,j,2} = 1 - p_{A,j,1} \tag{3.37}$$

*The average number of particles emitted from fission will normally be a non-integer value

and

$$x_1 = \begin{cases} \lfloor c_{A,j}(E') \rfloor & \text{if } c_{A,j}(E') \text{ not an integer} \\ c_{A,j}(E') & \text{otherwise} \end{cases} \tag{3.38}$$

$$x_2 = \lceil c_{A,j}(E') \rceil. \tag{3.39}$$

The expected value of the number of emitted particles, based on these probabilities and corresponding number of emitted particles, is $c_{A,j}(E')$ as required by the definition of the collision kernel.

By sampling from the collision kernel in its expanded form, particle multiplication will be treated explicitly. In this process of sampling from the expanded collision kernel one first samples the nuclide or element hit from the discrete PDF

$$\begin{aligned} p(A|\vec{r}, E') &= \sum_A p_A(\vec{r}, E') \\ &= \sum_A \frac{\Sigma_A(\vec{r}, E')}{\Sigma_T(\vec{r}, E')}. \end{aligned} \tag{3.40}$$

With the nuclide or element A selected, the reaction type is sampled from the discrete PDF

$$\begin{aligned} p(j|A, E') &= \sum_j p_{A,j}(E') \\ &= \sum_j \frac{\sigma_{A,j}(E')}{\sigma_A(E')} \end{aligned} \tag{3.41}$$

The number of particles emitted from the collision is then sampled from the discrete PDF

$$p(x_k|E') = \sum_k p_{A,j,k}(E'). \tag{3.42}$$

Finally, for each emitted particle l, the outgoing energy and direction is sampled from the transfer probability $p_{A,j,l}(E' \to E, \hat{\Omega}' \to \hat{\Omega})$.

In the sampling of the reaction type, if an absorption reaction is chosen, the random walk for the current particle ends. Therefore, at every collision, a random walk will end with probability

$$\frac{\Sigma_A(\vec{r}, E)}{\Sigma_T(\vec{r}, E)}.$$

This behavior mimics the behavior that was described in the random walk process

from the previous chapter. Instead of separately sampling whether a random walk ends, it is now incorporated into the sampling of a new particle state.

3.8 The Emission and Collision Density Random Walk PDFs

With the state transition kernels $K(y \to x)$ and $L(y \to x)$ fully characterized, the Monte Carlo random walk process for radiation transport can be completely specified:

$$\chi(x) \text{ Random Walk (implicit mult.):} \begin{cases} p^1(x) & = \frac{S(x)}{\int_\Gamma S(x)dx} \\ p(y \to x) & = \frac{\overline{P}_{NA}(y)}{\bar{c}(y)} K(y \to x) \\ p(x) & = 1 - \overline{P}_{NA}(x), \end{cases} \tag{3.43}$$

$$\psi(x) \text{ Random Walk (implicit mult.):} \begin{cases} p^1(x) & = \frac{S_c(x)}{\int_\Gamma S_c(x)dx} \\ p(y \to x) & = \frac{P_{NA}(y)}{c(y)} L(y \to x) \\ p(x) & = 1 - P_{NA}(x) \end{cases} \tag{3.44}$$

and

$$\chi(x) \text{ Random Walk (explicit mult.):} \begin{cases} p^1(x) & = \frac{S(x)}{\int_\Gamma S(x)dx} \\ p(y \to x) & = K(y \to x) \\ p(x) & = 1 - \overline{P}_{NA}(x), \end{cases} \tag{3.45}$$

$$\psi(x) \text{ Random Walk (explicit mult.):} \begin{cases} p^1(x) & = \frac{S_c(x)}{\int_\Gamma S_c(x)dx} \\ p(y \to x) & = L(y \to x) \\ p(x) & = 1 - P_{NA}(x). \end{cases} \tag{3.46}$$

Note that the function $S_c(x)$ is simply the first collided source, which was shown in equation 3.27. The first set of processes is for treating multiplication implicitly*. The second set is for treating multiplication explicitly using the procedure outlined in the previous section. In the second set of processes, the termination probabilities

*It must be noted that the random walk procedures that treat multiplication implicitly will never be used. This is because they rely on the total transfer probability, which is challenging to obtain and even more challenging to sample from directly. However, they are shown to provide continuity between this chapter and the previous chapter.

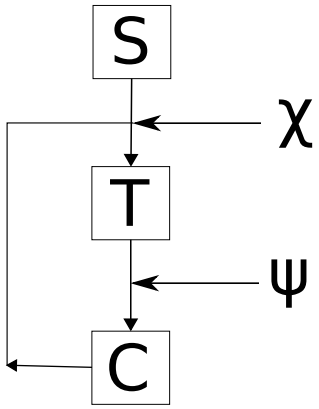

Figure 3.1: **Monte Carlo random walk procedure for radiation.** *A particle state is first sampled from the source distribution. The next collision point is sampled from the transport kernel T. Finally, the new particle energy and direction is sampled from the collision kernel, assuming that an absorption reaction wasn't sampled. If an absorption reaction was sampled, the random walk ends. Otherwise, the process continues. This procedure allows both the emission density and the collision density to be estimated.*

aren't sampled directly. Instead, a random walk can potentially be terminated when sampling from $p(y \to x)$.

While it might appear from the above PDFs that the random walk processes for the emission and collision density are completely different, because the kernels $K(y \to x)$ and $L(y \to x)$ only differ in the ordering of the collision and transport kernels and because of the relationship between the emission density and the collision density, both can be estimated during the same random walk process. Figure 3.1 illustrates the new combined random walk process. In this new process, particles always start in the true source and not the first collided source, which is advantageous because the first collided source would be challenging to evaluate in general. The emission density will always be estimated right after a collision (or birth) and the collision density will always be estimated right before a collision.

A common modification to the previous analogue random walk processes is to ignore absorption and instead use weights to account for the absorption probability.

This modification results in the following non-analogue random walk processes.

$$\chi(x) \text{ Random Walk (implicit mult.):} \begin{cases} p^1(x) & = \frac{S(x)}{\int_\Gamma S(x)dx} \\ p(y \to x) & = \frac{K(y \to x)}{\bar{c}(y)} \\ p(x) & = 0 \end{cases} \tag{3.47}$$

$$\psi(x) \text{ Random Walk (implicit mult.):} \begin{cases} p^1(x) & = \frac{S_c(x)}{\int_\Gamma S_c(x)dx} \\ p(y \to x) & = \frac{L(y \to x)}{c(y)} \\ p(x) & = 0 \end{cases} \tag{3.48}$$

$$\chi(x) \text{ Random Walk (explicit mult.):} \begin{cases} p^1(x) & = \frac{S(x)}{\int_\Gamma S(x)dx} \\ p(y \to x) & = \frac{K(y \to x)}{\bar{P}_{NA}(y)} \\ p(x) & = 0 \end{cases} \tag{3.49}$$

$$\psi(x) \text{ Random Walk (explicit mult.):} \begin{cases} p^1(x) & = \frac{S_c(x)}{\int_\Gamma S_c(x)dx} \\ p(y \to x) & = \frac{L(y \to x)}{P_{NA}(y)} \\ p(x) & = 0 \end{cases} \tag{3.50}$$

Russian roulette will have to be used with these random walk processes to force random walks to terminate when the particle weight becomes too small [5].

3.9 Estimating Responses

In typical radiation transport problems, the inner product of some function $a(\vec{r}, E, \hat{\Omega})$ and the flux $\varphi(\vec{r}, E, \hat{\Omega})$ is desired. If the function $a(\vec{r}, E, \hat{\Omega})$ is a cross section, the inner product that is calculated is often called a material response or reaction rate. Because it is challenging to estimate the flux directly using a Monte Carlo random walk procedure, equivalent inner products must be constructed that are either in terms of the collision density or the emission density:

$$I = \int\int\int a(\vec{r}, E, \hat{\Omega})\varphi(\vec{r}, E, \hat{\Omega})dVdEd\hat{\Omega} \tag{3.51}$$

$$= \int\int\int b(\vec{r}, E, \hat{\Omega})\psi(\vec{r}, E, \hat{\Omega})dVdEd\hat{\Omega} \tag{3.52}$$

$$= \int\int\int c(\vec{r}, E, \hat{\Omega})\chi(\vec{r}, E, \hat{\Omega})dVdEd\hat{\Omega}. \tag{3.53}$$

Based on the relationship between the collision density and the flux, $b(\vec{r}, E, \hat{\Omega})$ must be defined as

$$b(\vec{r}, E, \hat{\Omega}) = \frac{a(\vec{r}, E, \hat{\Omega})}{\Sigma_T(\vec{r}, E)}, \tag{3.54}$$

where $\Sigma_T(\vec{r}, E)$ is the total cross section. Similarly, the function $c(\vec{r}, E, \hat{\Omega})$ must be defined as

$$c(\vec{r}, E, \hat{\Omega}) = \int \frac{a(\vec{r}', E, \hat{\Omega})}{\Sigma_T(\vec{r}', E)} T(\vec{r} \to \vec{r}', E, \Omega) dV'. \tag{3.55}$$

Clearly, the function $b(\vec{r}, E, \hat{\Omega})$ will be easier to evaluate than the function $c(\vec{r}, E, \hat{\Omega})$. Using either of the estimators that were described in chapter 2 and the combined random walk process that was outlined in the previous section, an estimate for the value of I can be obtained.

In addition to the two estimators that were described in chapter 2, there is another estimator that can be used when dealing with the transport equation: the track-length estimator. The track-length estimator is very useful because it accumulates information every time a particle history passes through the region of interest. A derivation of this estimator, which is a limiting case of the event estimator, can be found in the work by Spanier and Gelbard [5]. If the function $a(\vec{r}, E, \hat{\Omega})$ is assumed to have the following form,

$$a(\vec{r}, E, \hat{\Omega}) = \begin{cases} f(\vec{r}, E, \hat{\Omega}) & \text{if } \vec{r} \in V_d \\ 0 & \text{otherwise,} \end{cases}$$

the track length estimator can be defined as

$$\eta^*(\alpha) = \sum_m W_m(\alpha) f_m d_m. \tag{3.56}$$

The variable α is used to represent all states of the random walk, as was done in section 2.3. The function $W_m(\alpha)$ defines the accumulated weight of the random walk up to the m^{th} event. This function also appeared in equation 2.18 for the event estimator. The value d_m is simply the length of the m^{th} particle track in the volume V_d. The value f_m is the value of the function $f(\vec{r}, E, \hat{\Omega})$ along the m^{th} particle track.

3.10 Chapter Summary

Before moving on to the next chapter, several points from this chapter must be emphasized:

- By performing a series of manipulations on the integro-differential form of the transport equation, a FIESK can be created that describes the flux, the emission density or the collision density of a system.
- The FIESK that describes the flux has several unfavorable properties that make the Monte Carlo random walk process challenging to conduct. In practice the flux FIESK and its associated random walk process are rarely used.
- The state transition kernels that appear in the emission density FIESK and the collision density FIESK can be decomposed into two constituent kernels: the collision kernel, which describes the movement of particles through energy and direction, and the transport kernel, which describes the movement of particles through space.
- Further, the collision kernel can be decomposed into its constituent reactions. If particle multiplication is treated explicitly this must be done.
- Due to the similarity between the emission density FIESK and the collision density FIESK, solutions to both FIESKs can be estimated using the same random walk process.
- Material responses are usually calculated from the inner product of the flux and a material response function. The emission density or collision density can be used instead of the flux if a modified material response function is used.

Chapter 4

The Monte Carlo Random Walk Process for Adjoint Radiation Transport

In section 2.4 the dual FIESK was introduced as a way to estimate the value of interest, which for radiation transport problems is defined in equation 3.51, at a point. In this chapter the dual emission density FIESK will be shown. In addition, more general PDFs that govern the random walk process for adjoint radiation will be derived. The same steps that were outlined in the previous chapter will be followed to derive these PDFs.

4.1 The Dual Emission Density FIESK

Using the procedure outlined in section 2.4, the dual emission density FIESK will be constructed. The function that will solve this dual equation will be called the *adjoint of the emission density*. It is not called the adjoint emission density because, as will be shown, the *adjoint of the emission density* does not behave like an emission density (or in general an event density). First, a linear operator will be constructed from equation 3.23, which is the emission density FIESK:

$$\begin{aligned} H_\chi \cdot \chi(\vec{r}, E, \hat{\Omega}) = \chi(\vec{r}, E, \hat{\Omega}) - \\ \iiint C(\vec{r}, E' \to E, \hat{\Omega}' \to \hat{\Omega}) T(\vec{r}' \to \vec{r}, E', \hat{\Omega}') \chi(\vec{r}', E', \hat{\Omega}') dV' dE' E \hat{\Omega}'. \end{aligned} \tag{4.1}$$

With the operator H_χ defined in this way it is clear from equation 3.23 that

$$H_\chi \cdot \chi(\vec{r}, E, \hat{\Omega}) = S(\vec{r}, E, \hat{\Omega}). \tag{4.2}$$

To define the adjoint operator, the following equality must hold:

$$\langle \chi^\dagger H_\chi \cdot \chi \rangle = \langle \chi H_\chi^\dagger \cdot \chi^\dagger \rangle.$$

The brackets indicate integration over all phase space. The function $\chi^\dagger(\vec{r}, E, \hat{\Omega})$ is the *adjoint of the emission density*. Since the operator H_χ is known, the left bracket

will be expanded:

$$\langle \chi^{\dagger} H_{\chi} \cdot \chi \rangle = \int\int\int \chi^{\dagger}(\vec{r}, E, \hat{\Omega}) \chi(\vec{r}, E, \hat{\Omega}) dV dE d\hat{\Omega} - \int\int\int \chi^{\dagger}(\vec{r}, E, \hat{\Omega})$$
$$\cdot \int\int\int C(\vec{r}, E' \to E, \hat{\Omega}' \to \hat{\Omega}') T(\vec{r}' \to \vec{r}, E', \hat{\Omega}') \chi(\vec{r}', E', \hat{\Omega}') dV' dE' d\hat{\Omega}' dV dE d\hat{\Omega}$$
$$= \int\int\int \chi^{\dagger}(\vec{r}, E, \hat{\Omega}) \chi(\vec{r}, E, \hat{\Omega}) dV dE d\hat{\Omega} - \int\int\int \chi(\vec{r}', E', \hat{\Omega}')$$
$$\cdot \int\int\int C(\vec{r}, E' \to E, \hat{\Omega}' \to \hat{\Omega}') T(\vec{r}' \to \vec{r}, E', \hat{\Omega}') \chi^{\dagger}(\vec{r}, E, \hat{\Omega}) dV dE d\hat{\Omega} dV' dE' d\hat{\Omega}'.$$

From this last manipulation, the adjoint operator can be deduced:

$$H_{\chi}^{\dagger} \cdot \chi^{\dagger}(\vec{r}, E, \hat{\Omega}) = \chi^{\dagger}(\vec{r}, E, \hat{\Omega}) -$$
$$\int\int\int T(\vec{r} \to \vec{r}', E, \hat{\Omega}) C(\vec{r}', E \to E', \hat{\Omega} \to \hat{\Omega}') \chi(\vec{r}', E', \hat{\Omega}') dE' d\hat{\Omega}' dV'. \tag{4.3}$$

In the previous chapter, the function $c(\vec{r}, E, \hat{\Omega})$ was defined in equation 3.55, which should be used with the emission density to calculate a response. By forcing the adjoint operator acting on the *adjoint of the emission density* to equal the function $c(\vec{r}, E, \hat{\Omega})$, the dual emission density FIESK can be created:

$$\chi^{\dagger}(\vec{r}, E, \hat{\Omega}) = c(\vec{r}, E, \hat{\Omega}) +$$
$$\int\int\int T(\vec{r} \to \vec{r}', E, \hat{\Omega}) C(\vec{r}', E \to E', \hat{\Omega} \to \hat{\Omega}') \chi^{\dagger}(\vec{r}', E', \hat{\Omega}') dE' d\hat{\Omega}' dV'. \tag{4.4}$$

Unfortunately, in the integral in equation 4.4, the transport and collision kernels are integrated over what were previously the final states. Therefore, the properties that were defined for these kernels in the previous chapter are no longer valid. In particular, the transport kernel is not normalized anymore and the collision kernel does not integrate to the the average number of particles emitted from a collision. To renormalize these kernels, the $\Sigma_T(\vec{r}', E)$ terms in both the transport and collision kernels will be allowed to cancel each other out. The modified transport kernel will now be examined:

$$\frac{T(\vec{r} \to \vec{r}', E, \hat{\Omega})}{\Sigma_T(\vec{r}', E)} = \exp\left[-\int_0^{|\vec{r}' - \vec{r}|} \Sigma_T(\vec{r}' - R'\hat{\Omega}, E) dR' \right] \frac{\delta\left(\hat{\Omega} - \left[\frac{\vec{r}' - \vec{r}}{|\vec{r}' - \vec{r}|}\right]\right)}{|\vec{r}'' - \vec{r}|^2}. \tag{4.5}$$

Based on the argument of the delta function,

$$\hat{\Omega} = \frac{\vec{r}' - \vec{r}}{|\vec{r}' - \vec{r}|}$$
$$\text{and}$$
$$\vec{r}' = \vec{r} + \hat{\Omega}|\vec{r}' - \vec{r}|. \tag{4.6}$$

This equation for $\vec{r}'$ can be substituted back into the equation 4.5:

$$\frac{T(\vec{r} \to \vec{r}', E, \hat{\Omega})}{\Sigma_T(\vec{r}', E)} = \exp\left[-\int_0^{|\vec{r}'-\vec{r}|} \Sigma_T\left(\vec{r} + \left[|\vec{r}' - \vec{r}| - R'\right]\hat{\Omega}, E\right) dR'\right] \frac{\delta\left(\hat{\Omega} - \left[\frac{\vec{r}'-\vec{r}}{|\vec{r}'-\vec{r}|}\right]\right)}{|\vec{r}' - \vec{r}|^2}.$$

A new variable of integration can be defined to simplify the exponent:

$$R'' = |\vec{r}' - \vec{r}| - R' \tag{4.7}$$
$$dR'' = -dR'$$

Note that $R'' = 0$ when $R' = |\vec{r}' - \vec{r}|$ and $R'' = |\vec{r}' - \vec{r}|$ when $R' = 0$. Equation 4.5 now becomes

$$\begin{aligned}
\frac{T(\vec{r} \to \vec{r}', E, \hat{\Omega})}{\Sigma_T(\vec{r}', E)} &= \exp\left[-\int_0^{|\vec{r}'-\vec{r}|} \Sigma_T\left(\vec{r} + R''\hat{\Omega}, E\right) dR''\right] \frac{\delta\left(\hat{\Omega} - \left[\frac{\vec{r}'-\vec{r}}{|\vec{r}'-\vec{r}|}\right]\right)}{|\vec{r}' - \vec{r}|^2} \\
&= \exp\left[-\int_0^{|\vec{r}-\vec{r}'|} \Sigma_T\left(\vec{r} + R''\hat{\Omega}, E\right) dR''\right] \frac{\delta\left(\hat{\Omega} + \left[\frac{\vec{r}-\vec{r}'}{|\vec{r}-\vec{r}'|}\right]\right)}{|\vec{r} - \vec{r}'|^2} \\
&= \tau(\vec{r}', \vec{r}, E, -\hat{\Omega}) \qquad (4.8) \\
&= \frac{T(\vec{r}' \to \vec{r}, E, -\hat{\Omega})}{\Sigma_T(\vec{r}, E)}. \qquad (4.9)
\end{aligned}$$

The dual emission density FIESK is therefore

$$\chi^\dagger(\vec{r}, E, \hat{\Omega}) = c(\vec{r}, E, \hat{\Omega}) + \int\int\int \tau(\vec{r}', \vec{r}, E, -\hat{\Omega})\Sigma_T(\vec{r}', E \to E', \hat{\Omega} \to \hat{\Omega}')dE'd\hat{\Omega}'dV'. \tag{4.10}$$

By comparing equation 4.10 to the flux FIESK given in equation 3.16, it is clear that the *adjoint of the emission density* behaves very similar to the flux. In the literature, the *adjoint of the emission density* is often called "flux-like" because of this similarity [16]. Though it will not be shown, the *adjoint of the collision density* is also "flux-like."

In section 3.3 it was shown that the random walk process to estimate the flux was not ideal. While a random walk process could be constructed for the *adjoint of the emission density*, given its flux-like nature, its random walk process will not be ideal either.

One way to construct a function that will be collision like and still retain the desired property of the dual FIESK (i.e. the response function becomes the source) is to multiply equation 4.10 by some function $\Sigma^*(\vec{r}, E)$, whose only necessary properties are that it is strictly positive and that it goes to zero in a vacuum. While this manipulation is encountered in several pieces of literature, and is in fact necessary in the derivation of the probability laws for coupled adjoint neutron and adjoint photon transport, it will be more instructive to take a step back and start over again with the adjoint transport equation [22–24]. In addition, the process for deriving the PDFs that govern the random walk process for the emission density and collision density outlined in the previous chapter can be followed.

4.2 The Adjoint Integro-Differential Boltzmann Equation

The integro-differential transport equation, given in equation 3.1 can also be written in an operator form. In the following equation, it is assumed that the flux distribution is time-independent:

$$H_B \cdot \varphi(\vec{r}, E, \hat{\Omega}) = S(\vec{r}, E, \hat{\Omega}). \tag{4.11}$$

Using the integro-differential transport operator, and the following equality

$$\langle \varphi^\dagger H_B \cdot \varphi \rangle = \langle \varphi H_B^\dagger \cdot \varphi^\dagger \rangle, \tag{4.12}$$

the adjoint integro-differential transport operator can be derived [7, 8]. This derivation is quite lengthy and will therefore not be shown. The interested reader should refer to the text by Lewis and Miller or the text by Bell and Glasstone for this derivation [7, 8]. The function $\varphi^\dagger(\vec{r}, E, \hat{\Omega})$ is the adjoint flux. The adjoint integro-differential transport operator, which operates on the adjoint flux, is

$$\begin{aligned} H_B^\dagger \cdot \varphi^\dagger(\vec{r}, E, \hat{\Omega}) = &\left[-\hat{\Omega} \cdot \vec{\bigtriangledown} + \Sigma_T(\vec{r}, E)\right] \varphi^\dagger(\vec{r}, E, \hat{\Omega}) - \\ &\int\int \Sigma_T(\vec{r}, E \rightarrow E', \hat{\Omega} \rightarrow \hat{\Omega}') \varphi^\dagger(\vec{r}, E', \hat{\Omega}') dE' d\hat{\Omega}'. \end{aligned} \tag{4.13}$$

The adjoint integro-differential transport equation can be derived by forcing $H_B^\dagger \cdot \varphi^\dagger(\vec{r}, E, \hat{\Omega})$ to equal the response function $a(\vec{r}, E, \hat{\Omega})$ that was used in equation 3.51. This will ensure that the inner product of the adjoint flux and the source will give the same value as the inner product of the flux and the response function:

$$\begin{aligned} I &= \langle \varphi H_B^\dagger \cdot \varphi^\dagger \rangle \\ &= \langle \varphi a \rangle \\ &= \langle \varphi^\dagger H_B \cdot \varphi \rangle \\ &= \langle \varphi^\dagger S \rangle. \end{aligned}$$

The adjoint integro-differential transport equation is

$$\begin{aligned} -\hat{\Omega} \cdot \vec{\nabla} \varphi^\dagger(\vec{r}, E, \hat{\Omega}) + \Sigma_T(\vec{r}, E)\varphi^\dagger(\vec{r}, E, \hat{\Omega}) = \\ a(\vec{r}, E, \hat{\Omega}) + \int\int \Sigma_T(\vec{r}, E \to E', \hat{\Omega} \to \hat{\Omega}')\varphi^\dagger(\vec{r}, E', \hat{\Omega}')dE'd\hat{\Omega}'. \end{aligned} \tag{4.14}$$

It must be noted that the double differential collision cross section in the adjoint integro-differential transport equation is identical to the one that appears in the integro-differential transport equation. However, it is now integrated over final energies and directions. Therefore, it is not clear what the normalization for the total double differential transfer function is or equivalently, what the mean number of adjoint particles emerging per collision is. These properties of the total double differential transfer function will be analyzed in the coming sections.

4.3 The Adjoint Transport Equation in Integral Form

In order to use the Monte Carlo random walk process that was discussed in the chapter 2, the integro-differential form of the adjoint transport equation must be converted to a FIESK. To do this, the adjoint transport equation will first be simplified by introducing the adjoint emission density:

$$\theta^\dagger(\vec{r}, E, \hat{\Omega}) = a(\vec{r}, E, \hat{\Omega}) + \int\int \Sigma_T(\vec{r}, E \to E', \hat{\Omega} \to \hat{\Omega}')\varphi^\dagger(\vec{r}, E', \hat{\Omega}')dE'd\hat{\Omega}'. \tag{4.15}$$

The adjoint emission density is the expected density of adjoint particles exiting a collision or the adjoint source. Using this definition for the adjoint emission density,

the simplified adjoint transport equation becomes

$$-\hat{\Omega}\cdot\vec{\bigtriangledown}\varphi^{\dagger}(\vec{r},E,\hat{\Omega},t)+\Sigma_{T}(\vec{r},E)\varphi^{\dagger}(\vec{r},E,\hat{\Omega},t)=\theta^{\dagger}(\vec{r},E,\hat{\Omega}). \tag{4.16}$$

From the reduced adjoint transport equation, the method of characteristics will be used to transform it to its integral form. The characteristic for the adjoint transport equation is the following parameterized line.

$$\vec{r}^{\,\prime}=\vec{r}+R\hat{\Omega} \tag{4.17}$$

Using equation 4.17 a directional derivative along the characteristic can be determined:

$$\begin{aligned}\frac{d}{dR}&=\frac{dx^{\prime}}{dR}\frac{\partial}{\partial x}+\frac{dy^{\prime}}{dR}\frac{\partial}{\partial y}+\frac{dz^{\prime}}{dR}\frac{\partial}{\partial z}\\&=\Omega_{x}\frac{\partial}{\partial x}+\Omega_{y}\frac{\partial}{\partial y}+\Omega_{z}\frac{\partial}{\partial z}\\&=\hat{\Omega}\cdot\vec{\bigtriangledown}.\end{aligned} \tag{4.18}$$

By using the directional derivative along the characteristic the adjoint transport equation can be reduced to a first order ODE:

$$-\frac{d}{dR}\varphi^{\dagger}(\vec{r}^{\,\prime},E,\hat{\Omega})+\Sigma_{T}(\vec{r}^{\,\prime},E)\varphi^{\dagger}(\vec{r}^{\,\prime},E,\hat{\Omega})=\theta^{\dagger}(\vec{r}^{\,\prime},E,\hat{\Omega}). \tag{4.19}$$

This ODE can be easily solved with the integrating factor

$$\exp\left[-\int_{0}^{R}\Sigma_{T}(\vec{r}+R^{\prime}\hat{\Omega},E)dR^{\prime}\right], \tag{4.20}$$

as will be shown.

First, the left two terms of equation 4.19 can combined into a single term using the integrating factor:

$$-\frac{d}{dR}\left[\varphi^{\dagger}(\vec{r}^{\,\prime},E,\hat{\Omega})\exp\left[-\int_{0}^{R}\Sigma_{T}(\vec{r}+R^{\prime}\hat{\Omega},E)dR^{\prime}\right]\right]=$$
$$\theta^{\dagger}(\vec{r}^{\,\prime},E,\hat{\Omega})\exp\left[-\int_{0}^{R}\Sigma_{T}(\vec{r}+R^{\prime}\hat{\Omega},E)dR^{\prime}\right].$$

Next, the derivative along the characteristic can be eliminated by integrating from

zero to infinity:

$$-\varphi^{\dagger}(\vec{r}+R\hat{\Omega},E,\hat{\Omega})\exp\left[-\int_0^R \Sigma_T(\vec{r}+R'\hat{\Omega},E)dR'\right]\Big|_0^{\infty} = \int_0^{\infty}\theta^{\dagger}(\vec{r}+R\hat{\Omega},E,\hat{\Omega})\exp\left[-\int_0^R \Sigma_T(\vec{r}+R'\hat{\Omega},E)dR'\right]dR.$$

If the adjoint flux is assumed to go to zero as R goes to infinity, the integral adjoint transport equation is obtained:

$$\varphi^{\dagger}(\vec{r},E,\hat{\Omega}) = \int_0^{\infty}\theta^{\dagger}(\vec{r}+R\hat{\Omega},E,\hat{\Omega})exp\left[-\int_0^R \Sigma_T(\vec{r}+R'\hat{\Omega},E)dR'\right]dR. \tag{4.21}$$

Like with the integral transport equation, it is often more convenient to represent the integral adjoint transport equation as an integral over all space. To do this, note that

$$\begin{aligned} R &= |\vec{r}' - \vec{r}|, \\ \hat{\Omega} &= \frac{\vec{r}' - \vec{r}}{|\vec{r}' - \vec{r}|} \text{ and} \\ dV' &= R^2 dR d\hat{\Omega}. \end{aligned} \tag{4.22}$$

With these definitions, the integral adjoint transport equation becomes

$$\varphi^{\dagger}(\vec{r},E,\hat{\Omega}) = \int \theta^{\dagger}(\vec{r}',E,\hat{\Omega})\exp\left[-\int_0^{|\vec{r}'-\vec{r}|}\Sigma_T(\vec{r}+R'\hat{\Omega},E)dR'\right]\frac{\delta\left(\hat{\Omega}-\left[\frac{\vec{r}'-\vec{r}}{|\vec{r}'-\vec{r}|}\right]\right)}{|\vec{r}''-\vec{r}|^2}dV'.$$

To further simplify the integral adjoint transport equation, one more function will be introduced:

$$\tau^{\dagger}(\vec{r}',\vec{r},E,\hat{\Omega}) = \exp\left[-\int_0^{|\vec{r}'-\vec{r}|}\Sigma_T(\vec{r}+R'\hat{\Omega},E)dR'\right]\frac{\delta\left(\hat{\Omega}-\left[\frac{\vec{r}'-\vec{r}}{|\vec{r}'-\vec{r}|}\right]\right)}{|\vec{r}''-\vec{r}|^2}. \tag{4.23}$$

By inspection it is clear that this function is simply the function introduced in equation 3.14 with a negative angular variable:

$$\tau^{\dagger}(\vec{r}',\vec{r},E,\hat{\Omega}) = \tau(\vec{r}',\vec{r},E,-\hat{\Omega}). \tag{4.24}$$

The simplified integral adjoint transport equation is now simply

$$\varphi^{\dagger}(\vec{r}, E, \hat{\Omega}) = \int \theta^{\dagger}(\vec{r}', E, \hat{\Omega}) \tau^{\dagger}(\vec{r}', \vec{r}, E, \hat{\Omega}) dV'. \tag{4.25}$$

Based on the lessons that were learned in the previous chapter, the adjoint flux FIESK will not be created and instead, the adjoint emission density FIESK will be derived next.

4.4 The Adjoint Emission Density FIESK

To construct the adjoint emission density FIESK the integral adjoint transport equation given in equation 4.25 must be substituted back into the adjoint emission density shown in equation 4.15:

$$\begin{aligned}\theta^{\dagger}(\vec{r}, E, \hat{\Omega}) &= a(\vec{r}, E, \hat{\Omega}) + \int\int \Sigma_T(\vec{r}, E \to E', \hat{\Omega} \to \hat{\Omega}') \int \theta^{\dagger}(\vec{r}', E', \hat{\Omega}') \tau^{\dagger}(\vec{r}', \vec{r}, E', \hat{\Omega}') dV' dE' d\hat{\Omega}' \\ &= a(\vec{r}, E, \hat{\Omega}) + \int\int\int \frac{\Sigma^{\dagger}(\vec{r}, E')}{\Sigma_T(\vec{r}, E')} \frac{\Sigma_T(\vec{r}, E \to E', \hat{\Omega} \to \hat{\Omega}')}{\Sigma^{\dagger}(\vec{r}, E')} \Sigma_T(\vec{r}, E') \tau^{\dagger}(\vec{r}', \vec{r}, E', \hat{\Omega}') \\ &\qquad \cdot \theta^{\dagger}(\vec{r}', E', \hat{\Omega}') dV' dE' d\hat{\Omega}'.\end{aligned}$$

The function $\Sigma^{\dagger}(\vec{r}, E')$ is called the total macroscopic adjoint cross section and is defined as

$$\Sigma^{\dagger}(\vec{r}, E') = \int\int \Sigma_T(\vec{r}, E \to E', \hat{\Omega} \to \hat{\Omega}') dE d\hat{\Omega}. \tag{4.26}$$

Two kernels and one weight factor must now be introduced to simplify the adjoint emission density FIESK. The first kernel will be called the adjoint collision kernel and is defined as

$$\begin{aligned}C^{\dagger}(\vec{r}, E' \to E, \hat{\Omega}' \to \hat{\Omega}) &= \frac{\Sigma_T(\vec{r}, E \to E', \hat{\Omega} \to \hat{\Omega}')}{\int\int \Sigma_T(\vec{r}, E \to E', \hat{\Omega} \to \hat{\Omega}') dE d\hat{\Omega}} \\ &= \frac{\Sigma_T(\vec{r}, E \to E', \hat{\Omega} \to \hat{\Omega}')}{\Sigma^{\dagger}(\vec{r}, E')}.\end{aligned} \tag{4.27}$$

The second kernel will be called the adjoint transport kernel and is defined as

$$\begin{aligned} T^{\dagger}(\vec{r}^{\,'} \rightarrow \vec{r}, E, \hat{\Omega}) &= \Sigma_T(\vec{r}, E)\tau^{\dagger}(\vec{r}^{\,'}, \vec{r}, E, \hat{\Omega}) \\ &= \Sigma_T(\vec{r}, E)\exp\left[-\int_0^{|\vec{r}^{\,'}-\vec{r}|}\Sigma_T(\vec{r}+R^{'}\hat{\Omega}, E)dR^{'}\right]\frac{\delta\left(\hat{\Omega}-\left[\frac{\vec{r}^{\,'}-\vec{r}}{|\vec{r}^{\,'}-\vec{r}|}\right]\right)}{|\vec{r}^{\,'}-\vec{r}|^2}. \end{aligned} \tag{4.28}$$

The quantity $T^{\dagger}(\vec{r}^{\,'} \rightarrow \vec{r}, E, \hat{\Omega})dV$ can be interpreted as the probability that an adjoint particle at $\vec{r}^{\,'}$ with energy E and direction $\hat{\Omega}$ will have its next collision in volume element dV at $\vec{r}$.

The weight factor will be called the adjoint weight factor. It is defined as

$$P^{\dagger}(\vec{r}, E) = \frac{\Sigma^{\dagger}(\vec{r}, E)}{\Sigma_T(\vec{r}, E)}. \tag{4.29}$$

The adjoint weight factor comes about from the construction of the adjoint collision kernel and the adjoint transport kernel. To construct the adjoint collision kernel from the double differential collision cross section, one must divide the double differential collision cross section by the total macroscopic adjoint cross section. To construct the adjoint transport kernel one must multiply the function $\tau^{\dagger}(\vec{r}^{\,'}, \vec{r}, E, \hat{\Omega})$ by the total macroscopic cross section. In general, the total macroscopic adjoint cross section and the total macroscopic cross section will not be equal, which is why the adjoint weight factor arises. In some literature, this factor is called the adjoint non-absorption probability [25]. However, as will be shown in the next chapter, this factor is not bounded in the interval (0,1) but is instead bounded in the interval (0,∞). It is therefore inappropriate to call this factor a probability*.

Using the above kernels and weight factor, the simplified adjoint emission density FIESK becomes

$$\begin{aligned} \theta^{\dagger}(\vec{r}, E, \hat{\Omega}) = a(\vec{r}, E, \hat{\Omega}) + \int\int\int C^{\dagger}(\vec{r}, E^{'} \rightarrow E, \hat{\Omega}^{'} \rightarrow \hat{\Omega})P^{\dagger}(\vec{r}, E^{'}) \\ \cdot T^{\dagger}(\vec{r}^{\,'} \rightarrow \vec{r}, E^{'}, \hat{\Omega}^{'})\theta^{\dagger}(\vec{r}^{\,'}, E^{'}, \hat{\Omega}^{'})dV^{'}dE^{'}d\hat{\Omega}^{'}. \end{aligned} \tag{4.30}$$

*This fact is noted in the reference that calls the factor the adjoint non-absorption probability [25].

The state transition kernel for the adjoint emission density FIESK is simply

$$\begin{aligned} M^{\dagger}(y \to x) &= M^{\dagger}(\vec{r}^{\,'} \to \vec{r}, E^{'} \to E, \hat{\Omega}^{'} \to \hat{\Omega}) \\ &= C^{\dagger}(\vec{r}, E^{'} \to E, \hat{\Omega}^{'} \to \hat{\Omega}) P^{\dagger}(\vec{r}, E^{'}) T^{\dagger}(\vec{r}^{\,'} \to \vec{r}, E^{'}, \hat{\Omega}^{'}). \end{aligned} \tag{4.31}$$

4.5 The Adjoint Collision Density FIESK

Like the collision density, the adjoint collision density can also be quite useful. It is related to the adjoint flux and the adjoint emission density by the following equations, which are analogous to the relationships between the collision density, flux and emission density:

$$\xi^{\dagger}(\vec{r}, E, \hat{\Omega}) = \Sigma_T(\vec{r}, E) \varphi^{\dagger}(\vec{r}, E, \hat{\Omega}) \tag{4.32}$$

$$= \int T^{\dagger}(\vec{r}^{\,'} \to \vec{r}, E, \hat{\Omega}) \theta^{\dagger}(\vec{r}^{\,'}, E, \hat{\Omega}) dV^{'}. \tag{4.33}$$

The adjoint collision density is the density of adjoint particles entering a collision.

To construct the adjoint collision density FIESK, equation 4.33 and the adjoint emission density FIESK given in equation 4.30 will be used:

$$\begin{aligned} \xi^{\dagger}(\vec{r}, E, \hat{\Omega}) = &\int a(\vec{r}^{\,'}, E, \hat{\Omega}) T^{\dagger}(\vec{r}^{\,'} \to \vec{r}, E, \hat{\Omega}) dV^{'} + \\ &\int\int\int T^{\dagger}(\vec{r}^{\,'} \to \vec{r}, E, \hat{\Omega}) C^{\dagger}(\vec{r}^{\,'}, E^{'} \to E, \hat{\Omega}^{'} \to \hat{\Omega}) P^{\dagger}(\vec{r}^{\,'}, E^{'}) \xi^{\dagger}(\vec{r}^{\,'}, E^{'}, \hat{\Omega}^{'}) dE^{'} d\hat{\Omega}^{'} dV^{'}. \end{aligned} \tag{4.34}$$

Notice that the source term for the adjoint collision density is a first collided source. To avoid confusion with the source term for the collision density, it will be referred to as the adjoint first collided source.

The state transition kernel for the collision density FIESK is simply

$$\begin{aligned} N^{\dagger}(y \to x) &= N^{\dagger}(\vec{r}^{\,'} \to \vec{r}, E^{'} \to E, \hat{\Omega}^{'} \to \hat{\Omega}) \\ &= T^{\dagger}(\vec{r}^{\,'} \to \vec{r}, E, \hat{\Omega}) C^{\dagger}(\vec{r}^{\,'}, E^{'} \to E, \hat{\Omega}^{'} \to \hat{\Omega}) P^{\dagger}(\vec{r}^{\,'}, E^{'}). \end{aligned} \tag{4.35}$$

4.6 Adjoint Emission and Collision Density State Transition Kernel Properties

Before the PDFs that govern the random walk process are derived, the adjoint transport kernel, adjoint collision kernel and adjoint weight factor must be investigated a bit further. A comparison of the adjoint transport kernel and the transport kernel reveals that the adjoint transport kernel is identical the the transport kernel with $\hat{\Omega} = -\hat{\Omega}$:

$$T^{\dagger}(\vec{r}' \rightarrow \vec{r}, E, \hat{\Omega}) = T(\vec{r}' \rightarrow \vec{r}, E, -\hat{\Omega}). \tag{4.36}$$

The significance of this relationship is that adjoint particles move in the direction opposite of the variable $\hat{\Omega}$. It is therefore inappropriate to interpret the variable $\hat{\Omega}$ of an adjoint particle as its direction. However, for convenience, it will continue to be referred to as an adjoint particle's direction. This relationship also indicates that the adjoint transport kernel is normalized for an infinite medium:

$$\int T^{\dagger}(\vec{r}' \rightarrow \vec{r}, E, \hat{\Omega}) dV = 1. \tag{4.37}$$

In problems where the domain of interest in finite, random walks should be terminated when they exit the domain of interest. This procedure was described in the previous chapter to account for the unnormalized transport kernel in finite domains. Because of the relationship between the transport kernel and the adjoint transport kernel, this procedure is also valid for the adjoint transport kernel.

Based on the definition of the adjoint collision kernel from equation 4.27 the adjoint collision kernel is also normalized to unity:

$$\begin{aligned}\int\int C^{\dagger}(\vec{r}, E' \rightarrow E, \hat{\Omega}' \rightarrow \hat{\Omega}) dE d\hat{\Omega} &= \int\int \frac{\Sigma_T(\vec{r}, E \rightarrow E', \hat{\Omega} \rightarrow \hat{\Omega}')}{\Sigma^{\dagger}(\vec{r}, E')} dE d\hat{\Omega} \\ &= 1.\end{aligned}$$

This property of the adjoint collision kernel hints at two interesting phenomena for adjoint particles. First, there are no absorption reactions for adjoint particles and second, there are no multiplying reactions for adjoint particles. Both of these properties become more obvious when the adjoint collision is expanded, which will be done in the next section. The consequence of the lack of an adjoint absorption reaction is that an analogue random walk process for the adjoint FIESKs is not possible. Russian roulette will have to be used to terminate histories.

As mentioned before, the adjoint weight factor $P^{\dagger}(\vec{r}, E)$ takes into account the fact that the total macroscopic cross section $\Sigma_T(\vec{r}, E)$, which is used to construct the adjoint transport kernel, is not equal to the total macroscopic adjoint cross section $\Sigma^{\dagger}(\vec{r}, E)$, which is used to construct the adjoint collision kernel. Unfortunately, this factor is not bounded to the interval (0,1), which means that it is likely to increase the variance of the estimators used.

Based on the properties of the adjoint transport kernel, adjoint collision kernel and the adjoint weight factor, the adjoint emission density state transition kernel normalization can be determined:

$$\begin{aligned}\int M^{\dagger}(y \to x)dx &= \int\int\int C^{\dagger}(\vec{r}, E' \to E, \hat{\Omega}' \to \hat{\Omega})P^{\dagger}(\vec{r}, E')T^{\dagger}(\vec{r}' \to \vec{r}, E', \hat{\Omega}')dEd\hat{\Omega})dV \\ &= \int P^{\dagger}(\vec{r}, E')T^{\dagger}(\vec{r}' \to \vec{r}, E', \hat{\Omega}')dEd\hat{\Omega})dV \\ &= \overline{P}^{\dagger}(\vec{r}', E'). \end{aligned} \tag{4.38}$$

The normalization function $\overline{P}^{\dagger}(\vec{r}', E')$ can be interpreted as the average adjoint weight factor along the line from $\vec{r}'$ to $\vec{r}$ given an adjoint particle of energy E'.

The adjoint collision density state transition kernel normalization can also be determined with the properties of the adjoint transport kernel, adjoint collision kernel and adjoint weight factor that were discussed:

$$\begin{aligned}\int N^{\dagger}(y \to x)dx &= \int\int\int T^{\dagger}(\vec{r}' \to \vec{r}, E, \hat{\Omega})C^{\dagger}(\vec{r}', E' \to E, \hat{\Omega}' \to \hat{\Omega})P^{\dagger}(\vec{r}', E')dVdEd\hat{\Omega}) \\ &= \int C^{\dagger}(\vec{r}', E' \to E, \hat{\Omega}' \to \hat{\Omega})P^{\dagger}(\vec{r}', E')dEd\hat{\Omega}) \\ &= P^{\dagger}(\vec{r}', E'). \end{aligned} \tag{4.39}$$

The properties of the two state transition kernels are summarized below.

1. $M^{\dagger}(y \to x) > 0$
   $N^{\dagger}(y \to x) > 0$

   and

2. $\int M^{\dagger}(y \to x)dx = \overline{P}^{\dagger}(y) < \infty$
   $\int N^{\dagger}(y \to x)dx = P^{\dagger}(y) < \infty$

Based on these properties for the two kernels and the fact that the adjoint survival probability is always unity due to the lack of an absorption reaction, it is clear that

an analogue random walk process for adjoint radiation transport is impossible. The adjoint collision kernel must still be expanded into its constituent parts, which will be shown in the next section, so that each individual adjoint reaction can be treated explicitly.

4.7 Expansion of the Adjoint Collision Kernel

As explained in the previous chapter, the total double differential transfer function, which appears in both the collision kernel and the adjoint collision kernel, is challenging to obtain. To conduct the random walks for adjoint radiation, each individual adjoint reaction has to be modeled. To do this, the adjoint collision kernel must be expanded:

$$\begin{aligned} C^{\dagger}(\vec{r}, E' \to E, \hat{\Omega}' \to \hat{\Omega}) &= \frac{\Sigma_T(\vec{r}, E \to E', \hat{\Omega} \to \hat{\Omega}')}{\Sigma^{\dagger}(\vec{r}, E')} \\ &= \sum_j \frac{\Sigma_j(\vec{r}, E) c_j(\vec{r}, E) f_j(E \to E', \hat{\Omega} \to \hat{\Omega}')}{\Sigma^{\dagger}(\vec{r}, E')} \\ &= \sum_A \frac{\Sigma_A^{\dagger}(\vec{r}, E')}{\Sigma^{\dagger}(\vec{r}, E')} \sum_j \frac{\sigma_{A,j}^{\dagger}(E')}{\sigma_A^{\dagger}(E')} \frac{\sigma_{A,j}(E) c_{A,j}(E) p_{A,j}(E \to E', \hat{\Omega} \to \hat{\Omega}')}{\sigma_{A,j}^{\dagger}(E')} \\ &= \sum_A p_A^{\dagger}(\vec{r}, E') \sum_j p_{A,j}^{\dagger}(E') p_{A,j}^{\dagger}(E' \to E, \hat{\Omega}' \to \hat{\Omega}). \end{aligned} \tag{4.40}$$

In this expansion, the subscript A denotes a particular nuclide or element and the subscript j denotes a particular type of reaction. The double differential transfer probability for a given reaction $p_{A,j}(E \to E', \hat{\Omega} \to \hat{\Omega}')$ is no longer normalized and cannot be used as a PDF for sampling the outgoing adjoint particle energy and direction. However, as indicated in equation 4.40 a new double differential transfer probability can be constructed for adjoint particles.

$$p_{A,j}^{\dagger}(E' \to E, \hat{\Omega}' \to \hat{\Omega}) = \frac{\sigma_{A,j}(E) c_{A,j}(E) p_{A,j}(E \to E', \hat{\Omega} \to \hat{\Omega}')}{\sigma_{A,j}^{\dagger}(E')} \tag{4.41}$$

The microscopic adjoint cross section for reaction j with nuclide or element A will be defined as follows.

$$\sigma_{A,j}^{\dagger}(E') = \int\int \sigma_{A,j}(E) c_{A,j}(E) p_{A,j}(E \to E', \hat{\Omega} \to \hat{\Omega}') dE d\hat{\Omega} \tag{4.42}$$

Therefore, the adjoint double differential transfer probability is indeed normalized to unity.

$$\int\int p^{\dagger}_{A,j}(E' \rightarrow E, \hat{\Omega}' \rightarrow \hat{\Omega}) dE d\hat{\Omega} = 1 \tag{4.43}$$

By sampling from the adjoint collision kernel in its expanded form, each individual adjoint reaction will be treated explicitly. In the process of sampling from the adjoint collision kernel one first samples the nuclide or element hit from the discrete PDF

$$\begin{aligned} p(A|\vec{r}, E') &= \sum_{A} p^{\dagger}_{A}(\vec{r}, E') \\ &= \sum_{A} \frac{\Sigma^{\dagger}_{A}(\vec{r}, E')}{\Sigma^{\dagger}(\vec{r}, E')}. \end{aligned} \tag{4.44}$$

With the nuclide or element A chosen, the reaction type is sampled from the discrete PDF

$$\begin{aligned} p(j|A, E') &= \sum_{j} p^{\dagger}_{A,j}(E') \\ &= \sum_{j} \frac{\sigma^{\dagger}_{A,j}(E')}{\sigma^{\dagger}_{A}(E')}. \end{aligned} \tag{4.45}$$

Finally, the outgoing energy and direction is sampled from the adjoint transfer probability $p^{\dagger}_{A,j}(E' \rightarrow E, \hat{\Omega}' \rightarrow \hat{\Omega})$.

To use this process, one must be able to calculate the microscopic adjoint cross sections and the adjoint double differential transfer probabilities. These calculations for photons will be discussed in the next chapter.

4.8 The Adjoint Emission Density and Adjoint Collision Density Random Walk PDFs

With the state transition kernels $M^{\dagger}(y \rightarrow x)$ and $N^{\dagger}(y \rightarrow x)$ fully characterized, the Monte Carlo random walk process for adjoint radiation transport can be completely

specified:

$$\theta^\dagger(x) \text{ Random Walk: } \begin{cases} p^1(x) & = \frac{a(x)}{\int_\Gamma a(x)\,dx} \\ p(y \to x) & = \frac{M^\dagger(y \to x)}{\overline{P}^\dagger(y)} \\ p(x) & = 0 \end{cases} \tag{4.46}$$

$$\xi^\dagger(x) \text{ Random Walk: } \begin{cases} p^1(x) & = \frac{S_c^\dagger(x)}{\int_\gamma S_c^\dagger(x)\,dx} \\ p(y \to x) & = \frac{N^\dagger(y \to x)}{P^\dagger(y)} \\ p(x) & = 0. \end{cases} \tag{4.47}$$

Note that the function $S_c^\dagger(x)$ is simply the adjoint first collided source, which was shown in equation 4.34.

While it might appear from the above PDFs that the two random walk processes for the adjoint emission and collision densities are completely different, because the kernels $M^\dagger(y \to x)$ and $N^\dagger(y \to x)$ only differ in the ordering of the adjoint transport kernel, adjoint collision kernel and adjoint weight factor, both the adjoint emission density and adjoint collision density can be estimated during the same random walk process. Figure 4.1 illustrates the new combined random walk process. In this new process, particles always start in the true adjoint source and not the adjoint first collided source, which is advantageous because the adjoint first collided source would be challenging to evaluate in general. The adjoint emission density will always be estimated right after a collision (or birth) and the adjoint collision density will always be estimated right before a collision and before multiplying the particle weight by the adjoint weight factor.

4.9 Estimating Responses

Due to the way that the adjoint transport equation is constructed, the inner product of the adjoint flux $\varphi^\dagger(\vec{r}, E, \hat{\Omega})$ and the source $S(\vec{r}, E, \hat{\Omega})$ will result in the same value as the inner product of the flux $\varphi(\vec{r}, E, \hat{\Omega})$ and the response function $a(\vec{r}, E, \hat{\Omega})$. Because it is not ideal to estimate the adjoint flux directly using a Monte Carlo random walk process, equivalent inner products must be constructed that are either

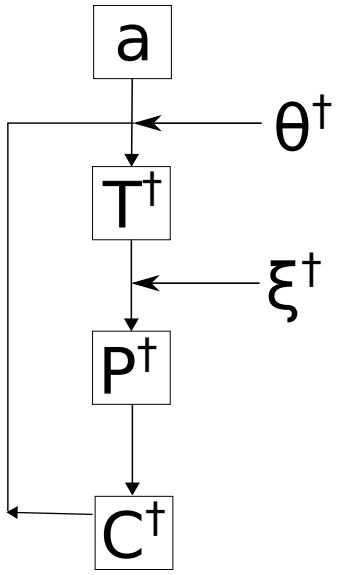

Figure 4.1: **Monte Carlo random walk process for adjoint radiation.** *A particle state is first sampled from the adjoint source distribution. The next collision point is sampled from the adjoint transport kernel $T^\dagger$. Next, the adjoint particle weight is multiplied by the adjoint weight factor $P^\dagger$. Finally, the new energy and direction is sampled from the adjoint collision kernel. This process continues until Russian roulette forces the random walk to terminate. This process allows both the adjoint emission density and the adjoint collision density to be estimated.*

in terms of the adjoint collision density or the adjoint emission density:

$$I = \int\int\int S(\vec{r}, E, \hat{\Omega})\varphi^\dagger(\vec{r}, E, \hat{\Omega})dVdEd\hat{\Omega} \tag{4.48}$$

$$= \int\int\int U(\vec{r}, E, \hat{\Omega})\xi^\dagger(\vec{r}, E, \hat{\Omega})dVdEd\hat{\Omega} \tag{4.49}$$

$$= \int\int\int V(\vec{r}, E, \hat{\Omega})\theta^\dagger(\vec{r}, E, \hat{\Omega}).dVdEd\hat{\Omega} \tag{4.50}$$

Based on the relationship between the adjoint collision density and the adjoint flux, $U(\vec{r}, E, \hat{\Omega})$ must be defined as

$$U(\vec{r}, E, \hat{\Omega}) = \frac{S(\vec{r}, E, \hat{\Omega})}{\Sigma_T(\vec{r}, E, \hat{\Omega})}. \tag{4.51}$$

Similarly, the function $V(\vec{r}, E, \hat{\Omega})$ must be defined as

$$V(\vec{r}, E, \hat{\Omega}) = \int \frac{S(\vec{r}', E, \hat{\Omega})}{\Sigma_T(\vec{r}', E, \hat{\Omega})} T^\dagger(\vec{r} \to \vec{r}', E, \hat{\Omega})dV'. \tag{4.52}$$

Clearly, the function $U(\vec{r}, E, \hat{\Omega})$ will be easier to evaluate than the function $V(\vec{r}, E, \hat{\Omega})$. Using either of the estimators that were described in chapter 2 or the track-length estimator that was described in chapter 3 and the combined random walk process that was outlined in the previous section, an estimate for the value I can be obtained.

4.10 Chapter Summary

Several points from this chapter must be emphasized before moving on:

- The dual emission density FIESK and the dual collision density FIESK describe "flux-like" quantities and should be avoided, based one of the main points from the previous chapter.
- The material response calculated from the inner product of the flux and the material response function can also be calculated from the inner product of the source function and a new quantity called the adjoint flux, which is described by the adjoint transport equation.
- The adjoint transport equation can be constructed from the transport equation using a similar procedure to the one that was outlined in chapter 2 for deriving a dual FIESK from a FIESK.
- By performing a set of manipulations similar to the ones outlined in the previous chapter, the integro-differential adjoint transport equation can be converted to a FIESK that describes the adjoint flux, the adjoint emission density or the adjoint collision density of a system.
- The adjoint emission density FIESK and the adjoint collision density FIESK are not equivalent to the dual emission density FIESK or the dual collision density FIESK respectively. However, they are related by a function $\Sigma^*(\vec{r}, E)$, which has some specific properties. This relationship becomes useful in the context of coupled adjoint neutron and adjoint photon transport.
- The state transition kernels that appear in the adjoint emission density FIESK and the adjoint collision density FIESK can be decomposed into two kernels and a weight factor: the adjoint collision kernel, which describes the movement of adjoint particles through energy and direction, the adjoint transport kernel, which describes the movement of adjoint particles through space, and the adjoint weight factor.

- The adjoint weight factor comes about from the construction of the adjoint collision kernel and the adjoint transport kernel, both of which are normalized to unity. The adjoint collision kernel is constructed with the total macroscopic adjoint cross section while the adjoint transport kernel is constructed with the total macroscopic cross section. These cross sections are in general not equal, which gives rise to the adjoint weight factor.
- The adjoint collision kernel can be decomposed into its constituent adjoint reactions so that each reaction can be modeled explicitly.
- Every adjoint reaction must be constructed from a corresponding forward reaction using the following equations:

$$\sigma^{\dagger}(E') = \int\int \sigma(E)c(E)p(E \to E', \hat{\Omega} \to \hat{\Omega}')dEd\hat{\Omega}$$

$$p^{\dagger}(E' \to E, \hat{\Omega}' \to \hat{\Omega}) = \frac{\sigma(E)c(E)p(E \to E', \hat{\Omega} \to \hat{\Omega}')}{\sigma^{\dagger}(E')}$$

- There are no adjoint absorption reactions or multiplication reactions. This is a result of the normalization of the adjoint collision kernel and the definition of the adjoint cross section.
- Due to the similarity between the adjoint emission density FIESK and the adjoint collision density FIESK, solutions to both FIESKs can be estimated using the same random walk process.

While all of the above points are important take-aways from this chapter, the most interesting are certainly the existence of the adjoint weight factor, the definition of the adjoint cross section and the nonexistence of adjoint absorption or multiplication reactions.

Chapter 5

Photon Interaction Cross Sections and Sampling Techniques

In the previous two chapters, the Monte Carlo random walk process for radiation characterized by the transport equation and the adjoint transport equation was described. An important part of the random walk process is the sampling from the expanded collision kernel, which requires information on the differential interaction cross sections for the particle of interest. In this chapter, four primary interactions of high energy photons with matter will be discussed: incoherent scattering, coherent scattering, pair production and the photoelectric effect. Photonuclear absorption, which can become important in high energy coupled neutron-photon transport simulations, will be discussed briefly. In addition, sampling procedures that can be used with each differential interaction cross section will be described. All secondary particles other than photons will be neglected from the cross sections and sampling procedures.

5.1 Incoherent Scattering

Incoherent or Compton scattering occurs when a photon scatters off of an orbital electron and loses some of its energy. The energy of the liberated electron is equal to the energy lost by the photon minus the binding energy of the shell the electron occupied. The differential incoherent scattering cross section (per atom) is usually expressed as the product of the differential Klein-Nishina scattering cross section per electron and the incoherent scattering function. Klein and Nishina developed the differential cross section under the assumption that the electron on which the photon scatters is free and at rest [26]. The incoherent scattering function is the correction to the Klein-Nishina scattering cross section from electron binding. The

differential incoherent scattering cross section is

$$\begin{aligned}\frac{d\sigma_{i.s.}(\alpha',\theta,Z)}{d\Omega} &= \frac{d\sigma_{K.N.}(\alpha',\theta)}{d\Omega}S(y,Z)\\ &= \frac{r_e^2}{2}\frac{\left[1+\cos^2\theta+\frac{\alpha'^2(1-\cos\theta)^2}{1+\alpha'(1-\cos\theta)}\right]}{\left[1+\alpha'(1-\cos\theta)\right]^2}S(y,Z)\end{aligned} \tag{5.1}$$

[2]. The value r_e^2 is the classical radius of the electron and α' is the energy of the incident photon in units of electron rest energy. The arguments of the scattering function are

$$y = \sin(\frac{\theta}{2})/\lambda' \tag{5.2}$$

and Z, the atomic number. The differential incoherent cross section will sometimes be expressed in terms of the outgoing photon energy as well:

$$\frac{d\sigma_{i.s.}(\alpha',\theta,Z)}{d\Omega} = \frac{r_e^2}{2}\left(\frac{\alpha}{\alpha'}\right)^2\left[\frac{\alpha}{\alpha'}+\frac{\alpha'}{\alpha}-1+\cos^2\theta\right]S(y,Z). \tag{5.3}$$

The alpha variables are simply the photon energy divided by the rest mass of the electron.

The later form of the differential incoherent cross section is made possible by the one-to-one correspondence between the outgoing energy and outgoing direction, which can be found using conservation of energy and momentum and the assumption that the electron is free and at rest (see Appendix A):

$$E = \frac{E'}{1+\frac{E'}{m_e c^2}(1-\cos\theta)}. \tag{5.4}$$

When binding effects cannot be neglected, which typically occurs when the incident photon energies are on the order of the electron binding energy, there will no longer be a one-to-one correspondence between the outgoing energy and the outgoing direction. Instead, there will be a distribution of outgoing energies that correspond to each outgoing direction. This phenomenon will be discussed more in the next section.

A PDF for the outgoing photon angle can be created by dividing the differential incoherent cross section by the total incoherent cross section at the incoming photon energy. Then, by reorganizing the PDF, the procedure for sampling an outgoing

photon direction and energy can be determined [27]:

$$\begin{aligned} p(\alpha', \theta, Z) &= \frac{1}{\sigma_{i.s.}(\alpha', Z)} \frac{d\sigma_{i.s.}(\alpha', \theta, Z)}{d\Omega} \\ &= \frac{S_{max}(y, Z)\sigma_{K.N.}(\alpha')}{\sigma_{i.s.}(\alpha', Z)} \left[\frac{S(y, Z)}{S_{max}(y, Z)}\right] \left[\frac{1}{\sigma_{K.N.}(\alpha')} \frac{d\sigma_{K.N.}(\alpha', \theta)}{d\Omega}\right] \\ &= C(\alpha', Z)R(y, Z)p_{K.N.}(\alpha', \theta). \end{aligned} \tag{5.5}$$

The scattering function increases monotonically from 0 when $y = 0$ to Z when $y = \infty$ and therefore,

$$S_{max}(y, Z) = S(y_{max}, Z).$$

The maximum value of y, which occurs when $\theta = \pi$ (corresponding to back scattering), is simply the inverse wavelength of the incoming particle (usually in cm^{-1}). Now, to sample the outgoing direction, one first samples an angle from the PDF for Compton Scattering off of a free electron, $p_{K.N.}(\alpha, \theta)$. Then one uses the rejection function R(y,Z) with the sampled angle to determine if it should be accepted or rejected. Several sampling techniques that can be used with the Klein-Nishina cross section will now be discussed.

For the purpose of sampling, it is useful to write the differential Klein-Nishina cross section in terms of a new variable whose inverse is the energy loss ratio:

$$\frac{1}{x} = \frac{\alpha}{\alpha'} \tag{5.6}$$

$$x = 1+\alpha'(1 - \cos\theta). \tag{5.7}$$

The differential Klein-Nishina cross section can then be written as

$$\frac{d\sigma_{K.N.}(\alpha',x)}{dx} = K\left[A + \frac{B}{x} + \frac{C}{x^2} + \frac{D}{x^3}\right] \tag{5.8}$$

where

$$K = \frac{\pi r_e^2}{\alpha'}$$
$$A = \frac{1}{\alpha'^2}$$
$$B = 1 - \frac{2(\alpha'+1)}{\alpha'^2}$$
$$C = \frac{1+2\alpha'}{\alpha'^2}$$
$$D = 1$$

[2]. The change of variables is carried out in Appendix A.

Now, a PDF for x can be created if the differential Klein-Nishina cross section is divided by the total Klein-Nishina cross section, which can be found by integrating the differential Klein-Nishina cross section from $x_{min} = 1$ to $x_{max} = 1 + 2\alpha'$*:

$$\sigma_{K.N.}(\alpha') = 2\pi r_e^2 \left(\frac{1+\alpha'}{\alpha'^2}\left[\frac{2+2\alpha'}{1+2\alpha'} - \frac{\ln(1+2\alpha')}{\alpha'}\right] + \frac{\ln(1+2\alpha')}{2\alpha'} - \frac{1+3\alpha'}{(1+2\alpha')^2}\right). \tag{5.9}$$

At low photon energies, the evaluation of this equation for the Klein-Nishina cross sections can lead to numerical errors due to the near-cancellation between logarithmic and algebraic terms [2]. An empirical formula was created that is correct to within 1.3% up to 100 MeV [28]. Due to the sampling techniques that will be used, the total Klein-Nishina cross section will only need to be evaluated when the incoming photon energy is above about 1.4 MeV. Therefore there is no need to use the empirical formula.

*The equation found in Lux and Koblinger's text book contains an error which is described in Appendix A

The PDF for x can be defined as

$$p_{K.N.}(\alpha', x) = \begin{cases} H \cdot \left[A + \frac{B}{x} + \frac{C}{x^2} + \frac{D}{x^3}\right] & \text{if } 1 \leqslant x \leqslant 1 + 2\alpha' \\ 0 & \text{otherwise} \end{cases} \tag{5.10}$$

where

$$H = \frac{K}{\sigma_{K.N.}(\alpha')}.$$

A direct inversion of this PDF is not possible. However, this PDF can still be sampled directly by using a combination of the probability mixing method and the inverse CDF method [29]*. To use these two sampling techniques, the PDF must be split into four terms:

$$p_{K.N.}(\alpha', x) = p_1(\alpha', x) + p_2(\alpha', x) + p_3(\alpha', x) + p_4(\alpha', x) \tag{5.11}$$

where

$$\begin{aligned} p_1(\alpha', x) &= HA \\ p_2(\alpha', x) &= \frac{HB}{x} \\ p_3(\alpha', x) &= \frac{HC}{x^2} \\ p_4(\alpha', x) &= \frac{HD}{x^3}. \end{aligned}$$

Now the probability of selecting the i^{th} term is

$$p_i = \int_1^{1+2\alpha'} p_i(\alpha', x)\,dx. \tag{5.12}$$

For the four functions above, the probabilities of being selected are

$$p_i = \begin{cases} \frac{2H}{\alpha'} & \text{if } i = 1 \\ H\left[1 - \frac{2+2\alpha'}{\alpha'^2}\right] \ln(1 + 2\alpha') & \text{if } i = 2 \\ \frac{2H}{\alpha'} & \text{if } i = 3 \\ \frac{H}{2}\left[1 - \frac{1}{(1+2\alpha')^2}\right] & \text{if } i = 4. \end{cases} \tag{5.13}$$

Take note that these probabilities contain the total Klein-Nishina cross section.

In order for this method to work, all of the probabilities must be positive. There-

*For a description of all sampling methods that one can use, please refer to refs. [2, 5, 29, 30].

fore, p_2 and p_4 impose limits on the values of α' where this method can be used. The probability p_2 is the more restrictive of the two. When the value of α' is less than $(1+\sqrt{3})$, p_2 will be negative and the method cannot be used. This corresponds to a photon energy of about 1.4 MeV. Below this energy another method must be used, which will be discussed shortly.

Once an i has been selected, the value of x is sampled from the inverse CDF of $p_i(\alpha', x)$. The inverse CDFs for the four functions are

$$P_1^{-1}(\alpha', \varepsilon) = 1 + 2\alpha'\varepsilon \tag{5.14}$$

$$P_2^{-1}(\alpha', \varepsilon) = (1 + 2\alpha')^{\varepsilon} \tag{5.15}$$

$$P_3^{-1}(\alpha', \varepsilon) = \frac{1 + 2\alpha'}{1 + 2\alpha'\varepsilon} \tag{5.16}$$

$$P_4^{-1}(\alpha', \varepsilon) = \left[1 - \varepsilon\left(1 - \frac{1}{(1+2\alpha')^2}\right)\right]^{-\frac{1}{2}}. \tag{5.17}$$

The uniform random number in the interval (0,1) required by the inverse CDF method is represented by the variable ε. Evaluating the inverse CDF with a random number yields a value of x from the Klein-Nishina differential cross section. The value of x can then be used to determine the new energy and direction (relative to the current direction) of the photon.

$$\alpha = \frac{\alpha'}{x} \tag{5.18}$$

$$\cos\theta = 1 + \frac{1 - x}{\alpha'} \tag{5.19}$$

When the energy of the incoming photon drops below 1.4 MeV, the rejection method can be used to sample values of x from the Klein-Nishina cross section. Kahn developed a rejection sampling procedure that can be used for any incoming photon energy. However the efficiency of the procedure is highest at lower energies [2, 31]. This procedure is shown in figure 5.1.

When the direct sampling method and the rejection method are used together, one can efficiently sample values from the Klein-Nishina cross section at any incoming photon energy. Figure 5.2 shows the efficiency of both Kahn's rejection sampling procedure and the combined sampling procedure. At around 1.4 MeV, the efficiency of the combined sampling procedure jumps to one because of the switch to the direct sampling method. This is a considerable improvement compared to only using Kahn's method.

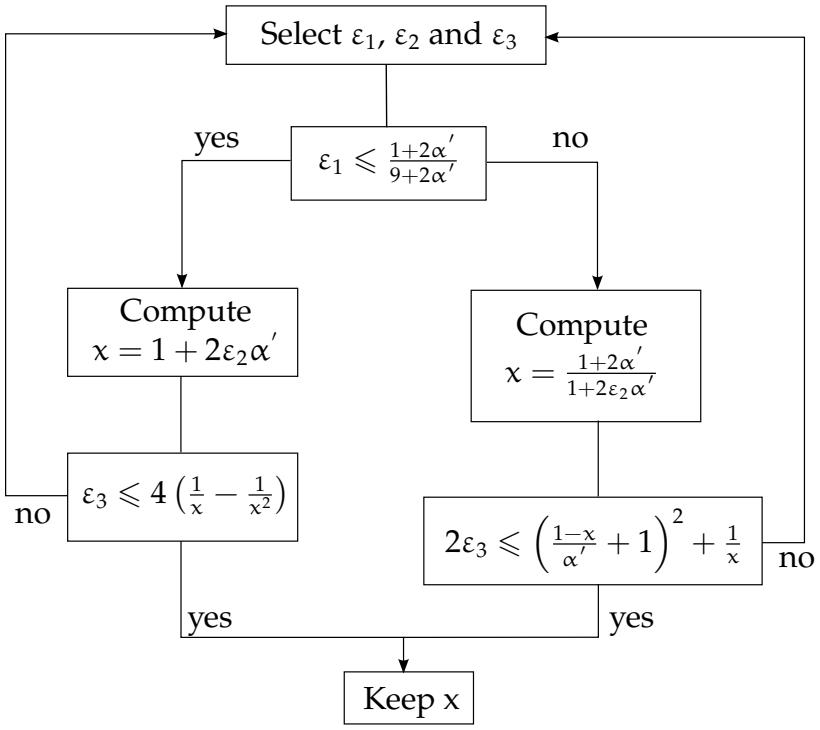

Figure 5.1: **Kahn's Rejection Sampling Procedure**. *This sampling procedure is used to sample a value of x from the differential Klein-Nishina cross section. One can use this sampling procedure at any incoming particle energy, however the efficiency of the procedure degrades at higher energies [2].*

Once an outgoing angle and energy have been selected from the PDF corresponding to the differential Klein-Nishina cross section, the rejection function $R(y, Z)$ from equation 5.5 must be used to determine if the outgoing energy and angle should be kept. This rejection function will affect the efficiency of the overall sampling procedure described by equation 5.5. Figure 5.3 shows the efficiency of the overall sampling procedure for a free electron, Aluminum and Lead. For lower energies and higher atomic numbers, the rejection function causes a large decrease in the efficiency of the sampling procedure compared to the free electron case (where the rejection function is equal to unity at all energies).

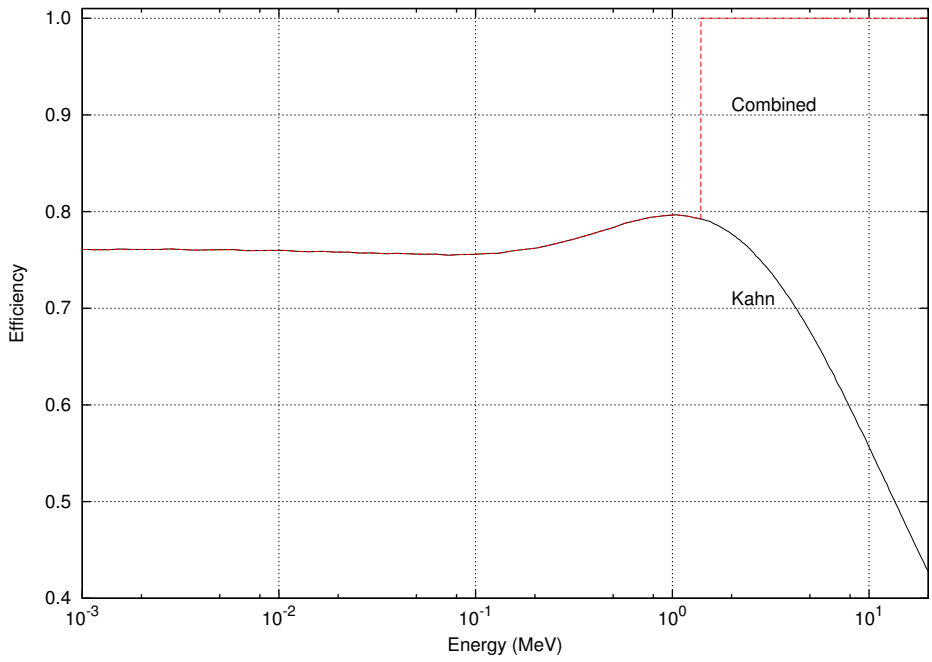

Figure 5.2: **Differential Klein-Nishina cross section sampling procedure efficiencies.** *The efficiency of Kahn's rejection sampling procedure is shown for energies between one keV and twenty MeV. The efficiency of this procedure begins to decline around a few MeV. When it is combined with Koblinger's direct sampling method, which can only be used above about 1.4 MeV, a very efficient sampling method is obtained for all photon energies.*

5.2 Doppler Broadening of Incoherently Scattered Photons

As mentioned in the previous section, the differential Klein-Nishina cross section assumes that the electron upon which the photon scatters is free and at rest. Atomic electrons are bound and consequently cannot be at rest. When the energy of the incoming photon is much greater than the binding energies of the electrons in the atom, binding effects are negligible and the incoherent cross section becomes simply the atomic number times the Klein-Nishina cross section. However, when the incoming photon energy is on the order of a few hundred keV or lower, binding effects must be taken into account [32]. Taking binding effects into account results in three significant changes to the simulated transport process. First, electron binding results in a reduction in the total incoherent cross section, which in turn results in larger mean free paths for the photon as it travels through the medium. This occurs because part of the differential cross section is suppressed because it would result

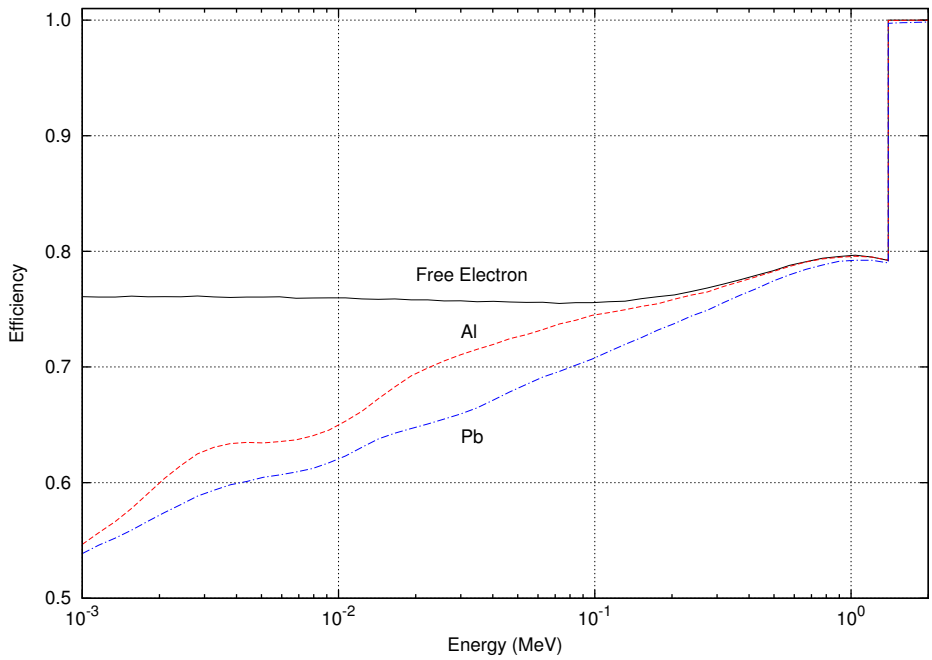

Figure 5.3: **Differential incoherent cross section sampling procedure efficiency.** *The efficiency of the combined method for sampling from the differential Klein-Nisha cross section with the subsequent evaluation of the rejection function (based on the scattering function) is shown. At lower energies and higher atomic numbers, the rejection function has a more deleterious effect on the sampling efficiency compared to the free electron case.*

in energetically impossible scattering events*. Second, the angular distribution of the scattered photon is modified, particularly in the forward direction. Finally, the Compton-scattered photon energy is broadened by the pre-collision motion of the electron [32]. In other words, the one-to-one correspondence between the outgoing photon direction and energy is broken and for each outgoing direction, there is an associated distribution of outgoing photon energies. The first two changes were taken into account in the last section by multiplying the differential Klein-Nishina cross section by the scattering function. In this section, the energy distribution will be dealt with.

To take into account the energy distribution, a double differential incoherent scattering cross section must be used. Using the Born and impulse approximations, Ribberfors was able to derive a double differential incoherent scattering cross section,

*Because the atomic system is a quantum-mechanical system, enough energy must be given to the electron to free it. Otherwise a reaction will not occur.

which is

$$\left(\frac{d^2\sigma(\alpha,\alpha',\theta,Z)}{d\Omega dE}\right)_i = \frac{r_e^2}{2c\left|\vec{\alpha'}-\vec{\alpha}\right|}\left(\frac{\alpha}{\alpha'}\right)\left(\frac{\alpha'}{\alpha_c}+\frac{\alpha_c}{\alpha'}-1+\cos^2\theta\right)J_i(p_z,Z) \quad (5.20)$$

[33]. This double differential cross section is given for each subshell of the atom, denoted by i. The value α_c is called the Compton line, which is the outgoing photon energy (divided by the electron rest mass) corresponding to the outgoing scattering angle assuming that the electron was stationary and free. The variable α is the true outgoing photon energy resulting from the collision with a bound, moving electron.

The function $J_i(p_z,Z)$ is the Compton profile for the i^{th} electron subshell for element Z. The argument p_z is the projection of the electron's initial momentum on the scattering vector $\vec{\alpha'}-\vec{\alpha}$. Because of the quantum mechanical nature of the atomic system, the electrons in each subshell have an associated probability distribution in momentum space, which is often denoted $n_i(\vec{p},Z)$. The Compton profile is simply the projection of this probability distribution along the scattering vector:

$$J_i(p_z,Z) = \int_{p_x}\int_{p_y} n_i(p_x,p_y,p_z,Z)\,dp_x\,dp_y \quad (5.21)$$

[34].

For the purposes of sampling from this double differential cross section it will be more useful to do a change of variables from outgoing energy to electron momentum projection p_z. Using conservation of energy and momentum, an equation for the electron momentum projection can be determined:

$$\begin{aligned} p_z &= m_e c\frac{\alpha-\alpha'+\alpha'\alpha(1-\cos\theta)}{\left|\vec{\alpha'}-\vec{\alpha}\right|} \\ &= m_e c\frac{\alpha-\alpha'+\alpha'\alpha(1-\cos\theta)}{\sqrt{\alpha'^2+\alpha^2-2\alpha'\alpha'^2\cos\theta}}. \end{aligned} \quad (5.22)$$

This derivation of this equation is shown in Appendix A.

The derivative of the electron momentum projection with respect to the outgoing photon energy is

$$\frac{dp_z}{d\alpha} = m_e c\frac{1+\alpha'(1-\cos\theta)}{\left|\vec{\alpha'}-\vec{\alpha}\right|} - p_z\frac{\left(\alpha-\alpha'\cos\theta\right)}{\left|\vec{\alpha'}-\vec{\alpha}\right|^2}. \quad (5.23)$$

Ribborfors suggested a simplification to this derivative based on some observations about the Compton profiles [33]. First, the Compton profiles are even functions. Therefore, the odd moments of p_z will be zero. Second, the Compton profiles drop off fairly rapidly so that the first moment can be approximated as

$$\langle p_z \rangle \approx \int_{-\infty}^{p_{i,max}} p_z J(p_z) dp_z = 0. \tag{5.24}$$

The limit of integration $p_{i,max}$ will be explained shortly. The second term in equation 5.23 can therefore be ignored because it will not contribute significantly to the total incoherent cross section:

$$\begin{aligned} \frac{dp_z}{d\alpha} &= m_e c \frac{1 + \alpha'(1 - \cos\theta)}{\left|\vec{\alpha'} - \vec{\alpha}\right|} \\ &= \frac{m_e c \alpha'}{\alpha_c \left|\vec{\alpha'} - \vec{\alpha}\right|}. \end{aligned} \tag{5.25}$$

Now the change of variables in the double differential cross section can be completed:

$$\begin{aligned} \left(\frac{d^2\sigma(p_z, \theta, Z)}{d\Omega dp_z}\right)_i &= \left(\frac{d^2\sigma(\alpha, \alpha', \theta, Z)}{d\Omega dE}\right)_i \frac{dE}{d\alpha}\frac{d\alpha}{dp_z} \\ &= \frac{r_e^2}{2}\left(\frac{\alpha\alpha_c}{\alpha'^2}\right)\left(\frac{\alpha'}{\alpha_c} + \frac{\alpha_c}{\alpha'} - 1 + \cos^2\theta\right) J_i(p_z, Z) \end{aligned} \tag{5.26}$$

[33].

The differential incoherent scattering cross section from the previous section can be recovered by integrating over all possible electron momentum projections and by summing up the resulting differential cross section for each shell. Because α and p_z are related by equation 5.22, this integral will be quite complicated. Fortunately, Ribberfors has shown that using the approximation $\alpha_c \approx \alpha$ results in negligible errors in the total incoherent scattering cross section [33]. The limit of integration $p_{i,max}$ is the maximum electron momentum projection that can occur. This maximum occurs when the outgoing photon energy is equal to $E - E_{i,b}$, where $E_{i,b}$ is the binding energy for the particular subshell. Unfortunately, $p_{i,max}$ is a function of θ

so this integral will still be complicated:

$$\begin{aligned}\frac{d\sigma_{i.s.}(\alpha',\theta,Z)}{d\Omega} &= \frac{r_e^2}{2}\left(\frac{\alpha_c}{\alpha'}\right)^2\left(\frac{\alpha'}{\alpha_c}+\frac{\alpha_c}{\alpha'}-1+\cos^2\theta\right)\sum_i\int_{-\infty}^{p_{i,max}} J_i(p_z,Z)dp_z \\ &= \frac{d\sigma_{K.N.}(\alpha',\theta)}{d\Omega}S^I(y,Z) \\ &= \frac{d\sigma_{K.N.}(\alpha',\theta)}{d\Omega}S(y,Z).\end{aligned}$$

The scattering function $S^I(y,Z)$ is the scattering function from the impulse approximation. The scattering function that is given in most tables and is recommended for use in Monte Carlo codes is based on the Waller-Hartree theory. Both of these scattering functions have been shown to be in close agreement for many elements though, which is why a direct substitution is justified [32].

The method proposed by Namito et al. for sampling an outgoing photon energy from the double differential incoherent cross section will now be discussed [32]. The first step is to sample an outgoing scattering angle from the differential incoherent cross section using the methods from the previous section. Next, the subshell containing the electron upon which the photon will scatter must be sampled. The most accurate way to sample the subshell would be to create a discrete PDF based on the total incoherent cross section for each subshell. This data isn't readily available in the popular tables [35]. The approximation used by Namito et al., which is only truly applicable when the incoming photon energy is much greater than the binding energy of the electron, is to sample the electron shell based on the number of electrons present in each shell (given as n_i):

$$\begin{aligned}p(i) &= \frac{(\sigma_{i.c.})_i}{\sigma_{i.c.}} \\ &\approx \frac{\sigma_{K.N.}n_i}{\sigma_{K.N.}Z} \\ &\approx \frac{n_i}{Z}.\end{aligned} \tag{5.27}$$

Finally, an outgoing photon energy must be sampled from the double differential incoherent cross section. A conditional PDF for the outgoing photon energy can be created by dividing the double differential incoherent cross section by the differential

incoherent cross section evaluated at a particular angle:

$$\begin{aligned} p_i(p_z, Z \mid \theta) &= \left(\frac{d\sigma_{i.s.}(\alpha', \theta, Z)}{d\Omega}\right)_i^{-1} \left(\frac{d^2\sigma(\alpha, \alpha', \theta, Z)}{d\Omega dp_z}\right)_i \\ &= \left(\frac{\alpha_c \alpha}{\alpha'^2}\right) \left(\frac{\alpha'}{\alpha_c}\right)^2 \frac{J_i(p_z, Z)}{S_i(y, Z)} \\ &= (1 + \alpha' \cos\theta) \left(\frac{\alpha}{\alpha'}\right) \left(\frac{J_i(p_z, Z)}{\int_{-\infty}^{p_{i,max}} J_i(p_z, Z) dp_z}\right) \\ &= C(\alpha', \theta) R(\alpha, \alpha') p(p_z, Z). \end{aligned} \tag{5.28}$$

The value of $p_{i,max}$ is calculated from the equation for p_z using the value of θ that was sampled and the substitution $\alpha = \alpha' - \frac{E_{i,b}}{m_e c^2}$.

One must sample a value of p_z from the PDF $p(p_z, Z)$ to determine the outgoing photon energy. Once the outgoing photon energy has been determined the rejection function $R(\alpha, \alpha')$ is used to determine if the value should be accepted or rejected. The CDF corresponding to the PDF for p_z is*:

$$P(p_z, Z) = \frac{\int_{-\infty}^{p_z} J_i(x, Z) dx}{\int_{-\infty}^{p_{i,max}} J_i(x, Z) dx}. \tag{5.29}$$

Because the Compton profiles are most commonly found in tabular form†, a table method must be used to sample the value of p_z. One first finds the value of the CDF corresponding to the momentum projection $p_{i,max}$. Then one finds the momentum projection associated with the CDF value $\varepsilon \int_{-\infty}^{p_{i,max}} J_i(x, Z) dx$, where ε is again a uniform random number. Using a standard binary search algorithm, this process can be done very efficiently.

The equation for the outgoing photon energy in terms of the momentum projec-

*Namito et al. actually recommend the CDF $\frac{\int_0^{p_z} J_i(x,Z) dx}{\int_0^{p_{i,max}} J_i(x,Z) dx}$, which appears to be an error.

†Biggs et al. have compiled the Compton profiles for atomic numbers 1-102[36].

tion is simply:

$$\alpha = \frac{-b}{2a} \pm \frac{\sqrt{b^2 - 4ac}}{2a} \tag{5.30}$$

where

$$a = \left(\frac{p_z}{m_e c}\right)^2 - \left(\frac{\alpha'}{\alpha_c}\right)^2$$

$$b = -2\alpha' \left[\left(\frac{p_z}{m_e c}\right)^2 \cos\theta + \frac{\alpha'}{\alpha_c}\right]$$

$$c = \alpha'^2 \left[\left(\frac{p_z}{m_e c}\right)^2 - 1\right].$$

When both values are energetically possible, one of the values must be randomly selected (with probability one half).

5.3 Coherent Scattering

Coherent or Rayleigh scattering occurs when a photon scatters off of an atom with negligible energy loss. It occurs rarely except for when low energy (keV) photons pass through a high atomic number material [2]. The differential coherent cross section (per atom) is usually expressed as a product of the classical Thompson differential cross section per electron and the atomic form factor squared. The differential coherent cross section is

$$\begin{aligned}\frac{d\sigma_{c.s.}(\alpha', \theta, Z)}{d\Omega} &= \frac{d\sigma_{Th.}(\theta)}{d\Omega} F^2(y, Z) \\ &= \frac{r_e^2}{2}(1 + \cos^2\theta) F^2(y, Z)\end{aligned} \tag{5.31}$$

[2]. The value r_e is the classical radius of the electron. The arguments of the atomic form factor are

$$y = \sin\frac{\theta}{2}/\lambda' \tag{5.32}$$

and Z, the atomic number.

A PDF for the outgoing photon angle can be created by dividing the differential coherent cross section by the total coherent cross section at the incoming photon energy. This PDF can be reorganized in an analogous way to the PDF for the

incoherent scattering cross section:

$$\begin{aligned} p(\alpha^{'}, \theta, Z) &= \frac{1}{\sigma_{c.s.}(\alpha^{'}, Z)} \frac{d\sigma_{c.s.}(\alpha^{'}, \theta, Z)}{d\Omega} \\ &= \frac{F^2_{max}(y, Z)\sigma_{Th.}(\theta)}{\sigma_{c.s.}(\alpha^{'}, Z)} \left[\frac{F^2(y, Z)}{F^2_{max}(y, Z)}\right] \left[\frac{1}{\sigma_{Th.}(\theta)} \frac{d\sigma_{Th.}(\theta)}{d\Omega}\right] \\ &= C(\alpha^{'}, Z)R(y, Z)p_{Th.}(\theta). \end{aligned}$$

Values of the scattering angle can be sampled from the PDF of the classical Thompson differential scattering cross section using a combination of the probability mixing and inverse CDF methods. Unfortunately, the rejection function R(y,Z) created from the atomic form factor that would be used with this method has a very low efficiency. Figure 5.4 shows the efficiency of this sampling procedure for aluminum and lead.

Another sampling procedure, which is much more efficient, exists [27]. This procedure requires that the PDF for the outgoing photon angle be changed to a PDF in terms of the atomic form factor argument squared:

$$\begin{aligned} y^2 &= \frac{\sin^2\left(\frac{\theta}{2}\right)}{\lambda^{'2}} \\ dy^2 &= \frac{\sin\theta}{2\lambda^{'2}} d\theta \end{aligned} \tag{5.33}$$

The following changes of variables need to be conducted to get the desired PDF:

$$\begin{aligned} p(\alpha^{'}, \theta, Z)d\theta &= p(\alpha^{'}, \theta, Z)d\Omega \\ &= \frac{\pi r_e^2}{\sigma_{c.s.}(\alpha^{'}, Z)}(1 + \cos^2\theta)F^2(y, Z)\sin\theta d\theta \\ p(\alpha^{'}, y^2, Z)dy^2 &= p(\alpha^{'}, \theta, Z)d\theta \\ &= \frac{2\pi r_e^2 \lambda^{'2}}{\sigma_{c.s.}(\alpha^{'}, Z)}(1 + \cos^2\theta)F^2(y, Z)dy^2. \end{aligned} \tag{5.34}$$

Now the PDF in terms of the atomic form factor argument squared can be reorganized into a PDF for sampling the atomic form factor argument squared and a

rejection function:

$$p(\alpha', y^2, Z) = \frac{4\pi r_e^2 \lambda'^2 \int_0^{y^2_{max}} F^2(y, Z)dy^2}{\sigma_{c.s.}(\alpha', Z)} \left[\frac{1+\cos^2\theta}{2}\right] \left[\frac{F^2(y, Z)}{\int_0^{y^2_{max}} F^2(y, Z)dy^2}\right]$$
$$= C(\alpha', Z)R(\cos\theta)p(y^2, Z). \quad (5.35)$$

To sample the outgoing photon direction, one first samples a squared argument from the PDF $p(y^2, Z)$. Then one uses the rejection function $R(\cos\theta)$ with the angle cosine corresponding to the squared argument

$$\cos\theta = 1 - 2\lambda'^2 y^2, \quad (5.36)$$

to determine if it should be accepted or rejected.

The CDF that would be used to sample a squared argument is simply

$$P(y^2, Z) = \frac{\int_0^{y^2} F^2(x, Z)dx^2}{\int_0^{y^2_{max}} F^2(x, Z)dx^2}. \quad (5.37)$$

Persliden recommended approximating the corresponding inverse CDF with polynomials and to then use the polynomials for sampling [27]. Another method that can be used is to create a new data table for each element that gets stored along with all of the other cross section tables. The independent variable of this table is y^2 and the dependent variable is $\int_0^{y^2} F^2(y, Z)dy^2$. To sample from this table, one finds the dependent value associated with y^2_{max}. Then one finds the independent value associated with the value $\varepsilon \int_0^{y^2_{max}} F^2(y, Z)dy^2$, where ε is a random number. By using a standard binary search, this method can be done very efficiently. In addition, the computation of the table only needs to be done once for each element.

Figure 5.4 shows the efficiency of Persliden's sampling method and the efficiency of the naive method that was discussed first.

5.4 Pair Production

Pair production occurs when the photon interacts with the electric field of an atom (screened nuclear field) producing an electron-positron pair. It can be subdivided into two separate phenomenon depending on the state of the atom after the interaction [37]. Coherent pair production occurs when the entire atom recoils from the interaction without any internal excitation. Incoherent pair production occurs

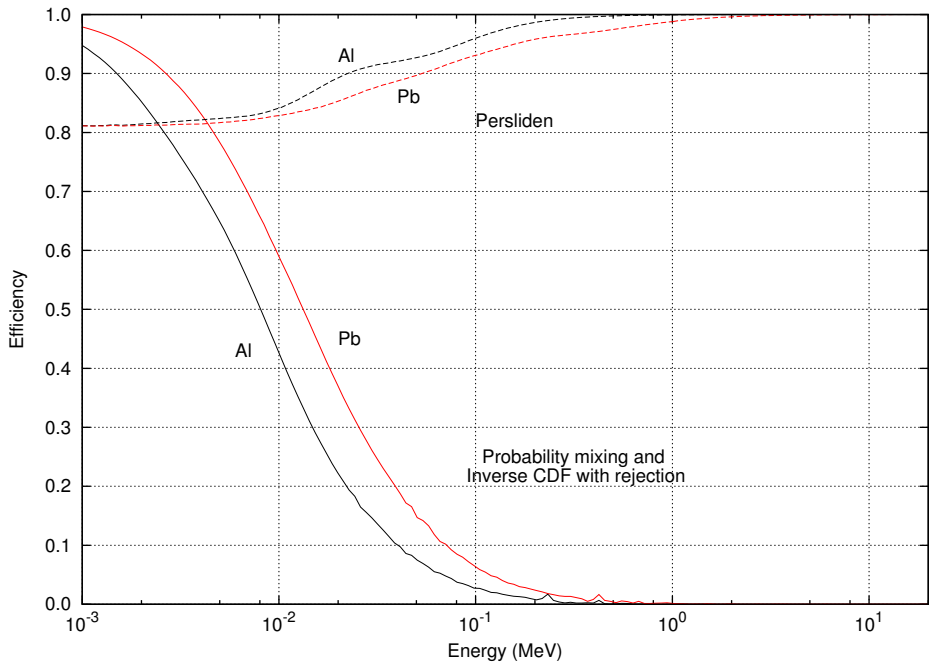

Figure 5.4: **Differential coherent cross section sampling procedure efficiencies.** *The efficiency of the probability mixing and inverse CDF sampling method with the atomic form factor rejection function and the efficiency of Persliden's sampling method is shown for energies between one keV and twenty MeV. Persliden's method is far superior as it has a high efficiency at all energies.*

when the atom is left in an excited or ionized state. Pair production resulting in the ionization of an atom is often called triplet production because three outgoing particles (two electrons and one positron) result from the interaction. However, triplet production is commonly used to refer to incoherent pair production (excitation and ionization).

The threshold for coherent pair production is $2m_ec^2$. The threshold for incoherent pair production is only slightly higher than the threshold for coherent pair production [37]. This is significantly different than the threshold for pair production in the field of a free electron (triplet production), which is $4m_ec^2$. However, the cross section for incoherent pair production below $4m_ec^2$ is very small and is usually neglected in data tables [37].

When one is conducting coupled photon-electron transport, the energy and direction of the outgoing electron and positron must be sampled. This can be done using the Bethe-Heitler expression for the coherent pair production cross section [38, 39]. When one is only interested in the transport of photons in the system, the

pair production cross section can be formulated differently. Several assumptions will be made in the formulation of this approximate cross section. The first is that the electron and positron deposit all of their energy locally (they stop immediately after being created). Since the mean free paths of electrons are generally much smaller than photons, this assumption is usually acceptable. The second is that the positron will only annihilate once its kinetic energy is essentially zero. In other words, the annihilation of positrons in flight will be neglected. This results in a very simple (isotropic) angular distribution of the annihilation photons. The final approximation is that the directions of the resulting annihilation photons are uncorrelated with the initial photon direction. Because of the torturous path taken by a typical electron or positron, this approximation is usually acceptable as well. The simplified treatment allows the pair production and triplet production cross sections to be combined into a single cross section. The resulting double differential pair production cross section is

$$\frac{d^2\sigma_{p.p.}(E', Z)}{d\Omega dE} = \frac{2[\sigma_{p.p.}(E', Z) + \sigma_{t.p.}(E', Z)]\delta(E - m_e c^2)}{4\pi} \tag{5.38}$$

[25, 40]. Note that the double differential pair production cross section contains the factor two to denote that two photons are created from the reaction.

During a random walk, a single outgoing photon can be followed as long as its weight is multiplied by two. Otherwise two photons must be followed. Both outgoing photons will have an outgoing energy equal to $m_e c^2$ as indicated by the delta function in the pair production cross section. The first photon will then have its outgoing direction sampled from an isotropic distribution. The direction of the second photon will then simply be the opposite direction of the first photon in accordance with conservation of momentum (and under the assumption that the positron-electron pair that annihilated had negligible momentum).

5.5 The Photoelectric Effect

The photoelectric effect occurs when a photon of energy E is absorbed by a target atom, which makes a transition to an excited state or becomes ionized. When ionization occurs, the ejected electron will have energy equal to the absorbed photon minus the binding energy of the electron. Atomic relaxation will occur after the vacancy has been created. This process results in the emission of Auger electrons and x-rays. The x-rays may be of significance in low energy photon simulations,

especially when high atomic number elements are present. It is therefore necessary to conduct a more detailed treatment of the photoelectric effect in photon transport codes. Salvat et al. recommended a procedure in which only the K and L shells are treated in a detailed way [39]. The outer shells are treated together. The PDF for selecting the shell containing the electron that is ejected is

$$p(i) = \begin{cases} \frac{\sigma_{i,pe}(E',Z)}{\sigma_{pe}(E',Z)} & \text{for K, L1, L2 or L3 shells} \\ 1 - p_K - p_{L1} - p_{L2} - p_{L3} & \text{otherwise.} \end{cases} \tag{5.39}$$

When ionization occurs in the K or L shell, the energy of the ejected electron is equal to the energy of the photon minus the binding energy of the particular shell. While this is also true for the outer shells, the binding energies are small enough that they can be neglected. If coupled photon-electron transport is not being conducted then all emitted electrons are ignored. When the K or L shells become ionized, the subsequent atomic relaxation has the possibility to result in the emission of x-rays with energy that can be significant depending on the calculation being done and must therefore be simulated. The emission of particles from atomic relaxation resulting from vacancies in the outer shells will always be ignored because of the low energy of these particles. The direction of all particles emitted from the relaxation process should be sampled from an isotropic distribution [39].

5.6 Photonuclear Absorption

Photonuclear absorption occurs when a gamma ray is absorbed by the nucleus of an atom resulting in the emission of one or more neutrons, charged particles or additional gamma rays. These reactions generally have small cross-sections and are usually neglected in photon transport codes. However, the cross sections do exhibit broad resonances in the 12 to 24 MeV energy range [2]. For high energy coupled neutron-photon transport this interaction can be important to include.

5.7 Other Interactions

There are many more interactions that can occur between a photon and an atom. These processes include Delbrück scattering, Raman scattering*, and photomeson

*Raman scattering is an inelastic scattering process that leaves the target atom in an excited state instead of ionized [35].

production. All of these interactions contribute less than 1% to the total cross section and are therefore neglected [2].

5.8 Adjoint Incoherent Scattering

To simulate adjoint incoherent scattering the differential adjoint incoherent scattering cross section must be derived using equations 4.41 and 4.42 from chapter 4. The mechanics of the interaction will be the same, except that they will proceed in reverse. In other words, an electron and photon will now interact at a point resulting in a single outgoing photon of higher energy. As mentioned previously, electron transport will be ignored so the electron will be ignored in the process. The collision mechanics are described in the following equation:

$$E = \frac{E'}{1 - \alpha'(1 - \cos\theta)} \tag{5.40}$$

[25]. This equation can be found by solving equation 5.4 for the incoming energy (and switching primed variables). This equation is interesting in that it exhibits a discontinuity when

$$\cos\theta = 1 - \frac{1}{\alpha'}. \tag{5.41}$$

Any value of $\cos\theta$ less than the above value will result in nonphysical (negative) energies. Acceptable values of $\cos\theta$ that approach the above value will result in very large outgoing adjoint photon energies.

Because of the discontinuity in the equation for the outgoing adjoint photon energy, the adjoint Compton scattering process is bound by a minimum scattering angle and not a minimum energy. The minimum angle is

$$\mu_{min} = \begin{cases} -1 & \text{if } \alpha' < \frac{1}{2} \\ 1 - \frac{1}{\alpha'} & \text{if } \alpha' \geqslant \frac{1}{2}. \end{cases} \tag{5.42}$$

The variable μ represents the cosine of the polar scattering angle. The maximum angle cosine is still unity.

The adjoint differential incoherent scattering cross section must now be derived

using the definition of the adjoint cross section from equations 4.41 and 4.42:

$$\begin{aligned} p^{\dagger}_{i.s}(E^{'} \rightarrow E, \hat{\Omega}^{'} \rightarrow \hat{\Omega}) &= \frac{\sigma_{i.s.}(E)c_{i.s.}(E)p_{i.s.}(E \rightarrow E^{'}, \hat{\Omega} \rightarrow \hat{\Omega}^{'})}{\sigma^{\dagger}_{i.s.}(E^{'})} \\ \sigma^{\dagger}_{i.s.}(E^{'})p^{\dagger}_{i.s}(E^{'} \rightarrow E, \hat{\Omega}^{'} \rightarrow \hat{\Omega}) &= \sigma_{i.s.}(E)c_{i.s.}(E)p_{i.s.}(E \rightarrow E^{'}, \hat{\Omega} \rightarrow \hat{\Omega}^{'}) \\ \sigma^{\dagger}_{i.s}(E^{'} \rightarrow E, \hat{\Omega}^{'} \rightarrow \hat{\Omega}) &= \sigma_{i.s.}(E \rightarrow E^{'}, \hat{\Omega} \rightarrow \hat{\Omega}^{'}). \end{aligned} \tag{5.43}$$

Generally, cross sections that are encountered are not dependent on the initial and final direction of the particle but on the cosine of the angle between these two directions. This is indeed what is observed in the incoherent scattering cross section for photons. Therefore, the relationship between the adjoint double differential incoherent scattering cross section and the double differential incoherent scattering cross section becomes

$$\begin{aligned} \sigma^{\dagger}_{i.s}(E^{'} \rightarrow E, \hat{\Omega}^{'} \rightarrow \hat{\Omega}) &= \sigma_{i.s.}(E \rightarrow E^{'}, \hat{\Omega} \rightarrow \hat{\Omega}^{'}) \\ \sigma^{\dagger}_{i.s}(E^{'} \rightarrow E, \hat{\Omega}^{'} \cdot \hat{\Omega}) &= \sigma_{i.s.}(E \rightarrow E^{'}, \hat{\Omega} \cdot \hat{\Omega}^{'}) \\ \sigma^{\dagger}_{i.s}(E^{'} \rightarrow E, \mu) &= \sigma_{i.s.}(E \rightarrow E^{'}, \mu), \end{aligned} \tag{5.44}$$

where μ is the cosine of the angle between the incoming and outgoing directions. A further simplification can be made by noting that the outgoing direction and energy are coupled in incoherent scattering. Therefore the differential incoherent scattering cross section differential in energy only can completely describe the interaction:

$$\begin{aligned} \sigma^{\dagger}_{i.s.}(E^{'} \rightarrow E) &= \sigma_{i.s.}(E \rightarrow E^{'}) \\ \frac{d\sigma^{\dagger}_{i.s.}(E^{'}, E, Z)}{dE} &= \frac{d\sigma_{i.s.}(E, E^{'}, Z)}{dE^{'}} \end{aligned} \tag{5.45}$$

The incoherent scattering cross section differential in outgoing energy, which was not shown in section 5.1, is

$$\frac{d\sigma_{i.s.}(\alpha^{'}, \alpha, Z)}{dE} = \frac{\pi r_e^2}{m_e c^2 \alpha'^2}\left[\frac{\alpha}{\alpha^{'}} + \frac{\alpha^{'}}{\alpha} - 1 + \cos^2\theta\right] S(y, Z). \tag{5.46}$$

From this equation, the adjoint differential incoherent scattering cross section is simply

$$\frac{d\sigma^{\dagger}_{i.s.}(\alpha^{'}, \alpha, Z)}{dE} = \frac{\pi r_e^2}{m_e c^2 \alpha^2}\left[\frac{\alpha^{'}}{\alpha} + \frac{\alpha}{\alpha^{'}} - 1 + \cos^2\theta\right] S(y, Z). \tag{5.47}$$

To construct this equation, all of the primed and unprimed variables in the previous

equation are switched in accordance with equation 5.45. It must also be noted that the first argument of the scattering function is now

$$y = \sin\frac{\theta}{2}/\lambda, \tag{5.48}$$

which is dependent on the outgoing photon wavelength.

A PDF for the outgoing energy can now be created, which will have a similar form to the PDF from equation 5.5 for incoherent scattering:

$$\begin{aligned} p^{\dagger}(\alpha|\alpha^{'}, Z) &= \frac{1}{\sigma^{\dagger}_{i.s.}(\alpha', Z)}\frac{d\sigma^{\dagger}_{i.s.}(\alpha^{'}, \alpha, Z)}{dE} \\ &= \frac{S_{max}(y, Z)\sigma^{\dagger}_{K.N.}(\alpha^{'})}{\sigma^{\dagger}_{i.s.}(\alpha', Z)}\left[\frac{S(y, Z)}{S_{max}(y, Z)}\right]\left[\frac{1}{\sigma^{\dagger}_{K.N.}(\alpha')}\frac{d\sigma^{\dagger}_{K.N.}(\alpha^{'}, \alpha)}{dE}\right] \\ &= C^{\dagger}(\alpha^{'}, Z)R(y, Z)p^{\dagger}_{K.N.}(\alpha|\alpha^{'}). \end{aligned} \tag{5.49}$$

Now, one samples an outgoing energy from the PDF $p^{\dagger}_{K.N.}(\alpha|\alpha^{'})$ and this energy is either accepted or rejected based on the rejection function $R(y, Z)$.

Using a similar change of variables to the one done for the differential Klein-Nishina cross section, the differential adjoint Klein-Nishina cross section can be written in terms of an inverse energy gain ratio:

$$\frac{1}{x} = \frac{\alpha}{\alpha^{'}} \tag{5.50}$$

$$x = 1 - \alpha^{'}(1 - \cos\theta). \tag{5.51}$$

The differential adjoint Klein-Nishina cross section can then be written as (see

Appendix A):

$$\frac{d\sigma^{\dagger}_{K.N.}(\alpha',x)}{dx} = K^{\dagger}\left[A^{\dagger}x^2 + B^{\dagger}x + C^{\dagger} + \frac{D^{\dagger}}{x}\right] \tag{5.52}$$

where

$$K^{\dagger} = \frac{\pi r_e^2}{\alpha'}$$
$$A^{\dagger} = \frac{1}{\alpha'^2}$$
$$B^{\dagger} = 1 + \frac{2(\alpha' - 1)}{\alpha'^2}$$
$$C^{\dagger} = \frac{1 - 2\alpha'}{\alpha'^2}$$
$$D^{\dagger} = 1.$$

Now, a PDF for x can be created if the differential adjoint Klein-Nishina cross section is divided by the total adjoint Klein-Nishina cross section. The total adjoint Klein-Nishina cross section can be found by integrating the differential Klein-Nishina cross section from $x_{min} = 1 - \alpha'(1 - \mu_{min})$ to $x_{max} = 1$. Unfortunately, when the initial energy of the adjoint photon is greater than $\frac{1}{2}m_e c^2$, the total adjoint Klein-Nishina cross section will be infinite. The cross section can be bounded if a maximum energy is set, which is an acceptable requirement since every physical problem will have a maximum source energy. Associated with this maximum energy will be a new minimum scattering angle cosine and consequently a new minimum inverse energy gain ratio:

$$\alpha_{max} = \frac{\alpha'}{1 - \alpha'(1 - \mu_{min})}$$

and

$$\mu_{min} = \begin{cases} -1 & \text{if } \alpha' < \frac{\alpha_{max}}{1+2\alpha_{max}} \\ 1 - \frac{1}{\alpha'} + \frac{1}{\alpha_{max}} & \text{if } \alpha' \geqslant \frac{\alpha_{max}}{1+2\alpha_{max}} \end{cases} \tag{5.53}$$

$$x_{min} = \begin{cases} 1 - 2\alpha' & \text{if } \alpha' < \frac{\alpha_{max}}{1+2\alpha_{max}} \\ \frac{\alpha'}{\alpha_{max}} & \text{if } \alpha' \geqslant \frac{\alpha_{max}}{1+2\alpha_{max}}. \end{cases} \tag{5.54}$$

The PDF for x can be defined as

$$p^{\dagger}_{K.N.}(x|\alpha', \alpha_{max}) = \begin{cases} H^{\dagger}\left[A^{\dagger}x^2 + B^{\dagger}x + C^{\dagger} + \frac{D^{\dagger}}{x}\right] & \text{if } x_{min} \leqslant x \leqslant 1 \\ 0 & \text{otherwise} \end{cases} \tag{5.55}$$

where

$$H^{\dagger} = \frac{K^{\dagger}}{\sigma^{\dagger}_{K.N.}(\alpha', \alpha_{max})}.$$

A direct inversion of this PDF is not possible. In addition, this PDF cannot be sampled directly using a combination of the probability mixing method and the inverse CDF method. If one were to split the PDF into a part for each term, as is done with the PDF associated with the differential Klein-Nishina cross section, the probability of selecting each part must be positive for the method to work. The probability of selecting the part containing the value $B^{\dagger}$ would only be positive when $\alpha' \geqslant -1 + \sqrt{3}$. The probability of selecting the part containing the value $C^{\dagger}$ would only be positive when $\alpha' \leqslant \frac{1}{2}$. These two constraints cannot be simultaneously satisfied and therefore, the PDF cannot be sampled directly.

The best remaining option is to create a rejection sampling scheme. An effective rejection sampling scheme becomes apparent if one reorganizes the PDF from equation 5.55:

$$\begin{aligned} p^{\dagger}_{K.N.}(x|\alpha', \alpha_{max}) &= \begin{cases} H^{\dagger}\left[x + \frac{1}{x} - 1 + \cos^2\theta\right] & \text{if } x_{min} \leqslant x \leqslant 1 \\ 0 & \text{otherwise} \end{cases} \\ &= \begin{cases} H^{\dagger}\left[\left(\frac{1}{x} - 1\right) + (x) + \left(\cos^2\theta\right)\right] & \text{if } x_{min} \leqslant x \leqslant 1 \\ 0 & \text{otherwise.} \end{cases} \end{aligned} \tag{5.56}$$

This equation has been split into three separate terms, two of which can be sampled from directly to create a very efficient rejection sampling procedure. The rejection sampling scheme is shown in figure 5.5. Refer to appendix A for a derivation of this rejection sampling scheme.

As shown in figure 5.6 (specifically the free electron case), the efficiency of this rejection sampling procedure is very good at all energies. At lower energies and larger atomic numbers, the rejection function $R(y, Z)$, which characterizes electron binding, causes a large decrease in the overall sampling procedure efficiency compared to the free electron case. The overall sampling procedure efficiency is still very good though.

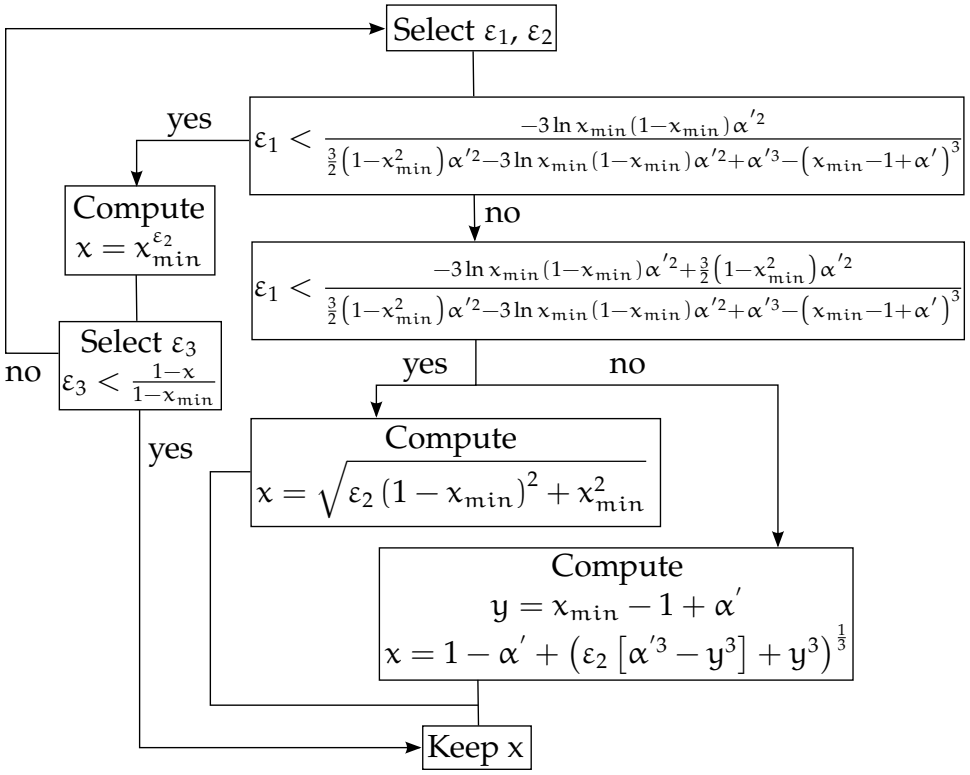

Figure 5.5: **Adjoint Klein-Nishina Rejection Sampling Procedure**. *This sampling procedure is used to sample a value of x from the differential adjoint Klein-Nishina cross section. One can use this sampling procedure at any incoming particle energy.*

Now that the procedure for sampling values from the differential adjoint incoherent cross section has been described, another important part of the adjoint random walk process must be addressed: the evaluation of the adjoint weight factor. To evaluate the adjoint weight factor, the adjoint incoherent cross section must be known. While this cross section is not provided in any of the popular tables, it can be determined by integrating equation 5.47 at an initial energy of interest (or many to create a table). As indicated previously, the adjoint incoherent cross section is a function of the maximum problem energy. Figure 5.7 shows the adjoint incoherent cross section for Aluminum as a function of initial energy and for three maximum problem energies: 1.0 MeV, 10.0 MeV and 20.0 MeV. As the maximum problem energy increases, the spike in the adjoint incoherent cross section centered at $\frac{\alpha_{max}}{1+2\alpha_{max}}$ increases. At the maximum problem energy, the adjoint incoherent cross section goes to zero.

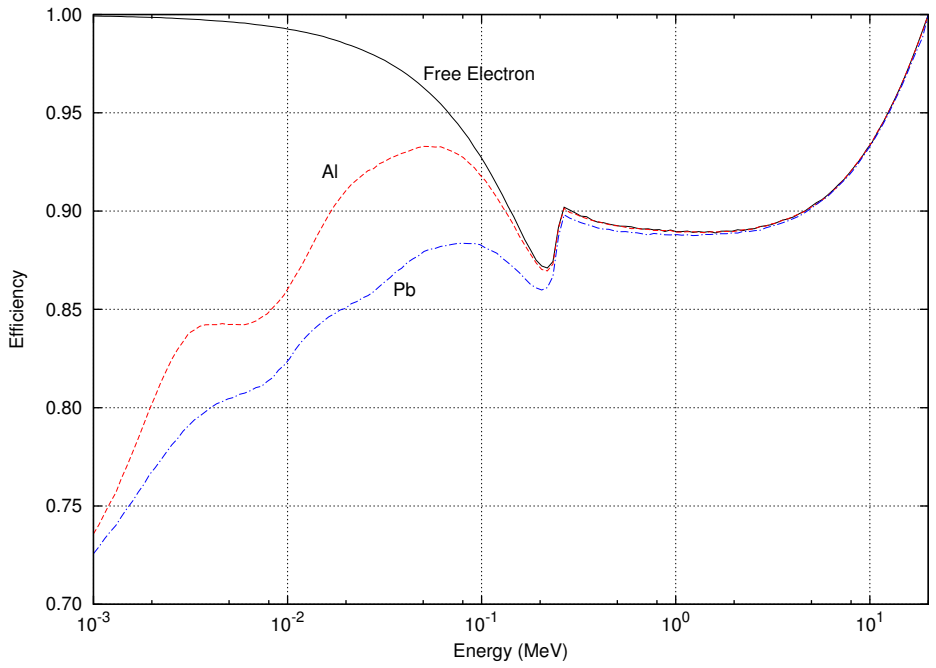

Figure 5.6: **Differential adjoint incoherent cross section sampling procedure efficiencies.** *The efficiency of the rejection sampling procedure for sampling from the differential adjoint Klein-Nishina cross section with the subsequent evaluation of the rejection function (based on the scattering function) is shown for energies between one keV and twenty MeV. At lower energies and higher atomic numbers, the rejection function has a larger effect on the sampling efficiency compared to the free electron case.*

5.9 Doppler Broadening of Incoherently Scattered Adjoint Photons

In section 5.2 Doppler broadening of incoherently scattered photons was discussed. While it hasn't been addressed in the literature yet, this process is also reversible. In this section, some arguments will be made to validate this claim. However, it must be noted that no simulations have been completed yet to confirm the validity of this claim.

In the derivation of the double differential incoherent scattering cross section, Ribberfors used the Born and impulse approximations. The impulse approximation is of particular importance because it allows the system to be treated identically immediately before and immediately after the collision. Therefore, the scattering mechanics using this approximation will be identical for the adjoint process, except that they will happen in reverse. In addition, the double differential incoherent

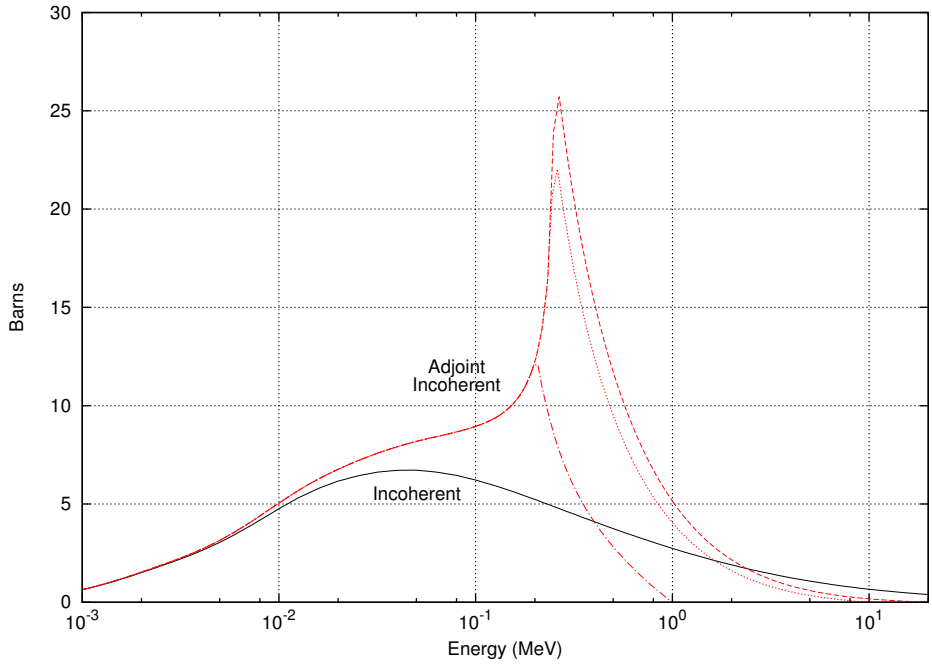

Figure 5.7: **Adjoint incoherent cross section for Aluminum.** *The adjoint incoherent cross section evaluated at a maximum problem energy of 20.0 MeV, 10.0 MeV and 1.0 MeV is shown. As the maximum problem energy increases, the spike in the adjoint incoherent cross section centered at* $\frac{\alpha_{max}}{1+2\alpha_{max}}$ *increases. At the maximum problem energy, the cross section goes to zero.*

scattering cross section is actually differential in the incoming and outgoing photon energy difference [34]. This variable will not change in the double differential adjoint incoherent scattering cross section despite the change in primed and unprimed variables. Before presenting the double differential adjoint incoherent scattering cross section, the adjoint incoherent scattering cross section differential in steradians must be determined. A change of variables will be done using equations 5.47 and 5.40:

$$\frac{d\sigma^{\dagger}_{i.s.}(\alpha', \alpha, Z)}{d\Omega} = \frac{r_e^2}{2}\left[\frac{\alpha'}{\alpha} + \frac{\alpha}{\alpha'} - 1 + \cos^2\theta\right] S(y, Z). \tag{5.57}$$

Now, the double differential adjoint incoherent scattering cross section is

$$\left(\frac{d\sigma^{\dagger}(\alpha', \alpha, \theta, Z)}{d\Omega dE}\right)_i = \frac{r_e^2}{2c\left|\vec{\alpha} - \vec{\alpha'}\right|}\left(\frac{\alpha'}{\alpha}\right)\left(\frac{\alpha'}{\alpha_c} + \frac{\alpha_c}{\alpha'} - 1 + \cos^2\theta\right) J_i(p_z, Z). \tag{5.58}$$

The variable α_c is now the adjoint Compton line, which is the outgoing adjoint photon energy in units of electron rest mass energy corresponding to the outgoing

scattering angle assuming that the electron upon which the adjoint photon scattered was stationary and free (see equation 5.40). The variable p_z is still the electron momentum projection. However, the primed and unprimed variables in equation 5.22 for p_z are switched:

$$\begin{aligned} p_z &= m_e c \frac{\alpha^{'} - \alpha + \alpha\alpha^{'}(1-\cos\theta)}{\left|\vec{\alpha} - \vec{\alpha^{'}}\right|} \\ &= m_e c \frac{\alpha^{'} - \alpha + \alpha\alpha^{'}(1-\cos\theta)}{\sqrt{\alpha^2 + \alpha^{'2} - 2\alpha\alpha^{'}\cos\theta}}. \end{aligned}$$

For the purposes of sampling from the double differential adjoint incoherent cross section, it will again be more useful to do a change of variables from outgoing energy to electron momentum projection p_z. The derivative of p_z with respect to the outgoing adjoint photon energy is

$$\frac{dp_z}{d\alpha} = m_e c \frac{-1 + \alpha^{'}(1-\cos\theta)}{\left|\vec{\alpha} - \vec{\alpha^{'}}\right|} - p_z \frac{\alpha - \alpha^{'}\cos\theta}{\left|\vec{\alpha} - \vec{\alpha^{'}}\right|^2}. \tag{5.59}$$

Using the same simplifications discussed in section 5.2 this derivative can be approximated as

$$\begin{aligned} \frac{dp_z}{d\alpha} &= m_e c \frac{-1 + \alpha^{'}(1-\cos\theta)}{\left|\vec{\alpha} - \vec{\alpha^{'}}\right|} \\ &= -\frac{m_e c \alpha^{'}}{\alpha_c \left|\vec{\alpha} - \vec{\alpha^{'}}\right|}. \end{aligned} \tag{5.60}$$

Now the change of variables in the double differential adjoint cross section can be completed:

$$\begin{aligned} \left(\frac{d\sigma^{\dagger}(p_z,\theta,Z)}{d\Omega dp_z}\right)_i &= \left(\frac{d\sigma^{\dagger}(\alpha^{'},\alpha,\theta,Z)}{d\Omega dE}\right)_i \frac{dE}{d\alpha}\left|\frac{d\alpha}{dp_z}\right| \\ &= \frac{r_e^2}{2}\left(\frac{\alpha_c}{\alpha}\right)\left(\frac{\alpha^{'}}{\alpha_c} + \frac{\alpha_c}{\alpha^{'}} - 1 + \cos^2\theta\right) J_i(p_z, Z). \end{aligned} \tag{5.61}$$

The differential adjoint incoherent scattering cross section from equation 5.57 can be recovered by integrating over all possible electron momentum projections and by summing up the resulting differential cross section for each shell. The approximation discussed in section 5.2 that $\alpha_c \approx \alpha$ will be used again here to

simplify the integral. The limit of integration $p_{i,max}$ is the same as before. However, it will now occur when the outgoing adjoint photon energy is equal to $E + E_{i,b}$, where $E_{i,b}$ is the binding energy for the particular subshell:

$$\begin{aligned}\frac{d\sigma^{\dagger}_{i.s.}(\alpha', \theta, Z)}{d\Omega} &= \frac{r_e^2}{2}\left[\frac{\alpha'}{\alpha} + \frac{\alpha}{\alpha'} - 1 + \cos^2\theta\right]\sum_i \int_{-\infty}^{p_{i,max}} J_i(p_z, Z)dp_z \\ &= \frac{d\sigma^{\dagger}_{K.N.}(\alpha', \theta, Z)}{d\Omega} S^I(y, Z) \\ &= \frac{d\sigma^{\dagger}_{K.N.}(\alpha', \theta, Z)}{d\Omega} S(y, Z).\end{aligned}$$

The fact that the differential adjoint incoherent cross section can be recovered using similar approximations to the ones used to recover the differential incoherent cross section is a promising result, which adds credibility to the claim that the photon Doppler broadening process is reversible.

A sampling method similar to the one proposed by Namito et al. for photon Doppler broadening can now be created for adjoint photon Doppler broadening. The first step is to sample an outgoing scattering angle from the differential adjoint incoherent cross section using the rejection method from the previous section. Next, the subshell containing the electron upon which the adjoint photon will scatter must be sampled. This will again be done by creating a discrete PDF based on the number of electrons in each shell.

$$p(i) = \frac{n_i}{Z}$$

Finally, an outgoing adjoint photon energy must be sampled from the double differential adjoint incoherent cross section. A conditional PDF for the outgoing photon energy can be created by dividing the double differential adjoint incoherent cross section by the differential adjoint incoherent cross section evaluated at a particular angle. The value of $p_{i,max}$ is calculated from the equation for p_z using the value of

θ that was sampled and the substitution $\alpha = \alpha' + \frac{E_{i,b}}{m_e c^2}$:

$$\begin{aligned} p_i^\dagger(p_z|\theta, Z) &= \left(\frac{d\sigma_{i.s.}^\dagger(\alpha', \theta, Z)}{d\Omega}\right)_i^{-1} \left(\frac{d\sigma^\dagger(p_z, \theta, Z)}{d\Omega dp_z}\right)_i \\ &= \left(\frac{\alpha_c}{\alpha}\right) \frac{J_i(p_z, Z)}{S_i(y, Z)} \\ &= \left(\frac{1}{1 - \alpha'(1 - \cos\theta)}\right) \left(\frac{\alpha'}{\alpha}\right) \left(\frac{J_i(p_z, Z)}{\int_{-\infty}^{p_{i,max}} J_i(p_z, Z) dp_z}\right) \\ &= C^\dagger(\alpha', \theta) R^\dagger(\alpha', \alpha) p(p_z, Z). \end{aligned} \tag{5.62}$$

One must sample a value of p_z from the PDF $p(p_z, Z)$ to determine the outgoing adjoint photon energy. The same table method discussed in section 5.2 can be used to sample a value of p_z from the PDF. Once the outgoing adjoint photon energy has been determined the rejection function $R^\dagger(\alpha, \alpha')$ is used to determine if the value should be accepted or rejected.

The equation for the outgoing adjoint photon energy in terms of the momentum projection is

$$\alpha = \frac{-b^\dagger}{2a^\dagger} \pm \frac{\sqrt{b^{\dagger 2} - 4a^\dagger c^\dagger}}{2a^\dagger} \tag{5.63}$$

where

$$\begin{aligned} a^\dagger &= \left(\frac{p_z}{m_e c}\right)^2 - \left(\frac{\alpha'}{\alpha_c}\right)^2 \\ b^\dagger &= -2\alpha' \left[\left(\frac{p_z}{m_e c}\right)^2 \cos\theta + \frac{\alpha'}{\alpha_c}\right] \\ c^\dagger &= \alpha'^2 \left[\left(\frac{p_z}{m_e c}\right)^2 - 1\right]. \end{aligned}$$

When both values are energetically possible, one of the values must be randomly selected (with probability one half).

5.10 Adjoint Coherent Scattering

As mentioned previously, photon cross sections are not dependent on the initial or final direction of the photon. They are only dependent on the cosine of the angle between these two directions. The coherent scattering cross section is unique in

that the photon's outgoing energy will always be equal to its incoming energy. The adjoint differential coherent scattering cross section must now be derived:

$$\begin{aligned}\sigma^{\dagger}_{c.s.}(E^{'} \rightarrow E, \hat{\Omega}^{'} \rightarrow \hat{\Omega}) &= \sigma_{c.s.}(E \rightarrow E^{'}, \hat{\Omega} \rightarrow \hat{\Omega}^{'}) \\ \sigma^{\dagger}_{c.s.}(E^{'}, \hat{\Omega}^{'} \cdot \hat{\Omega}) &= \sigma_{c.s.}(E^{'}, \hat{\Omega} \cdot \hat{\Omega}^{'}) \\ \sigma^{\dagger}_{c.s.}(E^{'}, \mu) &= \sigma_{c.s.}(E^{'}, \mu). \end{aligned} \tag{5.64}$$

Because the outgoing energy is always equal to the incoming energy, the differential cross section must be given in terms of the cosine of the scattering angle between the incoming and outgoing directions.

From the above equation it is clear that the differential adjoint coherent cross section is identical to the differential coherent cross section. Therefore, coherent scattering is identical for both photons and adjoint photons. All of the techniques discussed in section 5.3 for sampling an outgoing direction from the differential coherent scattering cross section should be used with adjoint photons.

5.11 Adjoint Pair Production

To simulate adjoint pair production the differential adjoint pair production cross section must be derived. This can be done using the definition of the adjoint cross section from equations 4.41 and 4.42. The pair production cross section, which was presented in 5.4, is only dependent on the cosine of the angle between the incoming and outgoing photon direction. In addition, the outgoing energy and the outgoing direction cosine are not coupled. The double differential pair production cross section therefore becomes:

$$\begin{aligned}\sigma^{\dagger}_{p.p.}(E^{'} \rightarrow E, \hat{\Omega}^{'} \rightarrow \hat{\Omega}) &= \sigma_{p.p.}(E \rightarrow E^{'}, \hat{\Omega} \rightarrow \hat{\Omega}^{'}) \\ \frac{d\sigma^{\dagger}_{p.p.}(E^{'} \rightarrow E)}{d\Omega} &= \frac{d\sigma_{p.p.}(E \rightarrow E^{'})}{d\Omega} \\ \frac{d^2\sigma^{\dagger}_{p.p.}(E^{'}, E, Z)}{d\Omega dE} &= \frac{d^2\sigma^{\dagger}_{p.p.}(E, E^{'}, Z)}{d\Omega dE^{'}} \end{aligned} \tag{5.65}$$

Using these relations, the double differential adjoint pair production cross becomes

$$\frac{d^2\sigma^{\dagger}_{p.p.}(E^{'}, E, Z)}{d\Omega dE} = \frac{2\left[\sigma_{p.p.}(E, Z) + \sigma_{t.p.}(E, Z)\right]\delta(E^{'} - m_e c^2)}{4\pi}, \tag{5.66}$$

where E is again the outgoing energy and $E^{'}$ is the incoming energy [40]. Inter-

estingly, the double differential adjoint pair production cross section will be zero unless the initial energy of the adjoint photon is equal to the rest mass of the electron. Therefore, the adjoint pair production process will never be sampled because the probability of an adjoint particle scattering into the energy $m_e c^2$ exactly during a random walk is zero. This issue indicates that the adjoint random walk process presented in chapter 4 is insufficient for adjoint photons. A modified adjoint random walk process must be derived which will enable adjoint pair production reactions to occur.

To start, recall the adjoint emission density FIESK:

$$\theta^\dagger(\vec{r}, E, \hat{\Omega}) = a(\vec{r}, E, \hat{\Omega}) + \int\int\int P^\dagger(\vec{r}, E') C^\dagger(\vec{r}, E' \to E, \hat{\Omega}' \to \hat{\Omega}) \cdot T^\dagger(\vec{r}' \to \vec{r}, E', \hat{\Omega}') \theta^\dagger(\vec{r}', E', \hat{\Omega}') dV' dE' d\hat{\Omega}'.$$

Using the definition of the adjoint collision density from equation 4.33, the adjoint emission density FIESK becomes

$$\theta^\dagger(\vec{r}, E, \hat{\Omega}) = a(\vec{r}, E, \hat{\Omega}) + \int\int P^\dagger(\vec{r}, E') C^\dagger(\vec{r}, E' \to E, \hat{\Omega}' \to \hat{\Omega}) \xi^\dagger(\vec{r}, E', \hat{\Omega}') dE' d\hat{\Omega}'.$$

The adjoint weight factor and the adjoint collision kernel will now be expanded:

$$\theta^\dagger(\vec{r}, E, \hat{\Omega}) = a(\vec{r}, E, \hat{\Omega}) + \int\int \sum_j \frac{\Sigma_j(\vec{r}, E) c_j(\vec{r}, E) f_j(E \to E', \hat{\Omega} \to \hat{\Omega}')}{\Sigma_T(\vec{r}, E')} \xi^\dagger(\vec{r}, E', \hat{\Omega}') dE' d\hat{\Omega}'.$$

The double differential adjoint pair production cross section will now be pulled

from the summation in the above equation creating a new term:

$$
\begin{aligned}
\theta^{\dagger}(\vec{r}, E, \hat{\Omega}) &= a(\vec{r}, E, \hat{\Omega}) \\
&\quad + \int\int \sum_{j \neq p.p.} \frac{\Sigma_j(\vec{r}, E) c_j(\vec{r}, E) f_j(E \rightarrow E', \hat{\Omega} \rightarrow \hat{\Omega}')}{\Sigma_T(\vec{r}, E')} \xi^{\dagger}(\vec{r}, E', \hat{\Omega}') dE' d\hat{\Omega}' \\
&\quad + \frac{2\left[\Sigma_{p.p.}(\vec{r}, E) + \Sigma_{t.p}(\vec{r}, E)\right]}{4\pi} \int\int \frac{\delta(E' - m_e c^2)}{\Sigma_T(\vec{r}, E')} \xi^{\dagger}(\vec{r}, E', \hat{\Omega}') dE' d\hat{\Omega}' \\
&= a(\vec{r}, E, \hat{\Omega}) \\
&\quad + \int\int \frac{\Sigma^{\dagger}_{i+c}(\vec{r}, E')}{\Sigma_T(\vec{r}, E')} \sum_{j \neq p.p.} \frac{\Sigma_j(\vec{r}, E) c_j(\vec{r}, E) f_j(E \rightarrow E', \hat{\Omega} \rightarrow \hat{\Omega}')}{\Sigma^{\dagger}_{i+c}(\vec{r}, E')} \xi^{\dagger}(\vec{r}, E', \hat{\Omega}') dE' d\hat{\Omega}' \\
&\quad + \frac{2\left[\Sigma_{p.p.}(\vec{r}, E) + \Sigma_{t.p}(\vec{r}, E)\right]}{4\pi \Sigma_T(\vec{r}, m_e c^2)} \int \xi^{\dagger}(\vec{r}, m_e c^2, \hat{\Omega}') d\hat{\Omega}' \\
&= a(\vec{r}, E, \hat{\Omega}) \\
&\quad + \int\int P^{\dagger}_{i+c}(\vec{r}, E') C^{\dagger}_{i+c}(\vec{r}, E' \rightarrow E, \hat{\Omega}' \rightarrow \hat{\Omega}) \xi^{\dagger}(\vec{r}, E', \hat{\Omega}') dE' d\hat{\Omega}' \\
&\quad + \frac{2\left[\Sigma_{p.p.}(\vec{r}) + \Sigma_{t.p}(\vec{r})\right]}{4\pi \Sigma_T(\vec{r}, m_e c^2)} \frac{\left[\Sigma_{p.p.}(\vec{r}, E) + \Sigma_{t.p}(\vec{r}, E)\right]}{\left[\Sigma_{p.p.}(\vec{r}) + \Sigma_{t.p}(\vec{r})\right]} \int \xi^{\dagger}(\vec{r}, m_e c^2, \hat{\Omega}') d\hat{\Omega}' \\
&= a(\vec{r}, E, \hat{\Omega}) \\
&\quad + \int\int P^{\dagger}_{i+c}(\vec{r}, E') C^{\dagger}_{i+c}(\vec{r}, E' \rightarrow E, \hat{\Omega}' \rightarrow \hat{\Omega}) \xi^{\dagger}(\vec{r}, E', \hat{\Omega}') dE' d\hat{\Omega}' \\
&\quad + \frac{1}{4\pi} P^{\dagger}_{p.p.}(\vec{r}, m_e c^2) p^{\dagger}_{p.p.}(\vec{r}, E) \int \xi^{\dagger}(\vec{r}, m_e c^2, \hat{\Omega}') d\hat{\Omega}'.
\end{aligned}
$$

The subscript (i+c) indicates that only incoherent and coherent scattering are considered in the particular factor or kernel.

As mentioned previously, the adjoint pair production cross section is zero except for when the incoming photon energy is exactly $m_e c^2$. Therefore, the following relations can be used to simplify the above equation:

$$C^{\dagger}_{i+c}(\vec{r}, E' \rightarrow E, \hat{\Omega}' \rightarrow \hat{\Omega}) = C^{\dagger}(\vec{r}, E' \rightarrow E, \hat{\Omega}' \rightarrow \hat{\Omega}) \tag{5.67}$$

$$P^{\dagger}_{i+c}(\vec{r}, E') = P^{\dagger}(\vec{r}, E'). \tag{5.68}$$

Using these relations the equation for the adjoint emission density becomes

$$\begin{aligned}\theta^{\dagger}(\vec{r},E,\hat{\Omega}) = {} & a(\vec{r},E,\hat{\Omega}) \\ & + \int\int\int P^{\dagger}(\vec{r},E')C^{\dagger}(\vec{r},E'\rightarrow E,\hat{\Omega}'\rightarrow\hat{\Omega})T^{\dagger}(\vec{r}'\rightarrow\vec{r},E',\hat{\Omega}')\theta^{\dagger}(\vec{r}',E',\hat{\Omega}')dV'dE'd\hat{\Omega}' \\ & + \frac{1}{4\pi}P^{\dagger}_{p.p.}(\vec{r},m_ec^2)p^{\dagger}_{p.p.}(\vec{r},E)\int\xi^{\dagger}(\vec{r},m_ec^2,\hat{\Omega}')d\hat{\Omega}'. \end{aligned} \tag{5.69}$$

The equation for the adjoint emission density is identical to the equation presented in chapter 4 except that there is now an additional term. This additional term, which was missed in the initial derivation, takes into account adjoint pair production. By manipulating this term further, the necessary modification to the adjoint random walk process will become apparent. This term will temporarily be referred to as T_3. The FIESK for the adjoint collision density, shown in equation 4.34 will now be substituted into T_3.

$$\begin{aligned}T_3 = {} & \frac{1}{4\pi}P^{\dagger}_{p.p.}(\vec{r},m_ec^2)p^{\dagger}_{p.p.}(\vec{r},E)\int\int T^{\dagger}(\vec{r}'\rightarrow\vec{r},m_ec^2,\hat{\Omega}')a(\vec{r}',m_ec^2,\hat{\Omega}')dV'd\hat{\Omega}' \\ & + \frac{1}{4\pi}P^{\dagger}_{p.p.}(\vec{r},m_ec^2)p^{\dagger}_{p.p.}(\vec{r},E)\int\int\int\int T^{\dagger}(\vec{r}'\rightarrow\vec{r},m_ec^2,\hat{\Omega}')C^{\dagger}(\vec{r},E''\rightarrow m_ec^2,\hat{\Omega}''\rightarrow\hat{\Omega}') \\ & \qquad \cdot P^{\dagger}(\vec{r}',E'')\xi^{\dagger}(\vec{r}',E'',\hat{\Omega}'')dE''d\hat{\Omega}''dV'd\hat{\Omega}'\end{aligned}$$

A new kernel will now be introduced, which is specific to adjoint pair production.

$$O^{\dagger}_{p.p.}(\vec{r}'\rightarrow\vec{r},m_ec^2\rightarrow E,\hat{\Omega}'\rightarrow\hat{\Omega}) = \frac{1}{4\pi}P^{\dagger}_{p.p.}(\vec{r},m_ec^2)p^{\dagger}_{p.p.}(\vec{r},E)T^{\dagger}(\vec{r}'\rightarrow\vec{r},m_ec^2,\hat{\Omega}') \tag{5.70}$$

The equation for T_3 then becomes

$$\begin{aligned}T_3 = {} & \int\int O^{\dagger}_{p.p.}(\vec{r}'\rightarrow\vec{r},m_ec^2\rightarrow E,\hat{\Omega}'\rightarrow\hat{\Omega})a(\vec{r}',m_ec^2,\hat{\Omega}')dV'd\hat{\Omega}' \\ & + \int\int O^{\dagger}_{p.p.}(\vec{r}'\rightarrow\vec{r},m_ec^2\rightarrow E,\hat{\Omega}'\rightarrow\hat{\Omega})\int\int\int M^{\dagger}(\vec{r''}\rightarrow\vec{r}',E''\rightarrow m_ec^2,\hat{\Omega}''\rightarrow\hat{\Omega}') \\ & \qquad \cdot\theta^{\dagger}(\vec{r}'',E'',\hat{\Omega}'')dV''dE''d\hat{\Omega}''dV'd\hat{\Omega}',\end{aligned} \tag{5.71}$$

where $M^{\dagger}$ is the state transition kernel for the adjoint emission density defined in equation 4.31.

The first term of T_3 is a new source term that accounts for adjoint particle emission from the adjoint source with energy exactly equal to the rest mass energy of the electron. The second term forces adjoint particles to scatter into the energy m_ec^2,

whenever energetically possible, at which point adjoint pair production occurs.

The modified random walk procedure is now completely defined by the third term of the adjoint emission density FIESK. The first modification is that the starting state of the adjoint particle must be sampled from either the adjoint source or the new source, which is

$$S^{\dagger}_{p.p.}(\vec{r}, m_e c^2, \hat{\Omega}) = \int\int O^{\dagger}_{p.p.}(\vec{r}^{\,'} \rightarrow \vec{r}, m_e c^2 \rightarrow E, \hat{\Omega}^{'} \rightarrow \hat{\Omega}) a(\vec{r}^{\,'}, m_e c^2, \hat{\Omega}^{'}) dV^{'} d\hat{\Omega}^{'}. \tag{5.72}$$

Sampling from this source will be done indirectly. Assume that the adjoint source has the following form:

$$a(\vec{r}, E, \hat{\Omega}) = f_{\vec{r}}(\vec{r}) f_E(E) f_{\hat{\Omega}}(\hat{\Omega}).$$

The PDF for selecting a particular starting energy is then

$$p_E(E) = \frac{f_E(E)}{\int f_E(E') dE'}.$$

Because every particle will be emitted from the new source with energy $m_e c^2$, the particles initial weight must be $p_E(m_e c^2)$. Next, a new position is sampled from the adjoint transport kernel. Then the weight of the particle is multiplied by the adjoint pair production weight factor. Finally, an outgoing energy is sampled from the adjoint pair production kernel. The last two steps will be discussed further shortly.

The next modification to the random walk process occurs when the expanded adjoint collision kernel is sampled from. If adjoint incoherent scattering is selected and it is energetically possible for the adjoint particle to scatter into the energy $m_e c^2$, a new random walk is initiated. The weight of this new random walk will be the weight of the initial random walk times the probability of scattering to the energy $m_e c^2$:

$$W = W_m p^{\dagger}_{i.s.}(E^{'} \rightarrow m_e c^2). \tag{5.73}$$

Given the properties of the adjoint incoherent scattering process, it will only be energetically possible for an adjoint photon to scatter into the energy $m_e c^2$ if its energy is in the following range:

$$\frac{1}{3} \leqslant \alpha^{'} \leqslant 1. \tag{5.74}$$

Next, a new position is sampled from the adjoint transport kernel. At the new

collision point, the weight of the adjoint photon is multiplied by the adjoint pair production weight factor, which is

$$P^{\dagger}_{p.p.}(\vec{r}, m_e c^2) = \frac{2\left[\Sigma_{p.p.}(\vec{r}) + \Sigma_{t.p}(\vec{r})\right]}{\Sigma_T(\vec{r}, m_e c^2)} \tag{5.75}$$

where

$$\Sigma_{p.p.}(\vec{r}) = \int_{2m_e c^2}^{E_{max}} \Sigma_{p.p.}(\vec{r}, E)\,dE \tag{5.76}$$

$$\Sigma_{t.p.}(\vec{r}) = \int_{4m_e c^2}^{E_{max}} \Sigma_{t.p.}(\vec{r}, E)\,dE. \tag{5.77}$$

As with the adjoint incoherent cross section, where a maximum problem energy must be set in order to keep the cross section finite, a maximum problem energy must also be set in order to keep the adjoint pair production weight factor finite.

Finally an outgoing energy is sampled from the PDF present in the adjoint pair production kernel, which has the following form:

$$\begin{aligned}
p^{\dagger}_{p.p.}(\vec{r}, E) &= \frac{\Sigma_{p.p.}(\vec{r}, E) + \Sigma_{t.p}(\vec{r}, E)}{\Sigma_{p.p.}(\vec{r}) + \Sigma_{t.p}(\vec{r})} \\
&= \frac{\Sigma_{p.p.}(\vec{r}, E)}{\Sigma_{p.p.}(\vec{r}) + \Sigma_{t.p}(\vec{r})} + \frac{\Sigma_{t.p.}(\vec{r})}{\Sigma_{p.p.}(\vec{r}) + \Sigma_{t.p}(\vec{r})} \\
&= \frac{\Sigma_{p.p.}(\vec{r})}{\Sigma_{p.p.}(\vec{r}) + \Sigma_{t.p}(\vec{r})} \frac{\Sigma_{p.p.}(\vec{r}, E)}{\Sigma_{p.p.}(\vec{r})} + \frac{\Sigma_{t.p.}(\vec{r})}{\Sigma_{p.p.}(\vec{r}, E) + \Sigma_{t.p}(\vec{r}, E)} \frac{\Sigma_{t.p.}(\vec{r}, E)}{\Sigma_{t.p.}(\vec{r})} \\
&= p^{\dagger}_{p.p.}(\vec{r}) \sum_A \frac{\Sigma_{p.p.,A}(\vec{r})}{\Sigma_{p.p.,A}(\vec{r})} \frac{\sigma_{p.p.}(E)}{\sigma_{p.p.,A}} + p^{\dagger}_{t.p}(\vec{r}) \sum_A \frac{\Sigma_{t.p.,A}(\vec{r})}{\Sigma_{t.p.,A}(\vec{r})} \frac{\sigma_{t.p.}(E)}{\sigma_{t.p.,A}} \\
&= \sum_{i=1}^{2} p^{\dagger}_i(\vec{r}) \sum_A p^{\dagger}_{i,A}(\vec{r}) p^{\dagger}_{i,A}(E).
\end{aligned} \tag{5.78}$$

Sampling from this PDF is essentially identical to sampling from the expanded adjoint collision kernel. Either the pair production or the triplet production distribution will be sampled from by selecting from the discrete PDF

$$p(i|\vec{r}) = \sum_{i=1}^{2} p^{\dagger}_i(\vec{r}). \tag{5.79}$$

Next, an element hit will be sampled from the discrete PDF

$$\begin{aligned} p(A|i,\vec{r}) &= p^{\dagger}_{i,A}(\vec{r}) \\ &= \sum_{A} \frac{\Sigma_{i,A}(\vec{r})}{\Sigma_{A}(\vec{r})}. \end{aligned} \tag{5.80}$$

Finally, an outgoing energy is sampled from the continuous PDF

$$\begin{aligned} p(E|i,A) &= p^{\dagger}_{i,A}(E) \\ &= \frac{\sigma_{i,A}(E)}{\sigma_{i,A}}. \end{aligned} \tag{5.81}$$

Once the outgoing energy has been chosen, this random walk will continue normally.

5.12 Discrete Energy Sources and Adjoint Photon Random Walks

Gamma ray sources commonly emit photons with only a few discrete energies. These sources are problematic for adjoint photon random walks because the probability of an adjoint photon scattering into one of the discrete source energies is zero. Fortunately, Gabler, Hennider and Reichelt have developed a simple and computationally efficient procedure for dealing with these types of sources [25].

Assume that the source is defined as

$$S(\vec{r},E,\hat{\Omega}) = \begin{cases} S_0 \sum_i p_i \delta(E - E_{s,i}) p_{s,\hat{\Omega}}(\hat{\Omega}) p_{s,\vec{r}}(\vec{r}) & \text{if } \vec{r} \in V_s \\ 0 & \text{otherwise.} \end{cases} \tag{5.82}$$

The only reaction for adjoint photons that can change the particles energy (given any initial energy) is adjoint incoherent scattering. Therefore, every time an adjoint incoherent scattering event is selected and the adjoint photon's energy is in the necessary energy window, an additional random walk must be initiated. The weight associated with this new random walk will be the weight of the main random walk times the probability of incoherently scattering from the current energy to the source

energy:

$$W = W_m p^{\dagger}_{A,i.s.}(\alpha_{s,i}|\alpha', Z) = \frac{W_m}{\sigma_{A,i.s.}(\alpha', Z)} \frac{d\sigma^{\dagger}_{A,i.s.}(\alpha', \alpha, Z)}{dE}\Big|_{E_{s,i}}. \quad (5.83)$$

The PDF from equation 5.49 is shown in the above equation. The outgoing direction cosine is directly coupled to the initial and outgoing energy:

$$\mu_{s,i} = 1 + \frac{1}{\alpha_{s,i}} - \frac{1}{\alpha'}. \quad (5.84)$$

The outgoing azimuthal angle is simply sampled from a uniform distribution over the interval (0,2π).

The necessary energy window for possible scattering into each discrete source energy is the following:

$$\frac{\alpha_{s,i}}{1 + 2\alpha_{s,i}} \leqslant \alpha' \leqslant \alpha_{s,i} \quad (5.85)$$

When the adjoint photon energy is in a region where two or more energy windows overlap, more than one additional random walk can be split off at each collision point.

The uncollided contribution to the inner product of interest must also be estimated. To do this assume that the adjoint source has the following form:

$$a(\vec{r}, E, \hat{\Omega}) = f_{d,\vec{r}}(\vec{r}) f_{d,E}(E) f_{d,\Omega}(\Omega). \quad (5.86)$$

A portion of the random walks that are generated must start with a discrete source energy $E_{s,i}$ and weight

$$W_0 = \frac{f_{d,E}(E_{s,i})}{\int f_{d,E}(E) dE}. \quad (5.87)$$

5.13 The Adjoint Weight Factor for Photons

As described in chapter 4, after an adjoint photon has been transported to the next collision site the weight must be multiplied by the adjoint weight factor. Because the adjoint weight factor is the ratio of the total macroscopic adjoint cross section to the total macroscopic cross section, it is not bound to the interval (0,1) but instead to the interval (0,∞). The adjoint weight factor will therefore have the potential to negatively affect the variance of the estimators used. By examining the adjoint

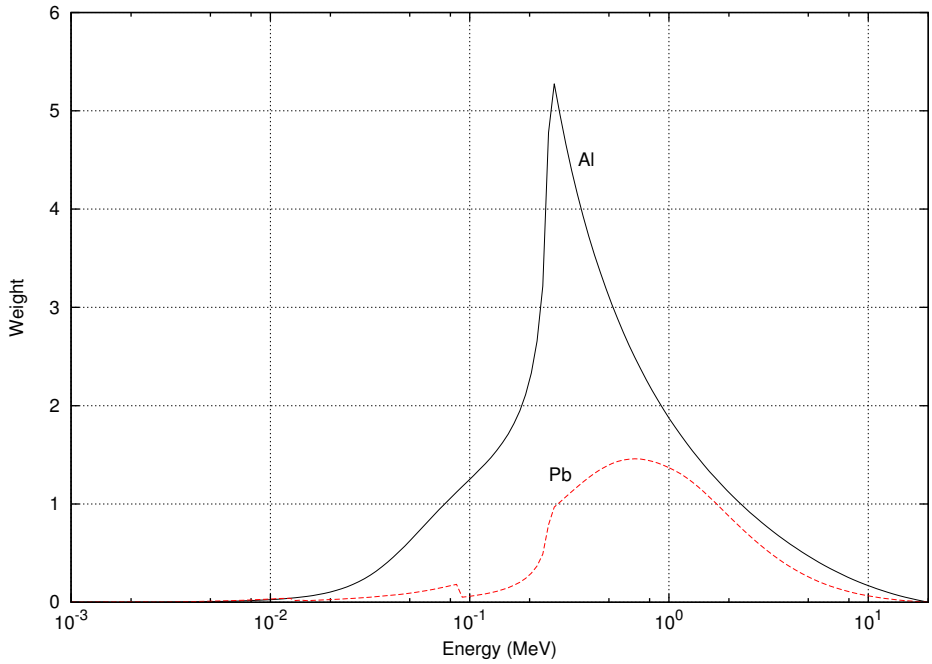

Figure 5.8: **The adjoint weight factor for Aluminum and Lead.** *The adjoint weight factor for Aluminum and Lead is shown for a maximum problem energy of 20.0 MeV. The adjoint weight factor for Aluminum is more problematic than the adjoint weight factor for Lead since it has a higher maximum value and a larger range of energies where it is above unity.*

weight factor for photons, the severity of the problem can be estimated. Figure 5.8 shows the adjoint weight factor for aluminum and lead with a maximum problem energy of 20.0 MeV. Interestingly, the problem is much less severe for lead since the adjoint weight factor only goes above unity for a small range of energies. In addition the maximum value of the adjoint weight factor for lead is much smaller than for aluminum. The true effect that the adjoint weight factor has on the variance of the estimator used can only be evaluated by running example problems.

Chapter 6

Neutron Interaction Cross Sections and Sampling Techniques

To conduct a Monte Carlo random walk for neutrons the individual reactions that make up the collision kernel must be discussed. In addition, the methods used to sample from the differential interaction cross sections must be discussed. Because of the increased complexity of reactions between a neutron and an a atomic nucleus compared to photon-atomic reactions, closed form differential interaction cross sections are quite rare. The models and procedures that are outlined in the ENDF manual will therefore be relied upon heavily. In this chapter all secondary particles other than neutrons will be neglected from the cross sections and sampling procedures.

6.1 Elastic and Inelastic Level Scatering

Elastic and inelastic level scattering are the two simplest scattering reactions between a neutron and an atomic nucleus. In elastic scattering the internal state of the atomic nucleus is left unchanged. In inelastic level scattering the atomic nucleus is excited to a particular state, which has an energy that will be denoted as Q above the ground state. Elastic scattering can therefore be regarded as a special case of inelastic scattering with Q set equal to zero. Because of the complicated nature of the interaction between a neutron and the atomic nucleus it is difficult to develop an equation for the differential elastic or inelastic level scattering cross section for all incoming neutron energies. The solution to this problem is to develop tabulated angular distributions for a range of incoming neutron energies, which can be found in the ENDF/B-VII.1 library [41].

According to the ENDF/B-VII.1 manual, the angular distrubitions for elastic and inelastic level scattering are expressed as normalized probability distributions.

$$p(\mu, E') = \frac{2\pi}{\sigma(E')}\sigma(\mu, E') \tag{6.1}$$

$$\int_{-1}^{1} p(\mu, E^{'}) d\mu = 1 \tag{6.2}$$

The angular distribition will be given in either a tabular form or as a Legendre polynomial series, which is shown below.

$$p(\mu, E^{'}) = \sum_{l=0}^{N} \frac{2l+1}{2} a_l(E^{'}) P_l(\mu) \tag{6.3}$$

In addition, the outgoing angle cosine can be given in either the lab frame or the center-of-mass (CM) frame. However, for two-body reactions like elastic and inelastic level scattering the scattering angle cosine will usually be given in the CM frame [41].

Sampling an outgoing angle from the PDF given in the ENDF library can be done in many ways [2]. In older Monte Carlo codes, including older versions of MCNP, the most common sampling technique was that proposed by Carter and Cashwell in which n equally probable intervals of the CDF are tabulated [42]. To select an outgoing angle cosine, one randomly selects an interval of the CDF and then selects the scattering angle cosine from a uniform PDF between the lower and upper boundaries of the selected interval [2]. This method is very computationally efficient but can become inaccurate when the PDF is given as a Legendre polynomial with many higher order terms [43]. The next best option is to use a 2-D tabular selection method [43]. This is very similar to the tabular selection method which was discussed in the previous chapter. At each of the selected incoming neutron energies the CDF corresponding to the PDF given in the ENDF library must first be calculated. To sample an outgoing angle cosine corresponding to a particular incoming neutron energy one must determine which energy bin the neutron's energy falls in, which can be accomplished with a binary search. Then one samples a random number and for the distribution corresponding to both energy bin boundaries, determines the outgoing angle cosine corresponding to that CDF value. The outgoing angle cosine corresponding to the incoming energy must then be found using interpolation between the two values. A set of appropriate interpolation schemes for 2-D tables are given in the ENDF/B-VII.1 manual [41].

Once the CM scattering angle cosine is sampled, it must be converted to the lab scattering angle cosine. This equation, which is shown below, can be derived using

conservation of energy and momentum in both reference frames (see Appendix **??**).

$$\mu_l = \frac{A\sqrt{1-\left(\frac{A+1}{A}\right)\frac{Q}{E'}}\mu_{cm}+1}{\sqrt{A^2\left[1-\left(\frac{A+1}{A}\right)\frac{Q}{E'}\right]+2A\mu_{cm}\sqrt{1-\left(\frac{A+1}{A}\right)\frac{Q}{E'}}+1}} \tag{6.4}$$

$$A = \frac{m_A}{m_n}$$

Because of the one-to-one correspondence between the outgoing energy and outgoing direction in the two-body reactions, once the outgoing angle cosine has been sampled the outgoing energy of the neutron can be determined. The equations that described this one-to-one correspondence can be found using conservation of energy and momentum and the assumption that the atomic nucleus upon which the neutron scatters is at rest. The outgoing energy from an inelastic level scattering interaction (in the lab frame) as a function of the initial energy and the scattering angle in the center of mass system is the following (see Appendix **??**).

$$E = E'\left(\frac{A^2\left[1-\left(\frac{A+1}{A}\right)\frac{Q}{E'}\right]+2A\mu_{cm}\sqrt{1-\left(\frac{A+1}{A}\right)\frac{Q}{E'}}+1}{(A+1)^2}\right) \tag{6.5}$$

The outgoing energy is limited to the following range.

$$\left(\frac{A\sqrt{1-\left(\frac{A+1}{A}\right)\frac{Q}{E}}-1}{A+1}\right)^2 E' \leqslant E \leqslant \left(\frac{A\sqrt{1-\left(\frac{A+1}{A}\right)\frac{Q}{E}}+1}{A+1}\right)^2 E' \tag{6.6}$$

The lower limit occurs when $\mu_{cm} = -1$ and the upper limit occurs when $\mu_{cm} = 1$.

6.2 Absorption Reactions

A neutron absorption reaction is any reaction in which an incident neutron is absorbed and another particle, whether a gamma ray, proton, alpha particle or some other atomic nucleus, is emitted. When neutrons are the only particle of interest, these reactions will all be combined into a single absorption reaction. However, in coupled particle transport calculations, these reactions along with the neutron collision density will function as the source term for the other particles of interest. Some of these reactions will be discussed further in the following chapter when

coupled neutron-photon transport will be discussed.

6.3 Other Non-fission Reactions

There are many other reactions which can also be important but are more complicated than the previous reactions that have been discussed. A few examples are the inelastic scattering to a continuum of energy levels, the (n,2n) reaction and the (n,3n) reaction. For a complete list of possible non-fission reactions, refer to the ENDF/B-VII.1 manual. In these reactions there is assumed to be no correlation between the outgoing energy and direction according to the ENDF/B-VII.1 manual [41]. This simplification of the reaction model means that conservation of energy and momentum will likely be violated during a given reaction modeled during the Monte Carlo random walk process. However the average of many individual reactions will still give the desired behavior. The neutron transfer probability for any of these reactions can be represented as follows.

$$\begin{aligned} f(E' \to E, \hat{\Omega}' \to \hat{\Omega}) &= p(E' \to E)p(\hat{\Omega}' \to \hat{\Omega}|E') \\ &= p(E' \to E)p(\hat{\Omega}' \cdot \hat{\Omega}|E') \\ &= p(E' \to E)p(\mu, E') \end{aligned} \tag{6.7}$$

As with elastic and inelastic level scattering the angular distributions are expressed as normalized PDFs [41].

$$p(\mu, E') = \frac{2\pi}{\sigma(E')}\sigma(\mu, E')$$

$$\int_{-1}^{1} p(\mu, E')d\mu = 1$$

In addition the angular distrubition will be given in either a tabular form or as a Legendre polynomial series. Usually, the outgoing angle cosine for these reactions will be given in the lab frame [41]. To sample an outgoing angle cosine, the same tabular procedure that was outlined in the previous section should be used.

The energy distributions are also expressed as normalized PDFs [41]. The variable c is the number of neutrons emitted from the reaction.

$$p(E' \to E) = \frac{1}{c\sigma(E')}\frac{d\sigma(E' \to E)}{dE} \tag{6.8}$$

$$\int_0^{E_{max}} p(E' \rightarrow E)dE = 1 \tag{6.9}$$

The energy distributions are given in either a tabular form or as an analytical formulation. The possible analytical formulations are the general evaporative spectrum or the evaporation spectrum [41]. The general evaporative spectrum has the following form.

$$p(E' \rightarrow E) = g(E/\theta(E')) \tag{6.10}$$

The function $\theta(E')$ is tabulated as a function of incident neutron energy and the function $g(x)$ is tabulated as a function of $x = E/\theta(E')$. To sample from this function a CDF corresponding to the pdf g(x) must be created. One then samples a random number and finds the value of x that corresponds to the random number in the CDF that was calculated. Finally, the outgoing energy is calculated as follows.

$$E = x\theta(E') \tag{6.11}$$

The evaporation spectrum, which is used for most non-fission reactions, has the following form [41].

$$p(E' \rightarrow E) = \frac{E}{I} exp\left[\frac{-E}{\theta(E')}\right] \tag{6.12}$$

$$I = \theta^2(E')\left[1 - exp\left[\frac{-(E'-U)}{\theta(E')}\right]\left(1 + \frac{E'-U}{\theta(E')}\right)\right] \tag{6.13}$$

The function $\theta(E')$ is again tabulated as a function of incident neutron energy and the variable U is introduced to define the proper upper limit for the final particle energy. Sampling from this distribution is also quite simple. However, the derivation of the sampling procedure is slightly complicated. Consider another PDF that has the same shape as the evaporation spectrum but extends to infinity (instead of $E' - U$).

$$f(E' \rightarrow E) = \frac{E}{\theta^2(E')} exp\left[\frac{-E}{\theta(E')}\right] \tag{6.14}$$

Also assume that the energy E is the sum of two values E_1 and E_2, which are independent of each other. If the PDF corresponding to E_1 is

$$f_1(E' \rightarrow E_1) = \frac{1}{\theta(E')} exp\left[\frac{-E_1}{\theta(E')}\right] \tag{6.15}$$

and the PDF corresponding to E_2 is

$$f_2(E' \to E_2) = \frac{1}{\theta(E')} exp\left[\frac{-E_2}{\theta(E')}\right] \tag{6.16}$$

then the PDF for E is the following [31].

$$\begin{aligned} f(E' \to E) &= \int_0^E f_1(E' \to E - E_2) f_2(E' \to E_2) dE_2 \\ &= \frac{1}{\theta^2(E')} \int_0^E exp\left[\frac{-(E - E_2)}{\theta(E')}\right] exp\left[\frac{-E_2}{\theta(E')}\right] dE_2 \\ &= \frac{1}{\theta^2(E')} exp\left[\frac{-E}{\theta(E')}\right] \int_0^E dE_2 \\ &= \frac{E}{\theta^2(E')} exp\left[\frac{-E}{\theta(E')}\right] \end{aligned} \tag{6.17}$$

Both E_1 and E_2 can be sampled from their respective PDFs using the inverse CDF method.

$$E_1 = -\theta(E') \ln \varepsilon_1 \tag{6.18}$$

$$E_2 = -\theta(E') \ln \varepsilon_2 \tag{6.19}$$

Since E is the sum of these two values, the equation for sampling E directly is the following [43].

$$\begin{aligned} E &= E_1 + E_2 \\ &= -\theta(E') \ln(\varepsilon_1 \varepsilon_2) \end{aligned} \tag{6.20}$$

Finaly, since E was sampled from a distrubition that wasn't truncated properly, the value of E must be rejected if it is greater than $E' - U$ to account for the improper truncation.

6.4 Neutron Induced Fission

Fission reaction must also be taken into account since for the random walk procedure that has been described, fission can occur as long as the system is subcritical. In fission reactions there is also assumed to be no correlation between outgoing energy and direction according to the ENDF/B-VII.1 manual [41]. The neutron transfer

probability for fission reactions will therefore have the same form as for the non-fission reactions from the previous section.

The energy distributions are again expressed as normalized PDFs [41]. The variable $\nu(E')$ is the average number of either prompt or delayed neutrons emitted by the fission reaction, depending on which distribution is of interest.

$$p(E' \rightarrow E) = \frac{1}{\nu(E')\sigma_f(E')} \frac{d\sigma_f(E' \rightarrow E)}{dE} \tag{6.21}$$

$$\int_0^{E_{max}} p(E' \rightarrow E) dE = 1 \tag{6.22}$$

The energy distributions are given in either a tabular form or as an analytical formulation. The possible analytical formulations are the evaporation spectrum, which was discussed in the previous section, the simple Maxwellian fission spectrum and the energy-dependent Watt spectrum [41]. The simple Maxwellian fission spectrum has the following form.

$$p(E' \rightarrow E) = \frac{\sqrt{E}}{I} exp\left[\frac{-E}{\theta(E')}\right] \tag{6.23}$$

$$I = \theta^{3/2}(E')\left[\frac{\sqrt{\pi}}{2} erf\left(\sqrt{\frac{(E'-U)}{\theta(E')}}\right) - \sqrt{\frac{(E'-U)}{\theta(E')}} exp\left[\frac{-(E'-U)}{\theta(E')}\right]\right] \tag{6.24}$$

The function $\theta(E')$ is tabulated as a function of incident neutron energy and the variable U is introduced to define the proper upper limit for the final particle energy. In the case of fission reactions, U is usually a large negative number since the outgoing neutrons can have an energy much higher than the incoming neutron [41]. Several methods are commonly used to sample from this distribution. All methods assume that the outgoing enegy can take on any value between zero and infinity, which results in a slightly different normalization of the distribution. The Maxwellian distribution falls off quickly enough that this difference is neglibible.

The first method for sampling from the Maxwellian is a direct sampling method, which is shown in the following equation [44].

$$E = -\theta(E')\left[cos^2\left(\frac{2}{\pi}\varepsilon_1\right) \ln \varepsilon_2 + \ln \varepsilon_3\right] \tag{6.25}$$

For a derivation of this method, refer to appendix **??**. The second method is a

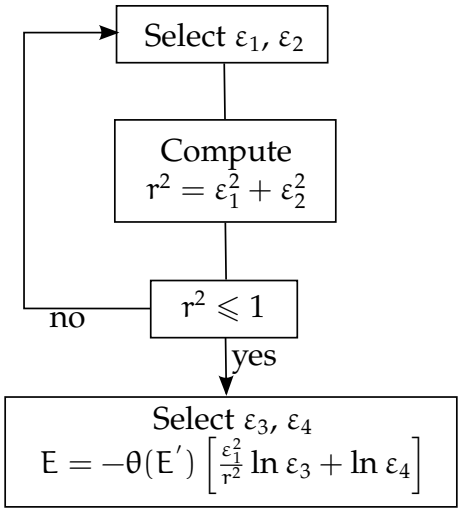

Figure 6.1: **Johnk's Algorithm**. *This sampling procedure is used to sample a value from the Maxwellian distribution. The efficiency of this procedure is about 0.78 and is independent of the incoming neutron energy [44].*

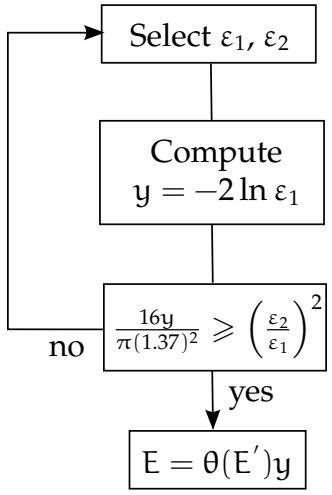

Figure 6.2: **Mohamed's Rejection Sampling Procedure**. *This sampling procedure is used to sample a value from the Maxwellian distribution. The efficiency of this procedure is about 0.73 and is independent of the incoming neutron energy [44].*

rejection sampling procedure. It is referred to by some authors as Johnk's algorithm* and is shown in figure 6.1 [44**?**]. The derivation of this method can also be found in appendix **??**. The final sampling method is also a rejection sampling procedure, which is shown in figure 6.2. Mohamed has shown that this method is the fastest of the three for generating random samples from a Maxwellian distribution despite

*This method is used in MCNP [43].

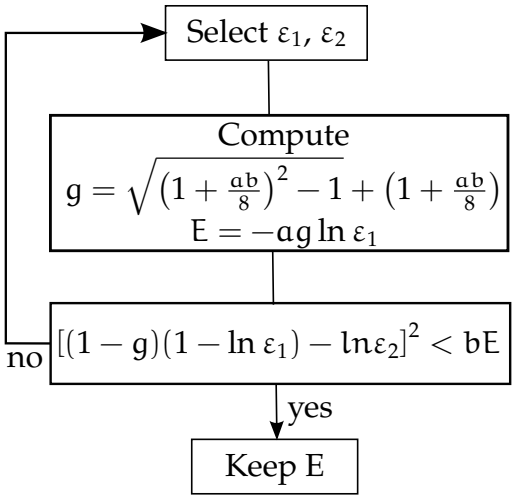

Figure 6.3: **Kalos's Algorithm**. *This sampling procedure is used to sample a value from the Watt fission spectrum. The efficiency of this procedure is about 0.67 and is independent of the incoming neutron energy [44].*

having an efficiency of only 0.73 [44]. The derivation of this method can also be found in appendix **??**.

The energy energy-dependent Watt spectrum has the following form.

$$p(E' \rightarrow E) = I^{-1} exp\left[\frac{-E}{a(E')}\right] sinh\left(\sqrt{b(E')E}\right) \tag{6.26}$$

$$I = \frac{1}{2}\sqrt{\frac{\pi a^3 b}{4}} exp\left(\frac{ab}{4}\right)\left[erf\left(\sqrt{\frac{E'-U}{a}} - \sqrt{\frac{ab}{4}}\right) + erf\left(\sqrt{\frac{E'-U}{a}} + \sqrt{\frac{ab}{4}}\right)\right] - a\exp\left[-\left(\frac{E'-U}{a}\right)\right] sinh\sqrt{b(E'-U)} \tag{6.27}$$

The functions $a(E')$ and $b(E')$ are tabulated as a function of incident neutron energy and the variable U is introduced to again define the proper upper limit for the final particle energy. Two methods are commonly used to sample from this distribution. Both methods assume that the outgoing energy can take on any value between zero and infinity, which results in a slightly different normalization of the distribution. However, the distribution falls off quickly enough thta this difference is negligible.

The first method is rejection sampling procedure referred to as Kalos's algorithm [44]. This method is shown in figure 6.3. The efficiency of this method is about 0.67. The second method is a direct sampling method, which is shown in the following

equation [44]. The variable y is a random number from a Maxwellian distribution with $\theta(E')$ replaced with $a(E')$. To generate this random number, any of the methods for sampling from a Maxwellian distribution can be used.

$$E = y + \frac{a^2 b}{4} + (2\varepsilon_1 - 1)\sqrt{a^2 b y} \tag{6.28}$$

When combined with Mohamed's rejection sampling procedure, the direct sampling method is the fastest at generating random samples from the Watt spectrum [44].

6.5 Thermal Scattering

In all previous sections it was assumed that the energy of the neutron was much greater than the thermal energy of the atoms upon which the neutron interacts. When the neutron energy drops below about one eV, this assumption is no longer valid. To account for the thermal motion of atoms upon which the neutron scatters, several models have been developed.

The most detailed model is the $S(\alpha, \beta)$ model, which can treat thermal neutron scattering by both molecules and crystalline solids [7, 41]. The $S(\alpha, \beta)$ data required for this model is only available for a few materials in the ENDF ENDF/B-VII.1 library [41].

When $S(\alpha, \beta)$ data is not available for a particular material another model that can lead to an accurate representation of thermal scattering is the free gas model. In this model, the atoms upon which the neutrons interact are assumed to be unbound with speeds characterized by a Maxwell-Boltzmann distribution [7]. This model is applicable to any mixture of materials as long as all scattering cross sections are independent of the relative speed of the neutron and scattering nucleus and all effective absoption cross sections are known [7].

The final model, which is the simplest and least accurate, is the one-velocity thermal energy group model. As its name implies, thermal neutrons are treated as if they all have the same energy with cross sections averaged over this thermal energy group used. Once a neutron scatters into the thermal group, its energy never changes due to scattering collisions and therefore, it never leaves the thermal group. Will many inaccuracies can arrise from this model, the largest is most likely from the generation of the average cross sections, which requires an assumption of the thermal neutron spectrum. Despite these limitations, this model will be employed initially because of the ease with which an equivalent adjoint model can be created.

The development of equivalent adjoint models for the other two models will be one of the primary focuses of the thesis.

The energy transfer probability for elastic scattering for the one-velocity thermal energy model is the following [16].

$$p(E' \rightarrow E) = \delta(E - E') \tag{6.29}$$

As soon as the neutron scatters to an energy below E_c, which is the energy cutoff for the thermal energy group, its energy will never change. Furthermore, the cross sections used will be the thermal group averaged cross sections, which are independent of the actual energy of the thermal neutron.

6.6 Adjoint Elastic and Inelastic Level Scattering

To model adjoint elastic and inelastic level scattering, the adjoint energy transfer probabilities and adjoint cross sections must be determined. For elastic and inelastic level scattering, the double differential transfer probability is represented by the following function [16].

$$p(E' \rightarrow E, \mu_{cm}) = p(\mu_{cm}, E')\delta\left(E - E'\left(\frac{A^2\left[1 - \left(\frac{A+1}{A}\right)\frac{Q}{E'}\right] + 2A\mu_{cm}\sqrt{1 - \left(\frac{A+1}{A}\right)\frac{Q}{E'}} + 1}{(A+1)^2}\right)\right) \tag{6.30}$$

The delta function in the above equation comes about from the one-to-one correspondence between the outgoing energy and outgoing direction. The energy transfer probability can now be deterimed by the following integral.

$$p(E' \rightarrow E) = \int_{-1}^{1} p(E' \rightarrow E, \mu_{cm}) d\mu_{cm} \tag{6.31}$$

Given that the delta function in the equation for the double differential transfer probability is in terms of the outgoing energy, the above integral will be more easily evaluated when the integration is over the outgoing energy. Based on equation 6.5,

$$d\mu_{cm} = \frac{(A+1)^2}{2AE'\sqrt{1 - \left(\frac{A+1}{A}\right)\frac{Q}{E'}}} dE. \tag{6.32}$$

Using the change of variables, the energy transfer probability is the following.

$$\begin{aligned} p(E^{'} \rightarrow E) &= \int_{-1}^{1} p(E^{'} \rightarrow E, \mu_{cm}) \frac{(A+1)^2}{2AE^{'}\sqrt{1-\left(\frac{A+1}{A}\right)\frac{Q}{E^{'}}}} dE \\ &= p(E^{'}, \mu_{cm}(E^{'}, E)) \frac{(A+1)^2}{2AE^{'}\sqrt{1-\left(\frac{A+1}{A}\right)\frac{Q}{E^{'}}}} \end{aligned} \tag{6.33}$$

The adjoint elastic and inelastic level scattering cross sections can now be determined using equation 4.42.

$$\sigma^{\dagger}_{e/i}(E^{'}) = \int_{E_{min}}^{E_{max}} \sigma_{e/i}(E) p(E \rightarrow E^{'}) dE \tag{6.34}$$

The last missing piece of information that is needed before the adjoint cross section can be evaluated is the limits of integrations. These limits can be determined by determining an equation for the incoming energy as a function of the outgoing energy (in the forward case). Unfortunately, one cannot simply solve equation 6.5 for $E^{'}$. As figure 6.5 shows, when the outgoing energy is less than $\frac{Q}{A(A+1)}$ and the CM scattering angle cosine is less than zero, there is not a one-to-one correspondance between incoming energy and the CM scattering angle cosine for fixed outgoing energy. If the outgoing energy is given as a function of incoming energy and the lab scattering angle instead, as shown in figure 6.5, there is a one-to-one correspondance between incoming energy and the lab scattering angle cosine for fixed outgoing energy. The incoming energy as a function of incoming energy and lab scattering angle cosine is shown in the following equation. It must also be noted that the primed and unprimed variables have been switched. The derivation of this equation is shown in appendix **??**.

$$E = E^{'}\left(\frac{A^2 - 1 + 2\mu_l^2 + A(A-1)\frac{Q}{E^{'}} - 2\mu_l\sqrt{A^2 - 1 + \mu_l^2 + A(A-1)\frac{Q}{E^{'}}}}{(A-1)^2}\right) \tag{6.35}$$

By using $\mu_l = 1$ and $\mu_l = -1$ in the above equation, the lower and upper energy bound of the adjoint elastic and inelastic level scattering process can be determined,

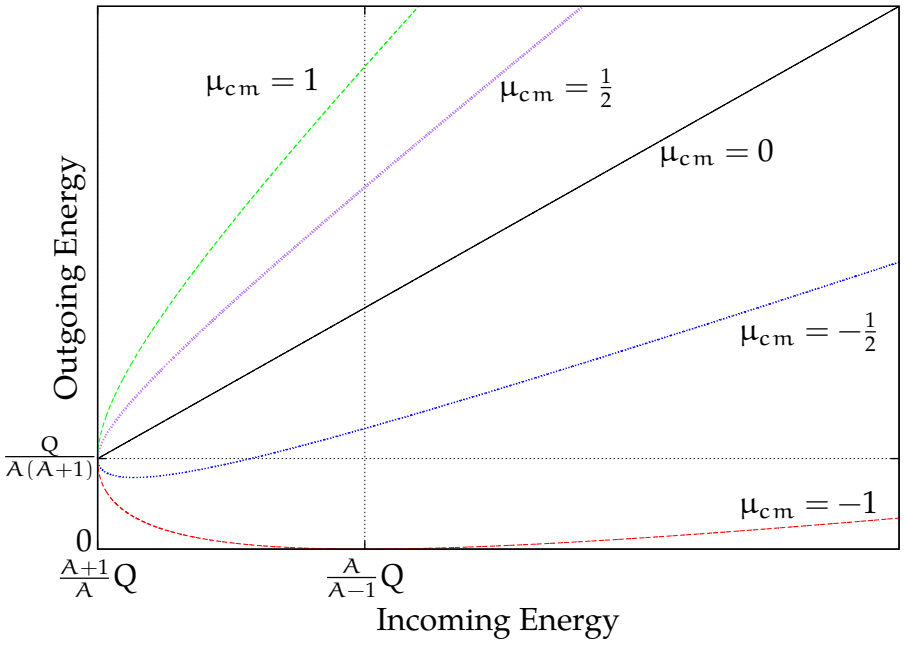

Figure 6.4: **Outgoing energy from forward reaction as a function of incoming energy and center-of-mass scattering angle cosine**. *For fixed incoming energy, there is a one-to-one correspondence between outgoing energy and center-of-mass scattering angle cosine. For fixed outgoing energy, there is only a one-to-one correspondence between incoming energy and center-of-mass scattering angle cosine if the outgoing energy is above* $\frac{Q}{A(A+1)}$ *or if the scattering angle cosine is above zero.*

repsectively.

$$\left(\frac{A\sqrt{1+\left(\frac{A-1}{A}\right)\frac{Q}{E'}}-1}{A-1}\right)^2 E' \leqslant E \leqslant \left(\frac{A\sqrt{1+\left(\frac{A-1}{A}\right)\frac{Q}{E'}}+1}{A-1}\right)^2 E' \tag{6.36}$$

With the adjoint cross section for elastic and inelastic level scattering completely defined, the adjoint energy transfer probability can now be determined using equation 4.41 [16].

$$\begin{aligned} p^\dagger(E' \to E) &= \frac{\sigma_{e/i}(E)p(E \to E')}{\sigma^\dagger_{e/i}(E')} \\ &= \frac{\sigma_{e/i}(E)}{\sigma^\dagger_{e/i}(E')}\frac{(A+1)^2}{2AE\sqrt{1-\left(\frac{A+1}{A}\right)\frac{Q}{E}}}p(E, \mu_{cm}(E, E')) \end{aligned} \tag{6.37}$$

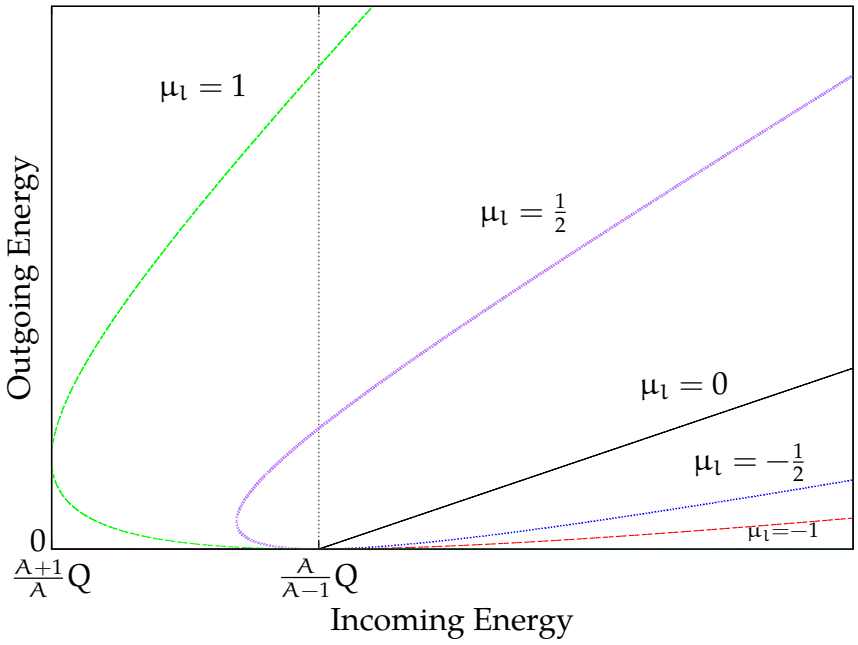

Figure 6.5: **Outgoing energy from forward reaction as a function of incoming energy and lab scattering angle cosine**. *For fixed incoming energy, there is only a one-to-one correspondence between outgoing energy and lab scattering angle cosine if the incoming energy is above* $\frac{AQ}{A-1}$. *For fixed outgoing energy, there is a one-to-one correspondence between incoming energy and lab scattering angle cosine.*

Efficient methods for sampling from this function will be a major focus of this work. However, it is likely that a tabular method will be used based on the seemingly complex nature of this PDF.

Because of the one-to-one correspondence between the outgoing energy and direction, once the outgoing energy has been selected the outgoing direction is known. The following equation must be used to determine the outgoind lab scattering angle cosine corresponding to the incoming and outgoing energy.

$$\mu_l = -\left[\frac{\left(\frac{E}{E'}\right)(A-1)^2 - A^2\left(1+\left(\frac{A-1}{A}\right)\frac{Q}{E'}\right)+1}{2\sqrt{\frac{E}{E'}}(A-1)}\right] \tag{6.38}$$

6.7 Other Non-fission Adjoint Reactions

6.8 Adjoint Neutron Induced Fission

6.9 Adjoint Thermal Scattering

Chapter 7

Overview of FACEMC

A professional software development process can be broken into five main phases: the problem definition, the requirements analysis, the high-level design, construction, and system testing [45]. The first three phases constitute the planning phase. They are considered the most important part of the development process [45].

The problem definition will not contain any reference to solution methods but should clearly define the problem that the software will solve. The problem definition for FACEMC was essentially given in the introduction and will therefore be neglected in this chapter.

During the requirements analysis one determines what the scope of the system is and more generally, what the system is supposed to do [45]. Completion of the requirements analysis is the first step towards a solution to the problem definition.

The high-level design or architecture identifies the subsystems and major classes and their interconnections that will allow for the requirements to be met. The architecture is very important because it determines the conceptual integrity of the software and provides guidance to programmers [45].

The construction phase is the only phase where the software is actually written. This phase will not be discussed further in this chapter. Though the system testing phase was listed last it does not only occur after the construction phase. A large part of this phase occurs in conjunction with the construction phase [45]. This phase is also very important and will be discussed in detail in one of the following sections.

7.1 Requirements

While more detail is certainly better when outlining the code requirements since they will lay the foundation for the entire code, only a brief discussion of the requirement for FACEMC will be given. The requirements that will be discussed fall into the following categories:

- user interface
- spatial domain modeling capabilities
- radiation modeling capabilities

- random number generation
- estimators
- variance reduction capabilities
- input file formats
- output file formats
- auxiliary capabilities
- parallelism

User Interface

The main user interface will be strictly a command-line interface (CLI). On the command-line, users will specify the necessary inputs, which will generally refer the code to the required input files and the desired output files.

Spatial Domain Modeling Capabilities

Two types of spatial domain modeling will be possible. The first type is based on a combinatorial method where Boolean combinations of geometric surfaces of order two or less are specified in order to create volumes. This modeling capability will be very similar to the one in MCNP5 [43]. Implementation details of this method can be found in the report by Hendricks [46]. The second type of spatial domain modeling is computer-aided drafting (CAD) based and will rely on the direct accelerated geometry (DAG) package in the mesh-oriented database (MOAB) [47, 48]. This modeling capability will allow for any types of surface to be modeled. Its use will also be contingent on the users accesses to another code called CUBIT, which is not open source [49].

Radiation Modeling Capabilities

As mentioned in the introduction, the types of radiation that the code will be able to model will be photons in the energy range of one keV to twenty MeV and neutrons in the energy range of 10^{-5} eV to twenty MeV. Adjoint photons and adjoint neutrons in the same energy ranges will also be able to be modeled. The code will not be able to model charged particles. The physics that describes the interaction of the

radiation with a material will be as detailed as possible. However, the user will have the option to select less detailed physics if speed is more important than accuracy.

To model photons and neutrons two cross section libraries will be used. For photons, the 1997 evaluated photon data library (EPDL97) will be used [35]. For neutrons, the seventh version of the evaluated nuclear data library (ENDF/B-VII.1) will be used [41]. While both of these libraries are text files, the Cross Section Evaluation Working Group has expressed interest in storing future versions of the ENDF/B data library in the binary HDF5 format [50]. Therefore, all processed cross section data will be stored in HDF5 format in order to be prepared for future versions of the cross section libraries.

Random Number Generation

Uniform random number generation is an integral part of the Monte Carlo random walk process. The linear congruential generator must be available due to its success in MCNP and many other Monte Carlo codes [51]. Other random number generators will also be available in order to test their speed in relation to the linear congruential generator.

Estimators

The collision estimator and the track length estimator will be available for the user to gather information about his or her model. No expected value estimators, such as the point detector, will be available. Many options will be available to further refine the behavior of these estimators. These options include phase space binning and for collision estimators, collision number binning. The known function which defines the estimator can be either a user defined function specified in the input file or a cross section present in the cross section library. The user will also have the ability to define new functions based on combinations of the previous two through basic mathematical operations.

Variance Reduction

In order to be able to generate results in a reasonable amount of time for deep penetration problems, which are commonly encountered, variance reduction techniques will have to be available. Only five commonly used techniques will be available in FACEMC. These techniques are implicit capture, Russian roulette, splitting, forced

collision, and weight windows. If the weight window technique is used, the user will be in charge of supplying an appropriate weight window mesh. A weight window generator will not be available in FACEMC.

Input File Formats

All input files other than the files that describe the CAD geometries will be in extensible markup language (XML) format. This decision was made because of the availability of XML parsers and because of the complexity involved in creating generic text file readers (based on previous experience). Further, two input files will always be necessary. One will describe the spatial domain and the other will describe all other details of the problem.

Output File Formats

All output files will also be written to XML files except when certain estimators with large phase space binning are used, in which case a Visualization ToolKit (VTK) file will be written. The VTK file format was chosen because of its compatibility with many visualization codes.

Parallelism

The code must also be able to run in parallel in order to solve larger and more complex problems. While several parallel algorithms exist that can be used in Monte Carlo codes, the hierarchical parallelism algorithm found in the paper by Brunner and Brantley will be implemented [52]. Their algorithm allows for domain decomposition, however, only domain replication* will be allowed. The message passing interface (MPI) will be used to implement the algorithm.

7.2 High-Level Design

To meet the requirements that were outlined in the previous section, several subsystems and major classes have been identified. The three main subsystems are the initialization subsystem, the problem simulation subsystem and the spatial domain plotting subsystem. These subsystems and their major components are

*Domain replication is where each processor receives a copy of the problem model. The maximum problem size is therefore limited by the processor with the smallest amount of memory available.

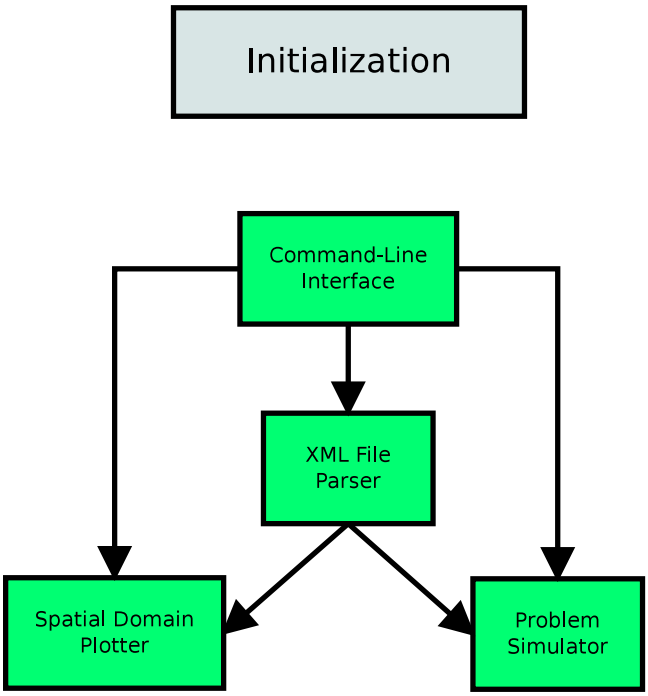

Figure 7.1: **Initialization Subsystem.** *The initialization subsystem consists of two major classes and two other subsystems. The two classes are the command-line interface and the XML file parser. The two subsystems are the spatial domain plotter and the problem simulator. Depending on the requests made by the user, either the problem simulator or the spatial domain plotter will be initialized.*

shown in figures 7.1, 7.2 and 7.3. A simple line between two components indicates that a component contains another component. The color of the two components will also be different to indicate the component hierarchy. A black arrow between two components in the same level of the hierarchy indicates the information flow between the two components. A red arrow between two components indicates that one component creates another component.

The first version of these components except for the XML parser and the geometry plotter are currently completed. The second version of several of these components are also currently completed. The second versions of these components will incorporate lessons learned from the first versions in addition to better programming practices.

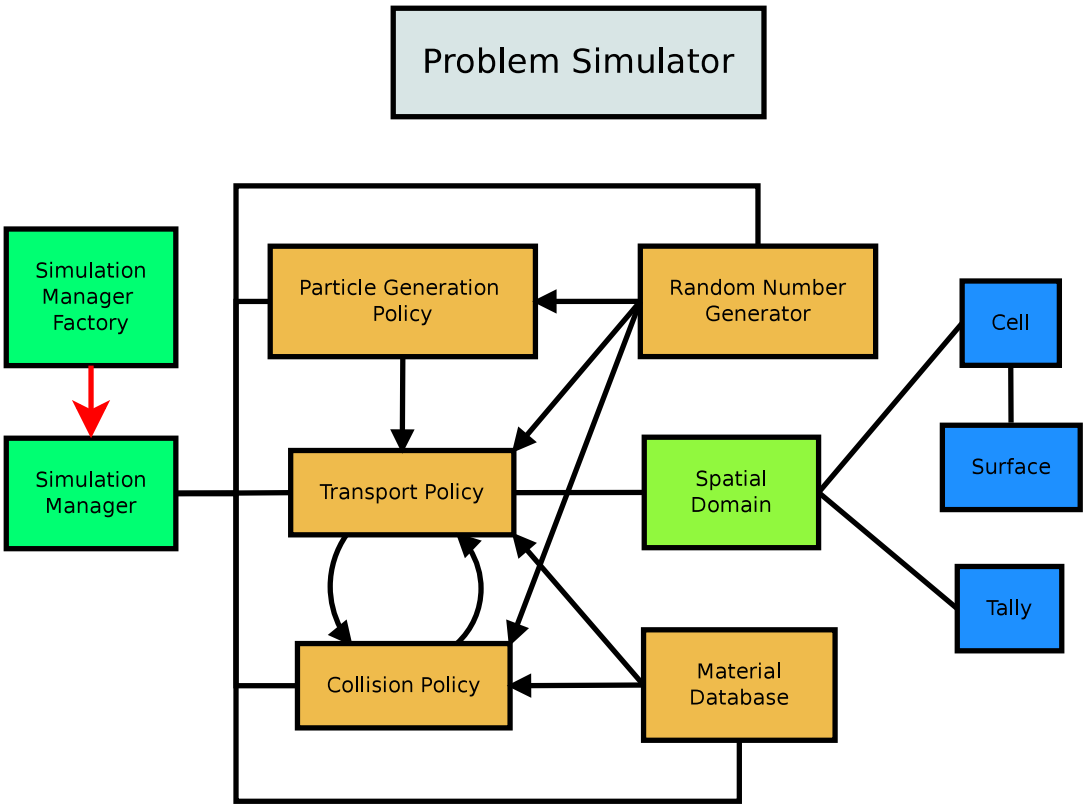

Figure 7.2: **Problem Simulation Subsystem.** *The problem simulation subsystem consists of several major classes. Based on the user inputs pulled from the XML file(s), the simulation manager factory will create the necessary simulation manager. The simulation manager will control the simulation of particles based on three policy classes: the particle generation policy, the transport policy, and the collision policy. The transport policy will contain the spatial domain class, which will contain all cells, surfaces and tallies.*

7.3 System Testing: Verification and Validation

System testing can be broken into two components: verification and validation. Verification, which is the process of determining whether or not particular components of the software fulfill a set of established requirements, occurs in conjunction with the construction phase [53]. Verification is accomplished with an on-going process of unit testing* during the construction phase. Verification of FACEMC through unit testing will not be discussed in this chapter.

Validation, which is the process of determining whether the software returns correct results for desired quantities, occurs at the end of the software development

*A unit test is written for one component of the code and test that expected outputs are returned for a set of inputs.

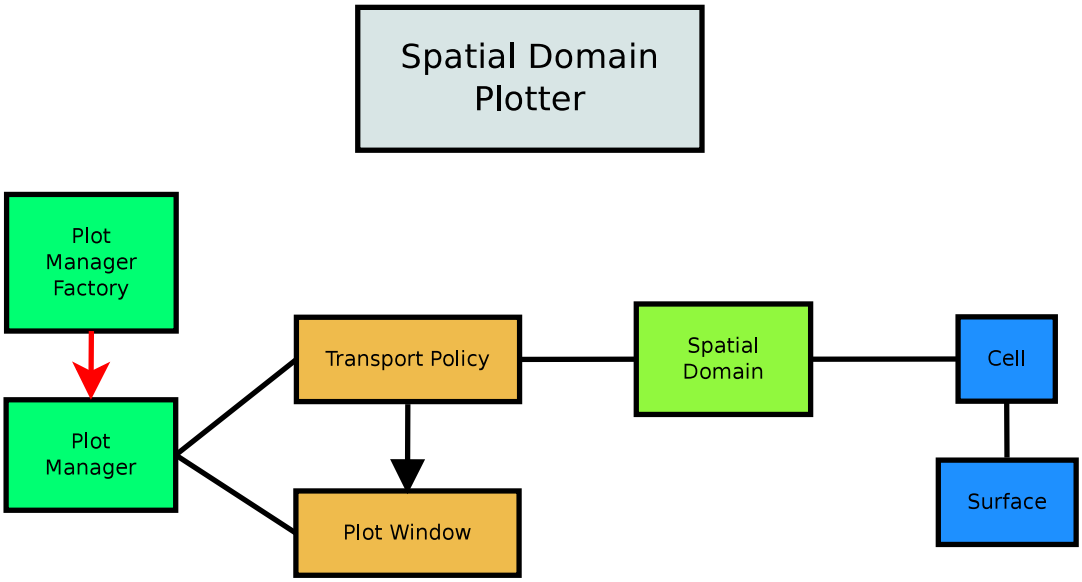

Figure 7.3: **Spatial Domain Plotting Subsystem.** *The spatial domain plotting subsystem consists of several major classes. Based on the user inputs pulled from the XML file(s), the plot manager factory will create the necessary plot manager. The plot manager will control how the spatial domain is plotted based on two classes: the transport policy, which is also a part of the simulation manager, and the plot window. The transport policy will primarily be used to visualize the spatial domain through ray-tracing.*

process. For FACEMC, the following validation plan has been created to ensure that the code functions properly:

1. Calculation of benchmark test problems for photons and neutrons
2. Code-to-code comparisons of integral quantities and photon or neutron spectra against other Monte Carlo codes that have been previously validated
3. Comparison of integral quantities and spectra from forward and reverse simulations

Validation Step 1

The first step of the validation plan will compare results from FACEMC forward simulations against data from benchmark test problems. For photons, the same problem that was used to validate GEANT4 photon simulations will be used [54]. Figure 7.4 shows the problem set up. In this problem, photon mass attenuation coefficients and partial interaction coefficients will be calculated at an array of

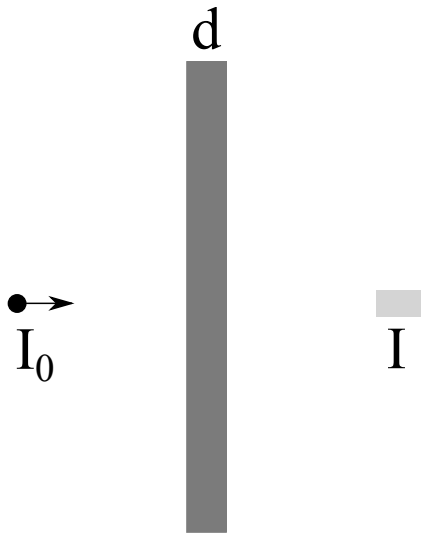

Figure 7.4: **Photon Benchmark Problem.** *A monoenergetic beam of photons is directed at a slab of thickness d. The current of uncollided photons that exits the slab is calculated.*

energies and for a variety of materials. The values that are calculated will then be compared to the values from the National Institute of Standards and Technology (NIST) XCOM database [54]. The mass attenuation coefficient can be calculated with the following formula:

$$\left(\frac{\mu}{\rho}\right) = -\frac{1}{\rho d} \ln\left(\frac{I}{I_0}\right). \tag{7.1}$$

If only a single reaction type is considered, the above equation can be used to determine the partial interaction coefficient corresponding to the reaction considered.

For neutrons, several experiments from the Shielding Integral Benchmark Archive Database (SINBAD) will be modeled and the resulting data will be compared to the experimental data in the database [55]. The exact problems that will be modeled have not been determined yet.

Validation Step 2

The second step of the validation plan will focus on code-to-code comparisons against other Monte Carlo codes that have been previously validated. Only a single problem, which is shown in figure 7.5 will be used in this step of the validation plan. The spatial domain is an infinite medium containing a point source at the center of five concentric spheres. Two surface flux estimators are used at each spherical surface. The first is used to estimate the total flux at the surface and the second

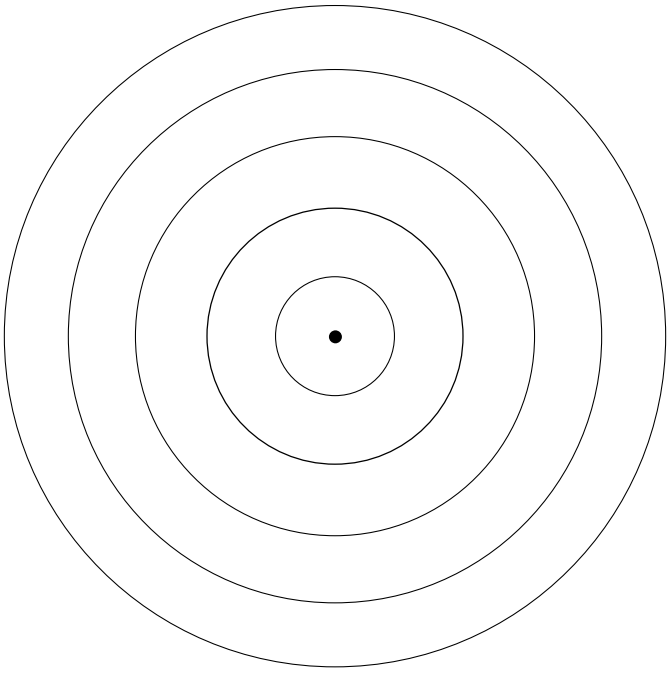

Figure 7.5: **Code-to-Code Comparison Problem.** *An isotropic point source is located at the center of five concentric spheres. The radii of the spheres are 10 cm, 20 cm, 30 cm, 40 cm and 50 cm. The spatial domain extends to infinity in every dimension. Only a single material is present throughout the spatial domain and there are no voids. Surface flux estimators are used on each sphere.*

is discretized in energy so that the energy spectrum of the particles crossing the surface can be estimated.

For photons, an isotropic point source with two discrete energies will be modeled. For neutrons, an isotropic point source with a fission spectrum will be modeled. An array of materials will also be used to ensure that cross sections have been processed correctly.

Two codes will be used to conduct the comparison for photons: MCNP5 and PENELOPE. Two codes will also be used to conduct the comparison for neutrons: MCNP5 and TART2005.

Validation Step 3

The third step of the validation plan will focus on comparisons between forward and reverse calculations done using FACEMC only. After the second step of the validation plan is complete the forward simulation mode can be deemed validated. It can therefore be used to validate the adjoint simulation mode.

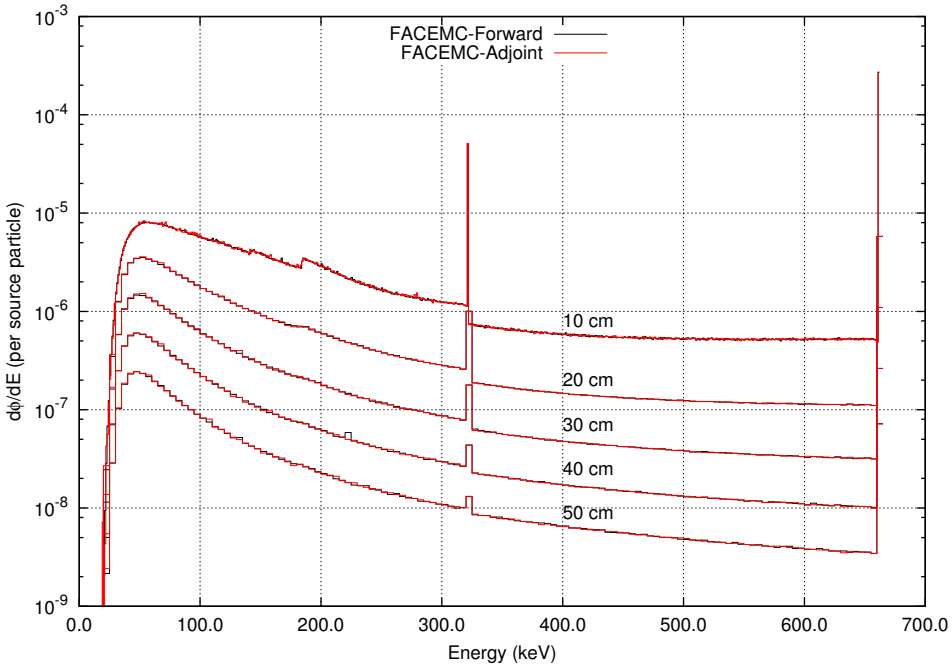

Figure 7.6: **Validation Plan Step 3 - Case 0: Photon Spectra in Water.** *The photon spectra computed using the forward and adjoint mode of FACEMC appear to be in very good agreement at all surfaces of interest. All relative errors are less than 1.5%.*

The same problem that was used in the second step of the validation plan, shown in figure 7.5, will be used in this step. Interestingly, the unique symmetry of this problem allows the reverse problem to be constructed identically to the forward problem. A proof of this symmetry is rather complex and requires the use of Green's functions [7]. It will therefore not be shown.

One case for photons has already been completed*. The material that is present is water and the two discrete source energies are 661.66 keV and 321.0 keV. The first discrete source energy corresponds to the primary Cs-137 decay line and the second discrete source energy is contrived. Figures 7.7 and 7.6 show the spectrum results for this case. From the figures, it is clear that the spectra calculated using the forward and adjoint capabilities of FACEMC are in good agreement. Table 7.1 shows the total flux results for this case. The total flux calculated with the forward and adjoint modes are also in very good agreement.

An interesting take away from table 7.1, which is unrelated to the validation of the code, is that the current implementation of the adjoint mode is more costly to

*This case was completed before the validation plan was developed, which is why it was done out of order.

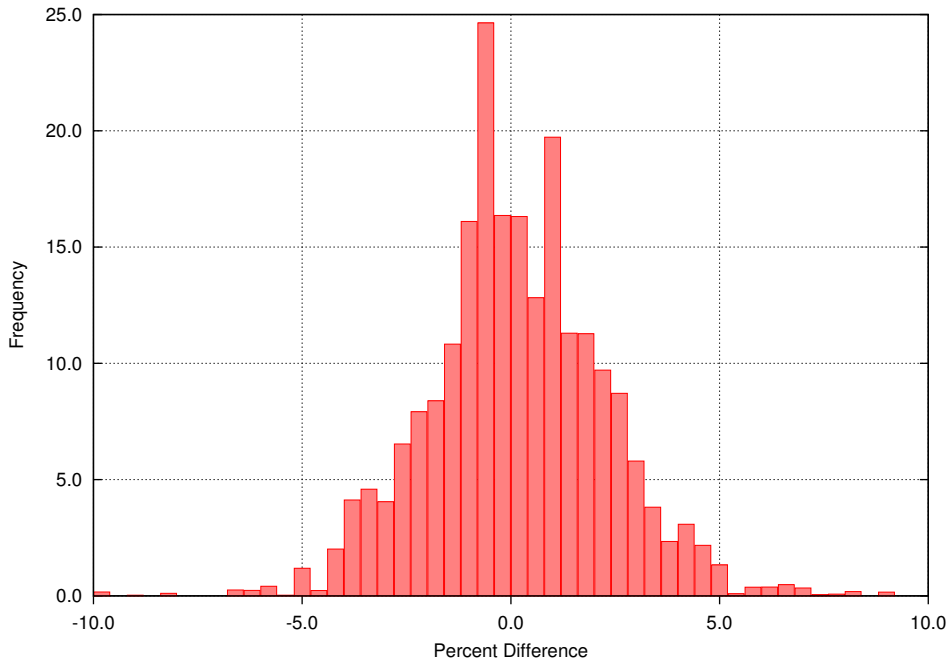

Figure 7.7: **Validation Plan Step 3 - Case 0: Photon Spectra Differences at 10 cm.** *This plot shows the percent difference between each bin of the spectrum at 10 cm computed using the forward mode of FACEMC and each bin of the spectrum at 10 cm computed using the adjoint mode of FACEMC. The majority of the percent differences are between -5.0% and 5.0%.*

Table 7.1: **Validation Plan Step 3 - Case 0: Photon Total Flux in Water.** *The photon total flux computed using the forward and adjoint mode of FACEMC are in very good agreement at all surfaces of interest.*

Distance (cm)	Flux (forward mode)	Relative Error	Flux (adjoint mode)	Relative Error	% Diff.
10	1.5748e-3	0.0007	1.5788e-3	0.0014	0.25
20	4.1291e-4	0.0007	4.1491e-4	0.0018	0.48
30	1.4150e-4	0.0007	1.4235e-4	0.0022	0.60
40	5.2255e-5	0.0011	5.2322e-5	0.0027	0.13
50	1.9963e-5	0.0014	2.0030e-5	0.0033	0.34

run than the implementation of the forward mode. Even when the same number of particles are modeled the relative error of the adjoint mode is higher than the forward mode. This is solely a result of the properties of the adjoint weight factor, which were described in the previous chapter, given that the problem is modeled identically in both the forward and adjoint modes. Hoogenboom has described

some methods that could potentially ameliorate this issue [16].

Chapter 8

Conclusion

The primary goals of this report were:

1. to present a detailed background of the Monte Carlo method beyond what is typically found in the literature,
2. to use this background to develop the Monte Carlo random walk process for adjoint particles,
3. to describe the adjoint cross sections and sampling procedures that will be used to conduct random walks with adjoint photons.
4. and to describe how all of this information will be incorporated into the FACEMC code.

While working to achieve these goals in this report several important points were made which must be summarized. In the following sections, the main points from each chapter will be given. Before finishing, all proposed future work will also be enumerated.

8.1 Monte Carlo Methods for Fredholm Integral Equations

The primary goal of chapter 2 was to give a very general description of the Monte Carlo random walk process and to show how one can use it to estimate solutions to a particular class of equations called FIESKs. The FIESK is an important equation with applications in radiation transport problems.

The Monte Carlo random walk process was shown to be governed by a set of PDFs that must be derived from the FIESK of interest. The process is very general and can in fact be applied to any FIESK as long as the PDFs derived from the FIESK have certain properties.

The concept of an estimator was also discussed in this chapter. To summarize briefly, the estimator accumulates information from a random walk and uses it to estimate the inner product of the solution of a FIESK and some known function.

The two estimators that were discussed were the termination estimator and the event estimator. The termination estimator estimates the solution of a FIESK every time a random walk ends in the region of interest. The event estimator estimates the solution of a FIESK every time a random walk has an event in the region of interest. In general, these estimators become ineffective when the region of interest is reduced to a single point of the phases space.

Finally, the estimation of the solution of a FIESK at a point was discussed. When this kind of estimate is desired the Dual FIESK and its associated Monte Carlo random walk process must be used. In the random walk process associated with the Dual FIESK random walks start in a detector region (or region of interest as its is sometimes referred to) and estimators accumulate information about the random walk in the source region. There are also special estimators that exist which can be used to estimate the value of certain FIESKs at a point, however these estimators are not applicable in general and were therefore not discussed. In general, if the size of the source region is larger than the size of the detector region, the Dual FIESK and its associated Monte Carlo random walk process should be used. This claim is based on the simple fact that a random walk will have a higher probability of entering a large region than a small region.

8.2 The Monte Carlo Random Walk Process for Radiation Transport

The primary goal of chapter 3 was to show how to create a FIESK from the integro-differental form of the transport equation and to then construct a Monte Carlo random walk process using the general theory from chapter 2. The idea was to take a very thorough approach to deriving the Monte Carlo random walk process for radiation transport even though most people are likely familiar with the process. Then, the same thorough approach could be used to derive the Monte Carlo random walk process for adjoint radiation, which is much less familiar.

Through a series of manipulations, it was shown in this chapter how to take the integro-differential tranport equation and create a FIESK that describes either the flux, the emission density or the collision density of a system. The flux FIESK was examined first and an associated Monte Carlo random walk process was created. This process was shown to have several unfavorable properties. By far the most unseemly was the potential for event locations to be sampled in a vacuum. This

property arose from the fact that the flux does not go to zero in a vacuum. Because of these unfavorable properties the flux FIESK and its associated random walk process are rarely used in practice.

The emission density FIESK and collision density FIESK were examined next. It was shown that the state transition kernels that appear in the emission density FIESK and collision density FIESK can be decomposed into two kernels: the collision kernel, which describes the movement of particles through energy and direction, and the transport kernel, which describes the movement of particles through space. It was also shown that the collision kernel can be further decomposed into its constituent reactions. When one wants to handle particle multiplication explicitly, which is usually done, this expansion of the collision kernel must be done. A sampling procedure was also given for sampling a particular reaction from the collision kernel.

Finally, the Monte Carlo random walk process for radiation transport was derived. Due to the similarities between the emission density FIESK and the collision density FIESK, solutions to both FIESKs can actually be estimated using the same random walk process. To quickly summarize this combined process, a random walk is always initiated in the problem source. The next collision point is then sampled from the transport kernel. At this new collision point a new energy and direction is sampled from the collision kernel. If a multiplying reaction was sampled additional random walks will start from this collision point. A new collision point will then be sampled for the original random walk and the process will continue until either an absorption reaction is chosen or the random walk exits the problem domain. During this process the emission density will always be estimated after a birth or after a particle exits a collision. The collision density will always be estimated upon entering a collision.

One final note was also given regarding the calculation of material responses. The material response is usually given as the inner product of the flux and a material response function. The emission density or the collision density can be used instead of the flux if a modified material response function is used.

8.3 The Monte Carlo Random Walk Process for Adjoint Radiation Transport

In chapter 4 all of the theories and procedures from chapters 2 and 3 were utilized to construct a Monte Carlo random walk process for adjoint radiation transport. The thorough approach to deriving the Monte Carlo random walk process for radiation transport in chapter 3 was particularly useful. Before this approach was mimicked for adjoint radiation transport, the dual emission density FIESK was constructed and examined.

Upon examination of the dual emission density FIESK it became clear that the *adjoint of the emission density*, which the dual emission density FIESK describes, was a "flux-like" quantity. Based on the observations made in chapter 3 about the Monte Carlo random walk process for the flux, it was determined that the dual emission density FIESK should be avoided. A modification to the dual emission density FIESK was also suggested to ameliorate its "flux-like" nature. It turns out that this modification results in the adjoint emission density FIESK, however this idea was not pursued further because it was desired to treat adjoint transport more generally.

As mentioned in chapter 3 a material response can be calculated from the inner product of the flux and the material response function. This material response function can also be calculated from the inner product of the source function and another quantity called the adjoint flux, which is described by the adjoint transport equation. The exact derivation of the adjoint transport equation was not given, though it is actually very similar to the derivation of the dual FIESK from a FIESK given in chapter 2.

Once the adjoint transport equation in integro-differential form was obtained, a set of manipulations similar to the ones shown in chapter 3 were done to obtain a FIESK that described the adjoint emission density or the adjoint collision density. The adjoint flux FIESK was avoided due to the negative properties of FIESKs that describe "flux-like" quantities. The state transition kernels that appeared in the adjoint emission density FIESK and the adjoint collision density FIESK were then examined.

Unlike the state transition kernels from the emission density FIESK and collision density FIESK, the state transition kernels from the adjoint emission density FIESK and adjoint collision density FIESK can actually be decomposed into three terms: the adjoint collision kernel, which describes the movement of adjoint particles through

energy and direction, the adjoint transport kernel, which describes the movement of adjoint particles through space, and the adjoint weight factor.

The adjoint weight factor, which is simply the ratio of the total macroscopic adjoint cross section to the total macroscopic cross section, is one of the very interesting and surprising properties of these state transition kernels. It comes about from the construction of the adjoint collision kernel and the adjoint transport kernel, both of which are normalized to unity. The adjoint collision kernel is constructed with the total macroscopic adjoint cross section while the adjoint transport kernel is constructed with the total macroscopic cross section, which allows for their normalization to unity. The total macroscopic adjoint cross section and the total macroscopic cross section are in general not equal, which gives rise to the adjoint weight factor.

An expansion of the adjoint collision kernel into its constituent adjoint reactions and a sampling procedure for sampling a particular reaction from this expanded adjoint collision kernel were also shown. This expansion and the associated sampling procedure is useful if one wants to model every adjoint reaction separately, which will usually be the case. Unfortunately, the adjoint cross section for each individual reaction is often unknown and must be constructed from the associated forward cross section. The equations for calculating the adjoint cross sections are an extremely important take-away from this report and will therefore be shown again:

$$\sigma^{\dagger}(E') = \int\int \sigma(E)c(E)p(E \to E', \hat{\Omega} \to \hat{\Omega}')dEd\hat{\Omega}$$

$$p^{\dagger}(E' \to E, \hat{\Omega}' \to \hat{\Omega}) = \frac{\sigma(E)c(E)p(E \to E', \hat{\Omega} \to \hat{\Omega}')}{\sigma^{\dagger}(E')}$$

An interesting property of adjoint radiation, which is apparent from both the normalization of the adjoint collision kernel and the definition of the adjoint cross section, is the lack of absorption reactions or multiplying reactions. For absorption reactions $c(E)$ is zero and the resulting adjoint cross section is zero. For multiplying reactions $c(E)$ gets integrated into the adjoint cross section. These properties highlight the necessity of the rigorous mathematical approach to deriving the Monte Carlo random walk process for adjoint radiation since they are very unintuitive.

Finally, the Monte Carlo random walk process for radiation transport was derived. Due to the similarities between the adjoint emission density FIESK and the adjoint collision density FIESK, solutions to both FIESKs can actually be estimated using the same random walk process. To quickly summarize this combined process, a random

walk is always initiated in the adjoint source (or detector). The next collision point is then sampled from the adjoint transport kernel. At this new collision point a new energy and direction is sampled from the adjoint collision kernel. A new collision point will then be sampled and the process will continue. Due to the lack of an absorption cross section, Russian roulette must be used to terminate these random walks. During this process the adjoint emission density will always be estimated after a birth or after an adjoint particle exits a collision. The adoint collision density will always be estimated upon entering a collision.

One final note was also given in this chapter regarding the calculation of material responses. The material response defined as the inner product of the adjoint flux and the source can also be defined in terms of the adjoint emission density or the adjoint collision density and a modified source function.

8.4 Photon Interaction Cross Sections and Sampling Techniques

Chapter 5 was intended to described completely all photon and adjoint photon interactions and associated sampling procedures. The primary interactions that were discussed for photons were incoherent scattering (with and without Doppler broadening), coherent scattering, pair production and the photoelectric effect. For adjoint photons the interactions that were discussed were adjoint incoherent scattering (with and without Doppler broadening), adjoint coherent scattering and adjoint pair production.

The main take-away from this chapter is that nearly all photon phenomena can be modeled with either photons or adjoint photons with the same degree of accuracy. The one phenomena that can't currently be accounted for by adjoint photons is the release of low energy x-rays due to atomic relaxation after a photoelectric effect event. In applications where low energy photons are important this limitation could be a problem. Solutions to this problem will be part of the future work.

It must also be noted that this chapter presented some genuinely novel work: the Doppler broadening of incoherently scattered adjoint photons. The theoretical work that was presented still needs to be tested. However, if it is indeed correct, the ability to model the Doppler broadening of incoherently scattered adjoint photons will be a capability unique to FACEMC.

8.5 Overview of FACEMC

The main take-away from chapter 7 is that FACEMC is already in a state where problems can be modeled and data can be acquired. The first version of the code is currently being updated to make it faster and easier to use. Adjoint neutron capabilities are also being added to the code.

An extensive validation plan was also presented in this chapter. Completion of this plan should ensure that FACEMC is working properly.

8.6 Future Work

Though much work has been completed towards the development of FACEMC both in terms of theory and coding, there is still much work to be done. In terms of theory, the following items have been identified as needing more work:

- The low energy x-ray emission problem for adjoint photons.
- The background work on neutron and adjoint neutron transport cross sections and sampling techniques.

In terms of coding, the following items must still be completed:

- The coding of the second version of all major FACEMC components outlined in chapter 7.
- The computation of adjoint neutron cross sections and storage in an HDF5 format library.

In terms of analysis work, the following items will be proposed:

- Complete the FACEMC validation plan.
- Calculate the adjoint data required for brachytherapy treatment planning optimization using data from a patient.
- Calculate the adjoint data required for external beam treatment planning using a standard phantom.
- Run a full scale shutdown dose calculation for a fusion device using the R2SA method.

- Run a shielding problem using the adjoint neutron transport capabilities of FACEMC.

These final items should be challenging enough to test the capabilities of FACEMC.

To complete the items listed above in a timely fashion, the following timeline has been created:

1. Complete all theoretical work by September 1st, 2013.
2. Complete all coding work by March 1st, 2014.
3. Complete the validation plan by April 1st, 2014.
4. Complete all of the the challenge problems by June 1st, 2014.
5. Ideal thesis completion date: August 1st, 2014 - September 1st, 2014

Based on experience gained writing the first version of FACEMC, this timeline should be feasible.

Appendix A

Photon Interaction Physics and Sampling Derivations

In chapter 5 the derivation of several important equations and sampling schemes were omitted. In this appendix the details of many of these derivations will be shown.

A.1 Compton Scattering from Free and Bound Electrons

The process of Compton scattering off of a free electron is represented by figure A.1. Conservation of energy and momentum will be used to determine the final energy of the photon after the collision with the electron. First, the momentum of the particle system will be analyzed. In the transverse direction, momentum conservation is:

$$P \sin\theta = P_e \sin\phi.$$

In the longitudinal direction, momentum conservation is.

$$P' = P\cos\theta + P_e \cos\phi.$$

Both of these equations will now be squared and added together:

$$P'^2 - 2P'P\cos\theta + P^2(\cos^2\theta + \sin^2\theta) = P_e^2(\cos^2\phi + \sin^2\phi)$$
$$P_e^2 = P'^2 - 2P'P\cos\theta + P^2. \tag{A.1}$$

This equation for the electron momentum will be useful in the equation for the conservation of energy of the particle system.

Now, the energy of the particle system will be analyzed:

$$E' + m_e c^2 = E + E_e$$

$$E' - E + m_e c^2 = E_e$$

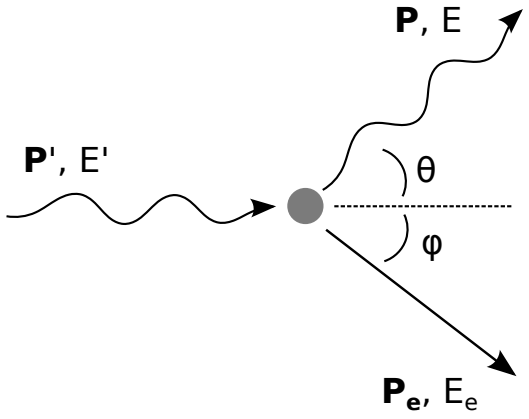

Figure A.1: **Compton scattering off of a free electron.**

$$(P^{'} - P)c + m_e c^2 = \sqrt{(P_e c)^2 + (m_e c^2)^2}$$

$$(P^{'} - P)^2 c^2 + 2m_e c^3 (P^{'} - P) + m_e^2 c^4 = P_e^2 c^2 + m_e^2 c^4$$

$$P^{'2} c^2 - 2P^{'} P c^2 + P^2 c^2 + 2m_e c^3 (P^{'} - P) = P^{'2} c^2 - 2P^{'} P \cos\theta c^2 + P^2 c^2$$

$$2m_e c^3 (P^{'} - P) = 2P^{'} P c^2 (1 - \cos\theta)$$

$$m_e c^3 P^{'} = Pc(P^{'} c(1 - \cos\theta) + m_e c^2)$$

$$\begin{aligned} E &= \frac{m_e c^2 E^{'}}{E^{'}(1 - \cos\theta) + m_e c^2} \\ &= \frac{E^{'}}{1 + \frac{E^{'}}{m_e c^2}(1 - \cos\theta)} \end{aligned} \tag{A.2}$$

$$\alpha = \frac{\alpha^{'}}{1 + \alpha^{'}(1 - \cos\theta)}. \tag{A.3}$$

The process of Compton scattering off of a bound electron is represented by figure A.2. Conservation of energy and momentum will again be used to determine the quantity of interest, which in this case is the initial electron momentum, $\vec{P_e^{'}}$, projected onto the photon scattering vector, $\vec{P} - \vec{P^{'}}$. The z-axis of the system will be set parallel to the scattering vector. Therefore, the electron momentum projection will be represented by the variable p_z.

Before analyzing the energy of the particle system, then energy of the electron

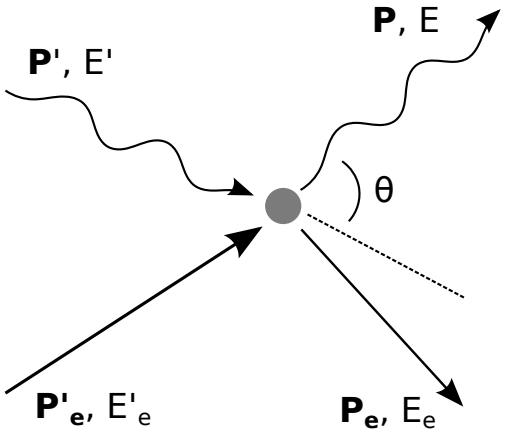

Figure A.2: **Compton scattering off of a bound electron.**

will be examined:

$$\begin{aligned} E_e^2 &= m_e^2c^4 + P_e^2c^2 \\ &= \left(m_ec^2 + E_{e,k}\right)^2. \end{aligned}$$

$$P_e^2c^2 = 2m_ec^2E_{e,k} + E_{e,k}^2. \tag{A.4}$$

The kinetic energy of the electron is represented by, $E_{e,k}$. The binding energy of the electron is will be represented by E_b. The energy of the particle system is

$$E^{'} + E_{e,k}^{'} + m_ec^2 = E + E_{e,k} + m_ec^2 + E_b$$

and

$$\begin{aligned}
E' - E - E_b &= E_{e,k} - E'_{e,k} \\
\left(E' - E - E_b\right)^2 &= \left(E_{e,k} - E'_{e,k}\right)^2 \\
&= E_{e,k}^2 - 2E_{e,k}E'_{e,k} + E'^2_{e,k} \\
&= P_e^2c^2 - 2m_ec^2E_{e,k} - 2E_{e,k}E'_{e,k} + P'^2_e c^2 - 2m_ec^2E'_{e,k} \\
&= \left(P_e^2 + P'^2_e\right)c^2 - 2m_ec^2E'_{e,k} - 2E_{e,k}\left(m_ec^2 + E'_{e,k}\right) \\
&= \left(P_e^2 + P'^2_e\right)c^2 - 2m_ec^2E'_{e,k} - 2\left(E' - E - E_b + E'_{e,k}\right)\left(m_ec^2 + E'_{e,k}\right) \\
&= \left(P_e^2 + P'^2_e\right)c^2 - 4m_ec^2E'_{e,k} - 2E'^2_{e,k} - 2\left(E' - E - E_b\right)\left(m_ec^2 + E'_{e,k}\right) \\
&= \left(P_e^2 - P'^2_e\right)c^2 - 2\left(E' - E - E_b\right)\left(m_ec^2 + E'_{e,k}\right) \\
\left(P_e^2 - P'^2_e\right)c^2 &= \left(E' - E - E_b\right)^2 + 2\left(E' - E - E_b\right)\left(m_ec^2 + E'_{e,k}\right). \qquad \text{(A.5)}
\end{aligned}$$

The momentum of the particle system will now be analyzed:

$$\begin{aligned}
\vec{P'} + \vec{P'_e} &= \vec{P} + \vec{P_e} \\
m_ec\vec{\alpha'} + \vec{P'_e} &= m_ec\vec{\alpha} + \vec{P_e}.
\end{aligned}$$

The new variable $\vec{\alpha}$ is simply the momentum of the photon in units of m_ec. The magnitude of this vector has the following properties:

$$\begin{aligned}
|\vec{\alpha}| &= \alpha \\
&= \frac{P}{m_ec} \qquad \text{(A.6)} \\
&= \frac{E}{m_ec^2}. \qquad \text{(A.7)}
\end{aligned}$$

The equation for the momentum of the system must be rearranged further before moving on:

$$\begin{aligned}
\vec{P'_e} - \vec{P_e} &= \vec{q} \\
&= m_ec\left(\vec{\alpha} - \vec{\alpha'}\right)
\end{aligned}$$

$$\begin{aligned} q^2 &= (m_e c)^2 \left| \vec{\alpha} - \vec{\alpha'} \right| \\ &= (m_e c)^2 \left(\alpha'^2 + \alpha^2 - 2\vec{\alpha'} \cdot \vec{\alpha} \right) \\ &= (m_e c)^2 \left(\alpha'^2 + \alpha^2 - 2\alpha' \alpha \cos\theta \right). \end{aligned} \tag{A.8}$$

Now, using the equation for $\vec{q}$, the equation for the electron momentum projection can be determined:

$$\vec{P_e} = \vec{P'_e} - \vec{q}$$

$$P_e^2 = P_e'^2 + q^2 - 2\vec{P'_e} \cdot \vec{q}$$

$$2\vec{P'_e} \cdot \vec{q} = -\left(P_e^2 - P_e'^2 \right) + q^2$$

$$2p_z q = -\left(P_e^2 - P_e'^2 \right) + q^2$$

$$\begin{aligned} p_z &= \frac{1}{2q}\left[-\left(P_e^2 - P_e'^2 \right) + q^2 \right] \\ &= \frac{1}{2qc^2}\left[-(E' - E - E_b)^2 - 2(E' - E - E_b)(m_e c^2 + E'_{e,k}) + q^2 c^2 \right] \\ &= \frac{m_e^2 c^4}{2qc^2}\left[-\left(\alpha' - \alpha - \frac{E_b}{m_e c^2} \right)^2 - 2\left(\alpha' - \alpha - \frac{E_b}{m_e c^2} \right)\left(1 + \frac{E'_{e,k}}{m_e c^2} \right) + \left| \vec{\alpha} - \vec{\alpha'} \right|^2 \right] \\ &= \frac{m_e^2 c^2}{2q}\Bigg[-(\alpha' - \alpha)^2 + 2(\alpha' - \alpha)\left(\frac{E_b}{m_e c^2} \right) - \left(\frac{E_b}{m_e c^2} \right)^2 - 2(\alpha' - \alpha)\left(1 + \frac{E'_{e,k}}{m_e c^2} \right) + \\ &\qquad 2\left(\frac{E_b}{m_e c^2} \right)\left(1 + \frac{E'_{e,k}}{m_e c^2} \right) + \alpha'^2 + \alpha^2 - 2\alpha' \alpha \cos\theta \Bigg] \\ &= m_e c \frac{\left[(\alpha' - \alpha)\left(1 + \frac{E'_{e,k} - E_b}{m_e c^2} \right) + \alpha' \alpha (1 - \cos\theta) - \frac{1}{2}\left(\frac{E_b}{m_e c^2} \right)^2 + \left(\frac{E_b}{m_e c^2} \right)\left(1 + \frac{E'_{e,k}}{m_e c^2} \right) \right]}{\sqrt{\alpha'^2 + \alpha^2 - 2\alpha' \alpha \cos\theta}}. \end{aligned} \tag{A.9}$$

If the binding energy and kinetic energy of the electron are assumed to be small compared to the rest mass energy of the electron, they can be neglected. The resulting equation, which is often reported in the literature is

$$p_z = m_e c \frac{\left[\alpha - \alpha' + \alpha' \alpha (1 - \cos\theta) \right]}{\sqrt{\alpha'^2 + \alpha^2 - 2\alpha' \alpha \cos\theta}}. \tag{A.10}$$

Derivations that are similar to the ones just shown were completed by Sood [56].

A.2 The Klein-Nishin Cross Section Differential in Inverse Energy Loss Ratio

As mentioned in chapter 5, the differential Klein-Nishina cross section is most easily sampled when a change of variables from steradians to the inverse energy loss ratio is conducted. The energy loss ratio, which was originally shown in chapter 5, will be shown again:

$$\begin{aligned}\frac{1}{x} &= \frac{\alpha}{\alpha'} \\ &= \frac{1}{1+\alpha'(1-\cos\theta)}.\end{aligned}$$

The change of variables is conducted using the following relationship:

$$\frac{d\sigma_{K.N.}(\alpha', x)}{dx}dx = \frac{d\sigma_{K.N.}(\alpha', \theta)}{d\Omega}d\Omega$$

$$\frac{d\sigma_{K.N.}(\alpha', x)}{dx} = \frac{d\sigma_{K.N.}(\alpha', \theta)}{d\Omega}\left(\frac{d\Omega}{dx}\right).$$

Based on the equation for the energy loss ratio, the second term in the above equation can be determined:

$$\begin{aligned}x &= 1+\alpha'(1-\cos\theta) \\ dx &= -\alpha' d(\cos\theta)\end{aligned}$$

and

$$\begin{aligned}\frac{d\Omega}{dx} &= -2\pi\frac{d(\cos\theta)}{dx} \\ &= \frac{2\pi}{\alpha'}.\end{aligned} \tag{A.11}$$

The following relationships will also be useful while conducting the change of variables:

$$x-1 = \alpha'(1-\cos\theta) \tag{A.12}$$

$$\cos^2\theta = 1 - \frac{2(x-1)}{\alpha'} + \frac{(x-1)^2}{\alpha'^2}. \tag{A.13}$$

Now, the change of variables can be completed:

$$\begin{aligned}
\frac{d\sigma_{K.N.}(\alpha', x)}{dx} &= \frac{r_e^2}{2}\frac{\left[1+\cos^2\theta+\frac{\alpha'^2(1-\cos\theta)^2}{1+\alpha'(1-\cos\theta)}\right]}{\left[1+\alpha'(1-\cos\theta)\right]^2}\left(\frac{2\pi}{\alpha'}\right) \\
&= \left(\frac{\pi r_e^2}{\alpha' x^2}\right)\left[1+\left(1-\frac{2(x-1)}{\alpha'}+\frac{(x-1)^2}{\alpha'^2}\right)+\frac{(x-1)^2}{x}\right] \\
&= \left(\frac{\pi r_e^2}{\alpha' x^2}\right)\left[2-\frac{2x}{\alpha'}+\frac{2}{\alpha'}+\frac{x^2}{\alpha'^2}-\frac{2x}{\alpha'^2}+\frac{1}{\alpha'^2}+x-2+\frac{1}{x}\right] \\
&= \left(\frac{\pi r_e^2}{\alpha'}\right)\left[\frac{1}{\alpha'^2}+\frac{1}{x}\left(1-\frac{2}{\alpha'}-\frac{2}{\alpha'^2}\right)+\frac{1}{x^2}\left(\frac{2}{\alpha'}+\frac{1}{\alpha'^2}\right)+\frac{1}{x^3}\right] \\
&= K\left[A+\frac{B}{x}+\frac{C}{x^2}+\frac{D}{x^3}\right]. \qquad \text{(A.14)}
\end{aligned}$$

where

$$\begin{aligned}
K &= \frac{\pi r_e^2}{\alpha'} \\
A &= \frac{1}{\alpha'^2} \\
B &= 1-\frac{2(\alpha'+1)}{\alpha'^2} \\
C &= \frac{(1+2\alpha')}{\alpha'^2} \\
D &= 1
\end{aligned}$$

A.3 The Total Klein-Nishina Cross Section

Using the sampling methods from chapter 5 will sometimes require the total Klein-Nishina cross section. Using the Klein-Nishina cross section differential in the inverse energy loss ratio, the total Klein-Nishina cross section can be determined

rather easily:

$$
\begin{aligned}
\sigma_{K.N.}(\alpha') &= \int_1^{1+2\alpha'} \frac{d\sigma_{K.N.}(x)}{dx} dx \\
&= K\left(\int_1^{1+2\alpha'} A\,dx + \int_1^{1+2\alpha'} \frac{B}{x} dx + \int_1^{1+2\alpha'} \frac{C}{x^2} dx + \int_1^{1+2\alpha'} \frac{D}{x^3} dx\right) \\
&= K\left(Ax\Big|_1^{1+2\alpha'} + B\ln x\Big|_1^{1+2\alpha'} - \frac{C}{x}\Big|_1^{1+2\alpha'} - \frac{D}{2x^2}\Big|_1^{1+2\alpha'}\right) \\
&= K\left(2\alpha' A + B\ln(1+2\alpha') - \frac{C}{1+2\alpha'} + C - \frac{D}{2(1+2\alpha')^2} + \frac{D}{2}\right) \\
&= K\left(\frac{2}{\alpha'} + \ln(1+2\alpha') - \frac{2(\alpha'+1)}{\alpha'^2}\ln(1+2\alpha') - \frac{1}{\alpha'^2} + \frac{1+2\alpha'}{\alpha'^2} - \frac{1}{2(1+2\alpha'^2)^2} + \frac{1}{2}\right) \\
&= K\left(\frac{2}{\alpha'} + \ln(1+2\alpha') - \frac{2(\alpha'+1)}{\alpha'^2}\ln(1+2\alpha') + \frac{2}{\alpha'} + \frac{2\alpha'(1+\alpha')}{(1+2\alpha')^2}\right) \\
&= K\left(\frac{4(1+\alpha')^2}{\alpha'(1+2\alpha')} - \frac{4\alpha'}{1+2\alpha'} + \ln(1+2\alpha') - \frac{2(\alpha'+1)}{\alpha'^2}\ln(1+2\alpha') + \frac{2\alpha'(1+\alpha')}{(1+2\alpha')^2}\right) \\
&= K\left(\frac{2(1+\alpha')}{\alpha'}\left[\frac{2(1+\alpha')}{1+2\alpha'} - \frac{\ln(1+2\alpha')}{\alpha'}\right] + \ln(1+2\alpha') - \frac{4\alpha'}{1+2\alpha'} + \frac{2\alpha'(1+\alpha')}{(1+2\alpha')^2}\right) \\
&= K\left(\frac{2(1+\alpha')}{\alpha'}\left[\frac{2(1+\alpha')}{1+2\alpha'} - \frac{\ln(1+2\alpha')}{\alpha'}\right] + \ln(1+2\alpha') - \frac{2\alpha'(1+3\alpha')}{(1+2\alpha')^2}\right) \\
&= 2\pi r_e^2\left(\frac{(1+\alpha')}{\alpha'^2}\left[\frac{2(1+\alpha')}{1+2\alpha'} - \frac{\ln(1+2\alpha')}{\alpha'}\right] + \frac{\ln(1+2\alpha')}{2\alpha'} - \frac{(1+3\alpha')}{(1+2\alpha')^2}\right).
\end{aligned}
\tag{A.15}
$$

In the equation for the total Klein-Nishina cross section reported by Lux, the second and third terms have an error [2]. The second term is

$$\frac{\ln(1+2\alpha')}{2\alpha'}.$$

In the equation reported by Lux, this term is

$$\frac{\ln(1+2\alpha')}{2\alpha'^2}.$$

The third term is

$$-\frac{(1+3\alpha')}{(1+2\alpha')^2}.$$

In the equation reported by Lux, this term is

$$-\frac{(1+3\alpha')}{\alpha'(1+2\alpha')^2}.$$

A.4 Kahn's Klein-Nishina Rejection Sampling Procedure

As mentioned in chapter 5, below an incoming photon energy of about 1.4 MeV, Kahn's rejection sampling procedure must be used to sample the outgoing angle and energy of the photon after a Compton scattering event. In this section, the derivation of this rejection sampling procedure will be presented. First, rejection sampling must be explained.

Most PDFs can be expanded in the following way:

$$p(x) = \frac{\sum_i^m p_i T_i(x) n_i(x)}{\kappa}. \tag{A.16}$$

The number of factors, m, is arbitrary although splitting a PDF into more than one factor can improve the sampling efficiency [31]. The probability of selecting a value of x from a particular factor is p_i. The function $T_i(x)$ must be bounded in the interval (0,1). The efficiency of the sampling procedure is κ. Now, to sample a value of x, one first samples an index i from the discrete PDF $p(i) = p_i$. Then, one samples a value of x from the PDF $n_i(x)$. Finally, if the following equality holds, the value is accepted:

$$\varepsilon \leqslant T_i(x).$$

Otherwise the entire process is repeated. The quantity ε is a uniform random number in the interval (0,1).

The simplest possible expansion for rejection sampling would be the following:

$$\kappa p(x) = \left(\frac{p(x)}{C}\right)\left(\frac{1}{b-a}\right).$$

Using this expansion, one would sample a value of x from the uniform distribution in the interval (a,b). Then the rejection function $\frac{p(x)}{C}$ would be used to determine if x should be accepted or rejected. The value of C is simply the maximum value of the PDF $p(x)$.

Often, determining the expansion with the largest efficiency requires trial and error as many possible expansions can exist for each PDF. This is the case with the PDF corresponding to the differential Klein-Nishina cross section. Only the optimum expansion will be shown.

To begin, the PDF corresponding to the differential Klein-Nishina cross section will be derived. A change of variables to the inverse energy loss ratio must be conducted first, which is shown in section A.2:

$$\frac{d\sigma_{K.N.}(\alpha', x)}{dx} = \frac{\pi r_e^2}{\alpha' x^2}\left(\frac{1}{x} + x - 1 + \cos^2\theta\right).$$

The PDF corresponding to this cross section is simply

$$p(\alpha', x) = \begin{cases} \frac{1}{K(\alpha')x^2}\left(\frac{1}{x} + x - 1 + \cos^2\theta\right) & \text{if } 1 \leqslant x \leqslant 1 + 2\alpha' \\ 0 & \text{otherwise} \end{cases} \tag{A.17}$$

where

$$\begin{aligned} K(\alpha') &= \int_1^{1+2\alpha'} \frac{dx}{x^2}\left(\frac{1}{x} + x - 1 + \cos^2\theta\right) \\ &= \left(\frac{\alpha'}{\pi r_e^2}\right)\sigma_{K.N}(\alpha'). \end{aligned} \tag{A.18}$$

Now, the PDF will be factored into the following form:

$$\kappa p(\alpha', x) = p_1(\alpha')T_1(\alpha', x)n_1(\alpha', x) + p_2(\alpha')T_2(\alpha', x)n_2(\alpha', x).$$

The first factor $T_1(\alpha', x)n_1(\alpha', x)$ will have the following form:

$$T_1(\alpha', x)n_1(\alpha', x) = C_1(\alpha')\left(\frac{1}{x} - \frac{1}{x^2}\right).$$

The most efficient way to sample from this distribution is to sample a value of x from the uniform distribution:

$$n_1(\alpha', x) = \frac{1}{2\alpha'}. \tag{A.19}$$

The rejection function is then

$$T_1(\alpha', x) = C_{T1}\left(\frac{1}{x} - \frac{1}{x^2}\right).$$

This function evaluates to zero when $x = 1$. The maximum value of this function occurs when $x = 2$. Therefore, C_{T1} must equal four so that the function is always between zero and one:

$$T_1(\alpha', x) = 4\left(\frac{1}{x} - \frac{1}{x^2}\right). \tag{A.20}$$

The second factor $T_2(\alpha', x)n_2(\alpha', x)$ will have the following form:

$$T_2(\alpha', x)n_2(\alpha', x) = \frac{C_2(\alpha')}{x^2}\left(\cos^2\theta + \frac{1}{x}\right).$$

The most efficient way to sample from this distribution is to sample a value of x from the following distribution:

$$n_2(\alpha', x) = \frac{1 + 2\alpha'}{2\alpha' x^2}. \tag{A.21}$$

The rejection function is then

$$T_2(\alpha', x) = C_{T2}\left(\cos^2\theta + \frac{1}{x}\right).$$

The maximum value of this function occurs when x equals unity and correspondingly, $\cos\theta$ equals unity. To ensure that this function is always between zero and one, $C_{T2} = \frac{1}{2}$ giving

$$T_2(\alpha', x) = \frac{1}{2}\left(\cos^2\theta + \frac{1}{x}\right). \tag{A.22}$$

Now, the probabilities associated with each factor need to be determined:

$$\kappa p(\alpha', x) = \frac{2p_1(\alpha')}{\alpha'}\left(\frac{1}{x} - \frac{1}{x^2}\right) + \frac{1 + 2\alpha'}{4\alpha' x^2}p_2\left(\cos^2\theta + \frac{1}{x}\right)$$

$$\begin{aligned} \frac{2p_1}{\alpha'} &= \frac{1 + 2\alpha'}{4\alpha'}p_2 \\ &= \frac{1 + 2\alpha'}{4\alpha'}(1 - p_1) \\ p_1\left(\frac{2}{\alpha'} + \frac{1}{4\alpha'} + \frac{1}{2}\right) &= \frac{1 + 2\alpha'}{4\alpha'} \end{aligned}$$

$$p_1 = \frac{1 + 2\alpha'}{9 + 2\alpha'} \tag{A.23}$$

$$p_2 = \frac{8}{9 + 2\alpha'}. \tag{A.24}$$

The efficiency associated with this rejection scheme is

$$\kappa(\alpha') = \frac{2K(\alpha')(1 + 2\alpha')}{\alpha'(9 + 2\alpha')}. \tag{A.25}$$

Kahn's rejection sampling procedure corresponds to the above expansion.

A.5 The Adjoint Klein-Nishina Cross Section Differential in Inverse Energy Gain Ratio

In this section, the derivation of the adjoint Klein-Nishina cross section differential in inverse energy gain ratio will be shown. The energy gain ratio, which was originally shown in chapter 5, will be shown again:

$$\begin{aligned} \frac{1}{x} &= \frac{\alpha}{\alpha'} \\ &= \frac{1}{1 - \alpha'(1 - \cos\theta)}. \end{aligned}$$

The change of variables is conducted using the following relationship:

$$\begin{aligned} \frac{d\sigma^{\dagger}_{K.N.}(\alpha', x)}{dx} dx &= \frac{d\sigma^{\dagger}_{K.N.}(\alpha', \theta)}{dE} dE \\ \frac{d\sigma^{\dagger}_{K.N.}(\alpha', x)}{dx} &= \frac{d\sigma^{\dagger}_{K.N.}(\alpha', \theta)}{dE} \left| \frac{dE}{dx} \right|. \end{aligned}$$

Based on the equation for the energy gain ratio, the second term in the above equation can be determined:

$$\begin{aligned} x &= \frac{\alpha'}{\alpha} \\ dx &= -\frac{\alpha'}{\alpha^2} d\alpha \end{aligned}$$

and

$$\begin{aligned}\frac{dx}{dE} &= -\frac{\alpha'}{\alpha^2}\frac{d\alpha}{dE} \\ &= -\frac{\alpha'}{m_e c^2 \alpha^2}.\end{aligned} \tag{A.26}$$

The following relationship will also be useful while conducting the change of variables:

$$\cos^2\theta = 1 - \frac{2(1-x)}{\alpha'} + \frac{(1-x)^2}{\alpha'^2}. \tag{A.27}$$

Now the change of variables can be completed:

$$\begin{aligned}\frac{d\sigma^{\dagger}_{K.N.}(\alpha', x)}{dx} &= \frac{\pi r_e^2}{m_e c^2 \alpha^2}\left[x + \frac{1}{x} - 1 + \cos^2\theta\right]\left(\frac{m_e c^2 \alpha^2}{\alpha'}\right) \\ &= \frac{\pi r_e^2}{\alpha'}\left[x + \frac{1}{x} - 1 + \cos^2\theta\right] \qquad \text{(A.28)} \\ &= \frac{\pi r_e^2}{\alpha'}\left[x + \frac{1}{x} - 1 + 1 - \frac{2(1-x)}{\alpha'} + \frac{(1-x)^2}{\alpha'^2}\right] \\ &= \frac{\pi r_e^2}{\alpha'}\left[x + \frac{1}{x} - \frac{2}{\alpha'} + \frac{2x}{\alpha'} + \frac{1}{\alpha'^2} - \frac{2x}{\alpha'^2} + \frac{x^2}{\alpha'^2}\right] \\ &= \frac{\pi r_e^2}{\alpha'}\left[\frac{1}{x} + x\left(1 + \frac{2}{\alpha'} - \frac{2}{\alpha'^2}\right) + x^2\left(\frac{1}{\alpha'^2}\right) - \frac{2}{\alpha'} + \frac{1}{\alpha'^2}\right] \\ &= K^{\dagger}\left[A^{\dagger}x^2 + B^{\dagger}x + C^{\dagger} + \frac{D^{\dagger}}{x}\right] \qquad \text{(A.29)}\end{aligned}$$

where

$$\begin{aligned}K^{\dagger} &= \frac{\pi r_e^2}{\alpha'} \\ A^{\dagger} &= \frac{1}{\alpha'^2} \\ B^{\dagger} &= 1 + \frac{2(\alpha' - 1)}{\alpha'^2} \\ C^{\dagger} &= \frac{1 - 2\alpha'}{\alpha'^2} \\ D^{\dagger} &= 1.\end{aligned}$$

A.6 Efficient Adjoint Klein-Nishina Rejection Sampling Procedure

As explained in section A.4 and shown in equation A.16, a PDF can be split into many factors from which values of the PDF are sampled. In the case of the PDF corresponding to the differential adjoint Klein-Nishina cross section, three factors will used:

$$\begin{aligned}\kappa p^{\dagger}_{K.N.}(x|\alpha^{'},\alpha_{max}) = {} & p_1(\alpha^{'},\alpha_{max})T_1(\alpha^{'},\alpha_{max},x)n_1(\alpha^{'},\alpha_{max},x) \\ & + p_2(\alpha^{'},\alpha_{max})T_2(\alpha^{'},\alpha_{max},x)n_2(\alpha^{'},\alpha_{max},x) \\ & + p_3(\alpha^{'},\alpha_{max})T_3(\alpha^{'},\alpha_{max},x)n_3(\alpha^{'},\alpha_{max},x).\end{aligned}$$

The PDF corresponding to the differential adjoint Klein-Nishina cross section was shown in equation 5.56. It will be shown here again for convenience:

$$p^{\dagger}_{K.N.}(x|\alpha^{'},\alpha_{max}) = \begin{cases} H^{\dagger}\left[\left(\frac{1}{x}-1\right)+(x)+\left(\cos^2\theta\right)\right] & \text{if } x_{min} \leqslant x \leqslant 1 \\ 0 & \text{otherwise.}\end{cases} \tag{A.30}$$

The three terms from which the three factors will be derived are shown in parenthesis in the above equation.

The first factor $T_1(\alpha^{'},\alpha_{max},x)n_1(\alpha^{'},\alpha_{max},x)$ will have the following form:

$$T_1(\alpha^{'},\alpha_{max},x)n_1(\alpha^{'},\alpha_{max},x) = C_1(\alpha^{'},\alpha_{max})\left(\frac{1}{x}-1\right).$$

The most efficient way to sample from this distribution is to sample a value of x from the following distribution:

$$n_1(\alpha^{'},\alpha_{max},x) = -\frac{1}{x\ln x_{min}}. \tag{A.31}$$

The rejection function is then

$$T_1(\alpha^{'},\alpha_{max},x) = C_{T1}(\alpha^{'},\alpha_{max})(1-x).$$

This function evaluates to zero when $x = 1$. The maximum value of this function

occurs when $x = x_{min}$. Therefore, this function must be defined as follows:

$$T_1(\alpha', \alpha_{max}, x) = \frac{1-x}{1-x_{min}}. \tag{A.32}$$

The second factor $T_2(\alpha', \alpha_{max}, x)n_2(\alpha', \alpha_{max}, x)$ will have the following form:

$$T_2(\alpha', \alpha_{max}, x)n_2(\alpha', \alpha_{max}, x) = C_2(\alpha', \alpha_{max})x.$$

This distribution can be sampled from directly. Therefore a value of x will be sampled from the following distribution:

$$n_2(\alpha', \alpha_{max}, x) = \frac{2x}{1-x_{min}^2}. \tag{A.33}$$

The rejection function is then simply unity due to the direct sampling.

The third factor $T_3(\alpha', \alpha_{max}, x)n_3(\alpha', \alpha_{max}, x)$ will have the following form:

$$\begin{aligned} T_3(\alpha', \alpha_{max}, x)n_3(\alpha', \alpha_{max}, x) &= C_3(\alpha', \alpha_{max})\cos^2\theta \\ &= C_3(\alpha', \alpha_{max})\left(1 - \frac{1}{\alpha'} + \frac{x}{\alpha'}\right)^2 \\ &= \frac{C_3(\alpha', \alpha_{max})}{\alpha'^2}\left(x - 1 + \alpha'\right)^2. \end{aligned} \tag{A.34}$$

This distribution can also be sampled from directly. Therefore a value of x will be sampled from the following distribution:

$$n_3(\alpha', \alpha_{max}, x) = \frac{3\left(x - 1 + \alpha'\right)^2}{\alpha'^3 - \left(x_{min} - 1 + \alpha'\right)^3}. \tag{A.35}$$

The rejection function will again be unity due to the direct sampling.

Now the probabilities associated with each factor need to be determined:

$$\begin{aligned} \kappa p^{\dagger}_{K.N.}(x|\alpha', \alpha_{max}) = &-\frac{p_1(\alpha', \alpha_{max})}{x \ln x_{min}}\left(\frac{1-x}{1-x_{min}}\right) + \frac{2x p_2(\alpha', \alpha_{max})}{1-x_{min}^2} \\ &+ \frac{3p_3(\alpha', \alpha_{max})\left(x - 1 + \alpha'\right)^2}{\alpha'^3 - \left(x_{min} - 1 + \alpha'\right)^3} \end{aligned}$$

$$\frac{2p_2(\alpha^{'},\alpha_{max})}{1-x_{min}^2} = -\frac{p_1(\alpha^{'},\alpha_{max})}{\ln x_{min}\,(1-x_{min})} \tag{A.36}$$

$$\frac{2p_2(\alpha^{'},\alpha_{max})}{1-x_{min}^2} = \frac{3\alpha^{'2}p_3(\alpha^{'},\alpha_{max})}{\alpha^{'3}-(x_{min}-1+\alpha^{'})^3} \tag{A.37}$$

$$1 = p_1(\alpha^{'},\alpha_{max}) + p_2(\alpha^{'},\alpha_{max}) + p_3(\alpha^{'},\alpha_{max}). \tag{A.38}$$

By solving the above system of equations, the probabilities can be determined, which are shown below:

$$p_1(\alpha^{'},\alpha_{max}) = -\frac{3\ln x_{min}\,(1-x_{min})\,\alpha^{'2}}{\frac{3}{2}\left(1-x_{min}^2\right)\alpha^{'2}-3\ln x_{min}\,(1-x_{min})\,\alpha^{'2}+\alpha^{'3}-(x_{min}-1+\alpha^{'})^3} \tag{A.39}$$

$$p_2(\alpha^{'},\alpha_{max}) = \frac{\frac{3}{2}\left(1-x_{min}^2\right)\alpha^{'2}}{\frac{3}{2}\left(1-x_{min}^2\right)\alpha^{'2}-3\ln x_{min}\,(1-x_{min})\,\alpha^{'2}+\alpha^{'3}-(x_{min}-1+\alpha^{'})^3} \tag{A.40}$$

$$p_3(\alpha^{'},\alpha_{max}) = \frac{\alpha^{'3}-\left(x_{min}-1+\alpha^{'}\right)^3}{\frac{3}{2}\left(1-x_{min}^2\right)\alpha^{'2}-3\ln x_{min}\,(1-x_{min})\,\alpha^{'2}+\alpha^{'3}-(x_{min}-1+\alpha^{'})^3}. \tag{A.41}$$

The efficiency associated with this rejection scheme is

$$\kappa(\alpha^{'},\alpha_{max}) = \frac{\alpha^{'}\sigma_{K.N.}^{\dagger}(\alpha^{'},\alpha_{max})}{\pi r_e^2} \cdot\left(\frac{3\alpha^{'2}}{\frac{3}{2}\left(1-x_{min}^2\right)\alpha^{'2}-3\ln x_{min}\,(1-x_{min})\,\alpha^{'2}+\alpha^{'3}-(x_{min}-1+\alpha^{'})^3}\right). \tag{A.42}$$

Bibliography

[1] J. H. Halton, "A retrospective and prospective survey of the monte carlo method," *SIAM Review*, vol. 12, no. 1, pp. 1–63, Jan. 1970.

[2] I. Lux and L. Koblinger, *Monte Carlo Particle Transport Methods: Neutron and Photon Calculations*. CRC Press, 1991.

[3] S. J. Chucas and et al, "Preparing the monte carlo code MCBEND for the 21st century," Arlington, Texas, 1994.

[4] J. E. Hoogenboom, W. R. Martin, and B. Petrovic, "The monte carlo performance benchmark test - aims, specifications and first results." Rio de Janeiro, Brazil: American Nuclear Society, 2011.

[5] J. Spanier and E. M. Gelbard, *Monte Carlo Principles and Neutron Transport Problems*. Addison-Wesley, 1969.

[6] L. Desorgher, F. Lei, and G. Santin, "Implementation of the reverse/adjoint monte carlo method into geant4," *Nuclear Instruments and Methods in Physics Research Section A: Accelerators, Spectrometers, Detectors and Associated Equipment*, vol. 621, no. 1-3, pp. 247–257, 2010.

[7] G. I. Bell and S. Glasstone, *Nuclear Reactor Theory*. Krieger Pub Co, Jun. 1979.

[8] E. E. Lewis and W. F. Miller, *Computational methods of neutron transport*. Wiley, 1993.

[9] P. Pereslavtsev, U. Fischer, D. Leichtle, and R. Villari, "Novel approach for efficient mesh based monte carlo shutdown dose rate calculations," *Fusion Engineering and Design*, vol. 88, 2013.

[10] Y. Chen and U. Fischer, "Rigorous mcnp based shutdown dose rate calculations: computational scheme, verification calculations and application to ITER," *Fusion Engineering and Design*, vol. 63-64, pp. 107–114, Dec. 2002.

[11] A. Robinson, L. El-Guebaly, and D. Henderson, "Rigorous evaluation of biological dose for fusion systems and comparison with approximate contact dose approach," *Fusion Science and Technology*, vol. 60, no. 2, pp. 720–724, Aug. 2011.

[12] S. Yoo, "Optimization of brachytherapy treatment planning using adjoint functions," PhD, University of Wisconsin-Madison, 2003.

[13] V. Chaswal, "Adjoint based treatment planning for brachytherapy: Novel techniques and further developments," PhD, University of Wisconsin-Madison, 2007.

[14] B. Wang, M. Goldstein, X. G. Xu, and N. Sahoo, "Adjoint monte carlo method for prostate external photon beam treatment planning: an application to 3D patient anatomy," *Physics in Medicine and Biology*, vol. 50, no. 5, pp. 923–935, Mar. 2005.

[15] G. Sjoden, "Deterministic adjoint transport applications for he-3 neutron detector design," *Annals of Nuclear Energy*, vol. 29, no. 9, pp. 1055–1071, Jun. 2002.

[16] J. E. Hoogenboom, "Adjoint monte carlo methods in neutron transport calculations," PhD Thesis, Technishe Hogeschool Delft, 1977.

[17] M. J. Grimstone, "Extension of the MCBEND monte carlo code to perform adjoint calculations using point energy data," Nashville, TN, 1998.

[18] M. Rahman, *Integral Equations and their Applications*. WIT Press / Computational Mechanics, Jun. 2007.

[19] P. M. Morse and H. Feshbach, *Methods of Theoretical Physics, Part I*. McGraw-Hill Science/Engineering/Math, Jun. 1953.

[20] M. H. Kalos, "On the estimation of flux at a point by monte carlo," *Nuclear Science and Engineering*, vol. 16, p. 111, 1963.

[21] D. C. Irving, "The adjoint boltzmann equation and its simulation by monte carlo," *Nuclear Engineering and Design*, vol. 15, pp. 273–292, 1971.

[22] M. H. Kalos, "Monte carlo integration of the adjoint gamma-ray transport equation," *Nuclear Science and Engineering*, vol. 33, pp. 284–290, 1968.

[23] B. Eriksson, C. Johansson, and M. Leimdorfer, "Monte carlo integration of the adjoint neutron transport equation," *Nuclear Science and Engineering*, vol. 37, pp. 410–422, 1969.

[24] J. E. Hoogenboom, "Methodology of continuous-energy adjoint monte carlo for neutron, photon, and coupled neutron-photon transport," *Nuclear Science and Engineering*, vol. 143, pp. 99–120, 2003.

[25] D. Gabler, J. Henniger, and U. Reichelt, "AMOS - an effective tool for adjoint monte carlo photon transport," *Nuclear Instruments and Methods in Physics Research Section B: Beam Interactions with Materials and Atoms*, vol. 251, no. 2, pp. 326–332, Oct. 2006.

[26] Klein and Y. Nishina, "Uber die streuung von strahlung durch freie elektronen nach der neuen relativistischen quantendyamik," *Z. F. Phys.*, vol. 52, pp. 853–869, 1929.

[27] J. Persliden, "A monte carlo program for photon transport using analogue sampling of scattering angle in coherent and incoherent scattering processes," *Computer Programs in Biomedicine*, vol. 17, no. 1-2, pp. 115–128, Aug. 1983.

[28] C. H. Hastings, *Approximations for Digital Computers*. Princeton University Press, Dec. 1955.

[29] L. Koblinger, "Direct sampling from the klein–nishina distribution for photon energies above 1.4 mev," *Nucl. Sci. Eng.*, vol. 56, no. 2, pp. 218–219, Feb. 1975.

[30] R. N. Blomquist and E. M. Gelbard, "An assessment of existing klein-nishina monte carlo sampling methods," *Nucl. Sci. Eng.; (United States)*, vol. 83, no. 3, Mar. 1983.

[31] H. Kahn, "Applications of monte carlo," Technical Report AECU-3259, 1956.

[32] Y. Namito, S. Ban, and H. Hirayama, "Implementation of the doppler broadening of a compton-scattered photon into the EGS4 code," *Nuclear Instruments and Methods in Physics Research Section A: Accelerators, Spectrometers, Detectors and Associated Equipment*, vol. 349, no. 2-3, pp. 489–494, Oct. 1994.

[33] R. Ribberfors, "X-ray incoherent scattering total cross sections and energy-absorption cross sections by means of simple calculation routines," *Physical Review A*, vol. 27, no. 6, pp. 3061–3070, Jun. 1983.

[34] M. J. Cooper, "Compton scattering and electron momentum determination," *Reports on Progress in Physics*, vol. 48, no. 4, pp. 415–481, Apr. 1985.

[35] D. E. Cullen, J. H. Hubbel, and L. Kissel, "EPDL97 the evaluated data library, '97 version," University of California, Lawrence Livermore National Laboratory, Tech. Rep. UCRL-ID-50400, Sep. 1997.

[36] F. Biggs, L. Mendelsohn, and J. Mann, "Hartree-fock compton profiles for the elements," *Atomic Data and Nuclear Data Tables*, vol. 16, no. 3, pp. 201–309, Sep. 1975.

[37] J. H. Hubbell, H. A. Gimm, and I. Overbo, "Pair, triple, and total atomic cross sections (and mass attenuation coefficients) for 1 MeV-100GeV photons in elements z=1 to 100," *Journal of Physical and Chemical Reference Data*, vol. 9, no. 4, pp. 1023–1147, 1980.

[38] K. N. Mukhin, *Experimental Nuclear Physics, Volume 1: Physics of Atomic Nucleus*. Mir, 1987.

[39] F. Salvat, E. Acosta, J. M. Fernandez-Varea, and J. Sempau, "The physics of electron / positron transport in PENELOPE," Jul. 2001, pp. 1–5.

[40] J. Hoogenboom, "Adjoint monte carlo photon transport in continuous energy mode with discrete photons from annihilation," in *PHYSOR*, 2000, pp. 50–62.

[41] M. B. Chadwick, M. Herman, P. Oblozinsky, M. E. Dunn, Y. Danon, A. C. Kahler, D. L. Smith, B. Pritychenko, G. Arbanas, R. Arcilla, R. Brewer, D. A. Brown, R. Capote, A. D. Carlson, Y. S. Cho, H. Derrien, K. Guber, G. M. Hale, and others, "ENDF/B-VII.1 nuclear data for science and technology: Cross sections, covariances, fission product yields and decay data," *Nuclear Data Sheets*, vol. 112, no. 12, pp. 2887–2996, 2011.

[42] C. L. L. and C. E. D., "Particle-transport simulation with monte carlo method," National Technical Information Service, Springfield, Tech. Rep., 1975.

[43] X-5 Monte Carlo Team, "MCNP - a general monte carlo n-particle transport code, version 5," Los Alamos National Laboratory, Technical Report LA-UR-03-1987, 2003.

[44] N. Mohamed, "Efficient algorithm for generating maxwell random variables," *Journal of Statistical Physics*, vol. 145, no. 6, pp. 1653–1660, Dec. 2011.

[45] S. McConnell, *Code complete*. Redmond, Wash.: Microsoft Press, 2004.

[46] J. S. Hendricks, "Calculation of cell volumes and surface areas in MCNP," Los Alamos National Laboratory, Informal Report LA-8113-MS, 1980.

[47] T. J. Tautges, P. P. H. Wilson, J. Kraftcheck, B. F. Smith, and D. L. Henderson, "Acceleration techniques for direct use of CAD-Based geometries in monte carlo radiation transport," in *International Conference on Mathematics, Computational Methods & Reactor Physics (M&C 2009)*. Saratoga Springs, NY: American Nuclear Society, May 2009.

[48] T. J. Tautges, R. Meyers, K. Merkley, C. Stimpson, and C. Ernst, "MOAB: a mesh-oriented database," Sandia National Laboratories, SAND2004-1592, Apr. 2004, report.

[49] T. D. Blacker, W. J. Bohnhoff, and T. L. Edwards, "CUBIT mesh generation environment. volume 1: Users manual," Tech. Rep., May 1994.

[50] C. Mattoon, B. Beck, N. Patel, N. Summers, G. Hedstrom, and D. Brown, "Generalized nuclear data: A new structure (with supporting infrastructure) for handling nuclear data," *Nuclear Data Sheets*, vol. 113, no. 12, pp. 3145–3171, Dec. 2012.

[51] F. B. Brown and Y. Nagaya, "The MCNP5 random number generator," Los Alamos National Laboratory, Technical Report LA-UR-023782, 2002.

[52] T. A. Brunner and P. S. Brantley, "An efficient, robust, domain-decomposition algorithm for particle monte carlo," *Journal of Computational Physics*, vol. 228, pp. 3882–3890, 2009.

[53] R. J. Procassini, D. E. Cullen, G. M. Greenman, and C. A. Hagmann, "Verification and validation of MERCURY: a modern, monte carlo particle transport code," Lawrence Livermore National Laboratory, Technical Report UCRL-CONF-208667, 2004.

[54] K. Amako, S. Guatelli, V. Ivanchenko, M. Maire, B. Mascialino, K. Murakami, P. Nieminen, L. Pandola, S. Parlati, M. Pia, M. Piergentili, T. Sasaki, and L. Urban, "Comparison of geant4 electromagnetic physics models against the NIST reference data," *IEEE Transactions on Nuclear Science*, vol. 52, no. 4, pp. 910–918, 2005.

[55] I. Kodeli, E. Sartori, and B. Kirk, "SINBAD shielding benchmark experiments status and planned activities," Carlsbad New Mexico, 2006.

[56] A. Sood, "Doppler energy broadening for incoherent scattering in MCNP5, part i," Los Alamos National Laboratory, Los Alamos, NM, United States, Technical Report LA-UR-04–0487, 2004.